













































































































































































































































Several important observations can be made from the damage contours and field measurements presented in Figure 6-7 through Figure 6-11.

- In general, most of the predicted simulation results indicate fairly good agreement with the field performance observations.
- According to the results obtained from the dynamic modulus characteristic curves and the failure criterion lines for the FHWA-ALF mixtures, it was expected that the SBS mixture would perform the best and the control mixture would perform the worst out of all the mixtures. The trends observed in the damage contours and field measurements clearly show this prediction in Figure 6-11 (a) and (b). It also can be observed for this pavement that the damage was concentrated in the bottom of the asphalt concrete layer. This observation is in line with the generally accepted failure mechanism for thin asphalt pavements, i.e., bottom-up fatigue cracking.
- Warm mix additives seem to deteriorate the mixtures' fatigue resistance, although they decrease the stiffness and aging during compaction. Figure 6-8 (b) and (c) and Figure 6-9 summarize the damage contours for the Sasobit, Evotherm, Advera mixtures and the foamed mixture. The field data support the simulation results obtained from the LVECD program, as seen in Figure 6-11 (c) through (f).
- RAP is considered to be a material that decreases the fatigue resistance of a mixture due to the increase in material stiffness. However, the simulation results suggest otherwise and show that the inclusion of RAP improves the mixture's resistance to fatigue. Because the virgin binder grade used in this study is PG 76-22, which is fairly high, it is possible that the utilization of RAP had no significant effect on resistance to fatigue. Although the LVECD model rankings for the R and RW sections do not match the field measurements, both the LVECD model results and the field observations show a small amount of damage in Figure 6-11 (c) and (d).

- It is accepted that the addition of RAP up to 20% does not have any major effect on virgin mixture performance, according to many asphalt agencies. The LVECD simulation results for the MIT-RAP project presented Figure 6-10 (a) and (c) confirm this finding, because no major differences in fatigue cracking can be observed for both the LVECD model and field cracking results, whereas the utilization of RAP up to 50% led to pavement performance deterioration, as seen in Figure 6-10 (c) and (d). The use of soft binder led to some improvement in performance, as indicated in the  $G^R$  line for the MIT-R-50RSB mix compared with that of the MIT-R-50R mix; however, no major change in performance was observed.
- The key point that emerges from the comparisons of the field measurements versus the simulation predictions is that the magnitudes of the damage area (%) index are quite different from the observed cracking areas in the field, although rankings among the different sections match well. It is noted that the damage area index is calculated from the amount of damage in the cross-section of a pavement, whereas the field cracking areas are determined from the cracks on the pavement surface. This difference emphasizes the significance of transfer functions. The need for such a function is not unexpected for a simulation program such as the LVECD model. The concept of transfer functions will be better defined as other complex phenomena, such as asphalt material aging and healing, which are not included in the version of the LVECD program used in this study, become incorporated for future releases of the LVECD program.

## **6.10 Summary and Conclusions**

This section presents the predictions of the fatigue cracking performance for 18 pavement sections composed of 34 different asphalt mixtures using experimental, analytical, and computational methodologies. The 34 asphalt mixtures include WMA mixtures that incorporate several different WMA technologies and RAP mixtures with different RAP contents and virgin binders. The fatigue characterization at the material level was undertaken using cyclic direct tension tests in accordance with the AASHTO TP 107 protocol and the S-VECD model. The fatigue simulations at the pavement level were performed using the LVECD program developed at NC State University. A comparison between the measured and predicted performance results indicates that the growth trend of the ‘damage area’ in the cross-section of a pavement agrees well with the cracking area measured from the pavement surface. Although overall trends agree between the simulations and the field observations, it is evident that transfer functions are necessary in order to match the magnitude of the damage area and time scale in the LVECD simulations with the magnitude of the field surface cracking area and time scale. The S-VECD characterization and the LVECD simulations of the various modified mixtures, WMA mixtures, and RAP mixtures reveal the effects of different material factors (e.g., different modifications, WMA technologies, RAP contents, virgin binder grades) on the fatigue performance of asphalt mixtures as well as asphalt pavements.

# CHAPTER 7 NUMERICAL EVALUATION OF PAVEMENT DESIGN PARAMETERS FOR THE FATIGUE CRACKING AND RUTTING PERFORMANCE OF ASPHALT PAVEMENT<sup>4</sup>

## 7.1 Abstract

Over recent years, significant research has been conducted to investigate ways to predict fatigue cracking and permanent deformation (rutting), which are two common distresses found in asphalt pavements. These distresses are affected by material properties, environmental conditions, and the pavement's structure. This section investigates common pavement design parameters, including surface type, base layer thickness, base layer type, sub-base layer thickness, and an anti-frost layer, with regard to the asphalt pavement performance of the Korea Expressway Corporation (KEC) test road. Test roads are often regarded as the most realistic tools for evaluating the effects of various parameters because they are subjected to real traffic and environmental factors. The KEC test road is 7.7 km long and was constructed with the aim of developing a Korean mechanistic empirical pavement design guide using the newly developed Layered ViscoElastic pavement analysis for Critical Distresses (LVECD) program.

According to the findings, the base layer thickness and base layer material were found to affect the fatigue cracking and rutting performance, whereas the sub-base thickness and anti-frost layer were found not to affect the amount of distress significantly. The LVECD program was able to capture the effects of the changes in the aforementioned parameters on the amount of cracking and rut depths. Reasonable agreement was found between the

---

<sup>4</sup>This chapter was previously published as: **Norouzi, A.**, D. Kim, and Y. R. Kim (2014). Numerical Evaluation of Pavement Design Parameters for the Fatigue Cracking and Rutting Performance of Asphalt Pavements. *Journal of Materials and Structures*.

program simulations and the field data. However, it remains necessary to develop a simulation of field transfer functions in order to obtain true field performance predictions.

## 7.2 Introduction

For decades, the pavement industry has been endeavoring to improve pavement construction practices, extend the life of new pavements, and minimize the need for pavement rehabilitation efforts. It is now well accepted that fatigue cracking and rutting are two major distresses that occur in hot mix asphalt pavements. These phenomena have been reported in many parts of the United States as well as Europe and other countries.

In pavement analysis, two strains are considered to be critical for design purposes: the horizontal strain ( $\epsilon_h$ ) at the bottom of the asphalt layer, which is instrumental in initiating fatigue cracking, and the vertical compressive strain ( $\epsilon_v$ ) at the top of the subgrade layer, which causes permanent deformation in the asphalt pavement. A study by Behiry (2012) showed that the base layer type, base layer thickness, and the subgrade resilient modulus are the key elements that control the strain levels at the critical locations in the pavement structure. Therefore, the key step for performance predictions and design purposes is to utilize accurate methods that consider pavement life, traffic loading, and temperature variations to obtain reasonable stress-strain analysis results for both the vertical and horizontal directions throughout the depth of the pavement.

The basic approach for stress-strain analysis is layered elastic analysis, where the pavement layers are considered to be the elastic material under stationary axisymmetric loading (Huang 2003). However, layered elastic analysis is not an accurate tool for asphalt pavement because asphalt concrete exhibits viscoelastic behavior, especially under traffic loading. Layered viscoelastic moving load analysis, which is an improvement over layered elastic analysis, is considered also to be more reliable than linear viscoelastic analysis in the viscoelastic domain due to its efficient functions that account for the effects of moving loads and viscoelasticity (Eslaminia and Guddati 2010).

Generally, in order to predict asphalt performance, effective models that can reliably represent fatigue damage growth and permanent deformation are still in demand in addition to efficient tools for strain and stress calculations. The Simplified ViscoElastic Continuum Damage (S-VECD) model is a mechanistic approach that has been applied effectively to predict the performance of asphalt concrete mixtures during pre-localization stages under different modes of loading (Hou et al. 2010, Chehab et al. 2003, Underwood et al. 2010, Underwood et al. 2012). Zhang et al. (2013) developed an energy measure that represents the rate of damage growth using the S-VECD model and can predict fatigue failure. However, Zhang's approach is based on the controlled crosshead (CX) mode of loading only. Sabouri and Kim (2014) proposed a new energy-based failure criterion called the  $G^R$  method, which is independent of mode of loading, test temperature, and strain amplitude. This new criterion has been verified successfully for multiple mixtures that contain reclaimed asphalt pavement, warm mix additives, and modified binders (Norouzi et al. 2014, Sabouri et al. 2014, Tafreshi and Norouzi 2012).

In this study, the rutting performance of the study mixtures was evaluated using a permanent deformation model developed at North Carolina State University by Choi et al. (2012). This so-called *shift model* is capable of expressing the permanent strain growth of asphalt concrete in both the primary and secondary regions as a function of deviatoric stress, load time, and temperature, based on the time-temperature and time-stress superposition principles (Kim and Guddati 2011). These three factors (deviatoric stress, load time, and temperature) are important in predicting rut depths in asphalt pavements because they vary throughout the depth of the asphalt layer. The triaxial stress sweep (TSS) test used in this study was developed to predict the rutting performance of the study mixtures by calibrating the shift model.

However, performance predictions that are based solely on material testing cannot provide a comprehensive picture of the pavement's behavior. Because pavement is a layered structure, the stress and strain distributions vary from point to point, which results in complicated shear and flow zones (Gibson et al. 2009). The newly released LVECD program

is able to calculate linear viscoelastic pavement responses that can be used for both the shift model and the S-VECD model to predict rutting and fatigue cracking, respectively. Norouzi and Kim (2014) verified the LVECD program for multiple pavement sections in the United States and found strong agreement between the simulation results and the field observations.

Given the above considerations, the purpose of this study is to gain a better understanding of the effects of the design parameters, i.e., surface layer type, base layer material properties, base layer thickness, sub-base thickness, and subgrade properties, on the fatigue and rutting resistance of asphalt pavements using experimental material characteristics and simulation software. This study used the following test protocols to find the required parameters for the performance predictions: dynamic modulus tests (AASHTO TP 79), uniaxial fatigue tests using the S-VECD model (AASHTO TP 107), and TSS tests for permanent deformation. To verify the LVECD analysis results, field data were collected from the tested sections and compared with the program simulations.

## **7.3 Test Protocols**

### **7.3.1 Dynamic Modulus Testing**

Asphalt material is considered to be linear viscoelastic material at specific strain levels; therefore, viscoelastic materials have both viscous and elastic components. The dynamic modulus,  $|E^*|$ , can be expressed in the form of a mastercurve that exhibits frequency- and temperature-dependent behavior. In this study, dynamic modulus testing was performed in load-controlled mode in axial compression following AASHTO TP 79. The tests were carried out for all the study mixtures at 4°C, 20°C, 40°C, and 54°C and at frequencies of 25, 10, 5, 1, 0.5, and 0.1 Hz. The load levels were specified by trial and error so that the strain amplitudes were between 50 and 75 microstrain to prevent damage to the specimens. The dynamic modulus values were fitted for the coefficients of the sigmoidal function and time-temperature shift factors by optimizing the dynamic modulus mastercurves.

After determining the shift factors, the dynamic modulus was converted to the relaxation modulus. Finally, a power term, alpha ( $\alpha$ ), used in viscoelastic continuum damage (VECD) theory, was calculated from the maximum log-log slope,  $m$ , of the relaxation modulus and time using the relationship  $\alpha = 1 + \frac{1}{m}$ .

### 7.3.2 Cyclic Testing Using the S-VECD Model

The S-VECD fatigue performance model – which is the simplified form of the more rigorous VECD model and can be used to characterize the fatigue behavior of asphalt concrete using the elastic-viscoelastic correspondence principle, continuum damage mechanics, and time-temperature superposition principle – has been proven to be independent of loading. Controlled crosshead (CX) cyclic direct tension tests were performed at 10 Hz at different temperatures based on the binder performance grade (PG) following AASHTO TP 107. All the tests were performed at three different strain amplitudes (high, medium, and low). The strain amplitudes were selected in such a way to create a spread of numbers of cycles to failure ( $N_f$ ) in the range of 1,000 and 100,000 cycles. In addition to taking air void measurements, in order to check the variability of the fatigue test specimens more precisely, fingerprint dynamic modulus tests were conducted at 10 Hz and 50 cycles before running the CX cyclic direct tension tests. The dynamic modulus value measured from this test is specified as  $|E^*|_{\text{fingerprint}}$  and is used to calculate the dynamic modulus ratio (DMR) via Equation (7.1). A DMR value in the range of 0.9 to 1.1 guarantees that the linear viscoelastic properties obtained from the dynamic modulus tests can be used effectively in S-VECD analysis.

$$DMR = \frac{|E^*|_{\text{fingerprint}}}{|E^*|_{LVE}} \quad (7.1)$$

To determine failure for each sample, the corresponding cycle that is related to the sudden drop in the phase angle, which typically happens around the failure point, has been specified based on the Reese approach (1997). In order to minimize the effects of viscoplasticity, Sabouri and Kim (2014) suggested using the PG of the base binder to determine the proper testing temperature, as shown in Equation (7.2).

$$T(^{\circ}C) \leq \frac{\text{High temperature binder PG grade} + \text{Low temperature binder PG grade}}{2} - 3 \leq 19^{\circ}C \quad (7.2)$$

### 7.3.3 Fatigue Failure Criterion ( $G^R$ Method)

According to the S-VECD failure criterion (the  $G^R$  method), the maximum stored pseudo strain energy at each cycle represents the material's ability to store energy at that particular time. The material loses its stored energy as the damage grows for the same magnitude of applied pseudo strain due to the reduction in pseudo stiffness. The difference between the maximum stored pseudo strain energy and the corresponding undamaged state is referred to as the *total released pseudo strain energy* and is denoted as  $W_C^R$ . According to this criterion, a characteristic relationship exists between the rate of change of the averaged released pseudo strain energy ( $G^R$ ) during fatigue testing and the final fatigue life ( $N_f$ ). The  $G^R$  can be calculated using Equation (7.3). This failure criterion combines the advantages of the S-VECD model and this characteristic relationship, which both originate from fundamental mixture properties. Details regarding the  $G^R$  method and its corresponding calculations can be found in the paper by Sabouri and Kim (2014).

$$G^R = \frac{\frac{1}{2} \int_0^{N_f} (\varepsilon_{0,ta}^R)^2 (1 - F_i)}{N_f^2} \quad (7.3)$$

where

$$\begin{aligned} (\varepsilon_{0,ia}^R)_i &= \text{pseudo strain amplitude at cycle } i, \text{ and} \\ F_i &= \text{pseudo stiffness at cycle } i. \end{aligned}$$

### 7.3.4 Permanent Deformation (TSS testing)

The TSS test is composed of two type of tests: a reference test at the high temperature ( $T_H$ ) followed by three multiple stress sweep (MSS) tests at three different temperatures of low, intermediate, and high ( $T_L$ ,  $T_I$ , and  $T_H$ ), respectively. The reference test in this study utilizes a 0.4-second pulse with a 10-second rest period. This reference test provides permanent strain mastercurves by fitting the incremental model, which is expressed as Equation (7.4).

$$\varepsilon_{vp} = \frac{\varepsilon_0 \cdot N_{red}}{(N_I + N_{red})^\beta}, \quad (7.4)$$

$$\begin{aligned} a_{\xi_p} &= p_1 \log(\xi_p) + p_2, \\ a_{\sigma_v} &= d_1 (\sigma_v / P_a)^{d_2} + d_3. \end{aligned} \quad (7.5)$$

where

$$\begin{aligned} N_{red} &= \text{reduced number of cycles at reference loading conditions,} \\ p_1, p_2 &= \text{coefficients of reduced load time shift factor,} \\ d_1, d_2, d_3 &= \text{coefficients of deviatoric stress shift factor, and} \\ P_a &= \text{atmospheric pressure to normalize stress.} \end{aligned}$$

The MSS tests consist of three loading blocks with increases in deviatoric stress level (70, 100, and 130 psi) while the other loading conditions are kept constant. In this study, the shift factors were obtained by shifting the permanent strain of an individual loading block toward the permanent strain mastercurve, which was obtained from the reference test. The reduced load time shift factor and deviatoric stress shift factor are shown in Equation (7.5).

The physical number of cycles at a given condition was converted into a reduced number of cycles using the total shift factor, which is the sum of the deviatoric stress shift factor and the reduced load time shift factor. These two shift functions utilize temperature, load time, and vertical stress to calculate the shift factors. Details regarding the TSS test method and shift model can be found elsewhere (Choi et al. 2012).

## **7.4 Materials and Test Methods**

For this study, experiments were performed using five laboratory-produced mixtures. Of these mixtures, two types of asphalt mixtures were used at the surface to compare the rutting and crack propagation; these mixtures were an ASTM mix and a 19-mm nominal maximum aggregate size (NMAS) polymer-modified styrene butadiene styrene (SBS) mix, which is designated as *PMA* throughout the study. The intermediate layer consisted of a 25-mm NMAS BB5 mixture with 70 mm thickness. Mixes designated as BB1 (25 mm NMAS) and BB3 (40 mm NMAS), which are frequently used in South Korea, were used for the base layers.

Table 7-1 summarizes the volumetric properties of the mixtures used in the KEC test road sections. The sublayers below the base layer are composed mostly of sub-base and anti-frost layers that are placed on top of the subgrade. An anti-frost layer often is used to compensate for the level difference due to the base; however, the anti-frost layer was omitted from some sections for comparative purposes to evaluate the effectiveness of anti-frost layers on pavement performance. Figure 7-1 schematically presents the KEC pavement structure.

Table 7-1. Volumetric Properties of the KEC Mixtures

Type	Surface		Base		Intermediate
Mixture	ASTM	PMA	BB1	BB3	BB5
Binder Type	Unmodified	Styrene Butadiene Styrene	Unmodified		
Binder Grade	PG 64-22	PG 76-22	PG 64-22		
NMAS* (mm)	19		25	40	25
% Air Void (S-VECD)	5.9		5.7	7.6	7.5
% Air Void (Rutting)	5.9		6.0	8.0	9.9
Sieve Size	Gradation, % Passing				
37.5 mm	100.0		100.0	100.0	100.0
25.0 mm	100.0		100.0	88.6	100.0
19.0 mm	99.6		92.5	71.0	91.0
12.5 mm	84.9		72.9	51.1	67.5
9.5 mm	71.1		63.9	44.1	55.1
4.75 mm	49.3		48.5	38.1	31.2
2.36 mm	36.2		36.1	29.1	23.0
0.60 mm	18.1		18.0	15.1	12.8
0.30 mm	11.6		11.6	10.1	9.2
0.15 mm	7.4		7.3	6.8	6.7
0.075 mm	4.4		4.2	4.4	4.6

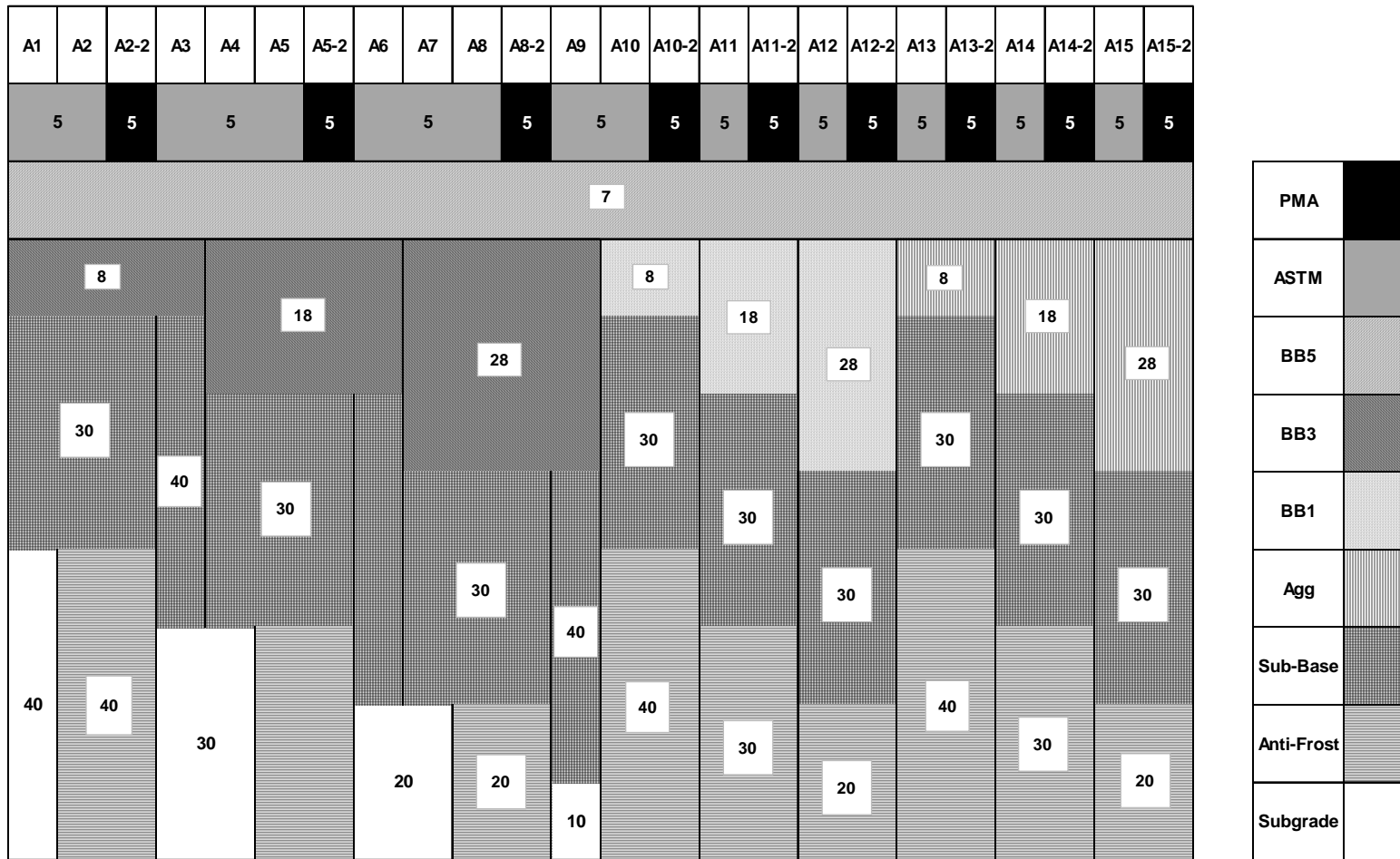
\* Nominal maximum aggregate size.

#### 7.4.1 Specimen Fabrication

To prepare the specimens, aggregate stockpiles were dried and sieved for batching. The aggregate particles were then heated to the mixing temperature for more than six hours before mixing. The asphalt binder and aggregates were mixed together using a bucket mixer. Then, the mixtures were short-term oven-aged for four hours at the compaction temperature.

All the test specimens were compacted to a height of 178 mm and a diameter of 150 mm using the Superpave Gyratory Compactor (SGC). To obtain specimens of uniform air void distribution, these samples were cored to a diameter of 100 mm and cut to a height of 130 mm (Lee et al. 2014) for fatigue cyclic testing, and to a diameter of 100 mm with the height of 150 mm for the dynamic modulus and the permanent deformation (TSS) testing.

The air void contents were measured using the CoreLok method for each specimen prior to testing. All the test samples met the target air void content by  $\pm 0.5$  percent. The direct tension test specimens were glued to metal plates using Devcon steel putty. Vertical deformations were measured using four linear variable differential transducers (LVDTs) with the gauge length of 70 mm at intervals of 90 degrees for both the dynamic modulus and CX cyclic tension tests.



\* The numbers in the figure are all in centimeters (cm).

Figure 7-1. Asphalt pavement sections at the KEC test road.

## 7.5 Test Results and Discussion

### 7.5.1 Dynamic modulus Values

Figure 7-2 presents the averaged dynamic modulus values of the replicates for the KEC mixtures, respectively, on the same graph. The comparison between the PMA and ASTM mixes clearly shows that the PMA mix exhibits low stiffness values at high reduced frequencies (low temperatures) and high stiffness values at low reduced frequencies (high temperatures). In other words, it seems that the PMA mix presents favorable characteristics for fatigue resistance at low temperatures and for rutting resistance at high temperatures. In general, the other unmodified mixtures have similar stiffness values, given the sample-to-sample variability.

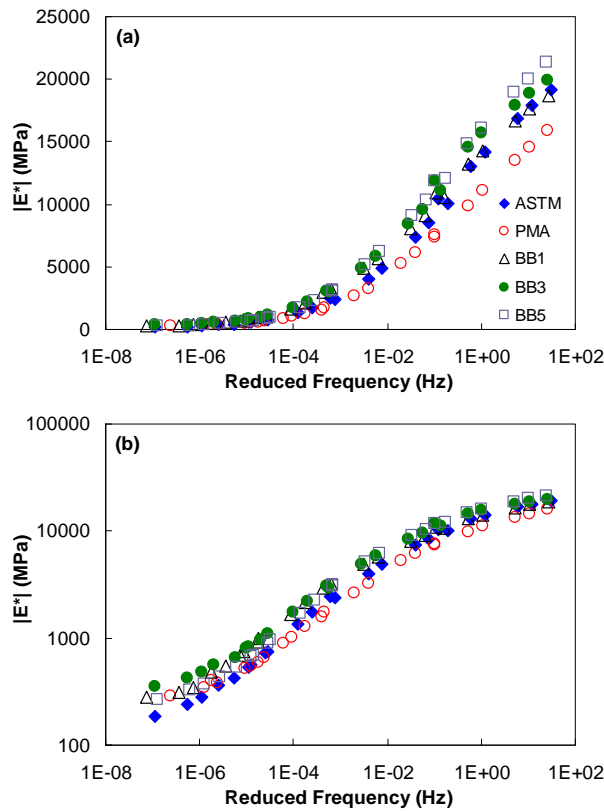


Figure 7-2. Dynamic modulus mastercurves for KEC test road mixtures: (a) in semi-log space and (b) in log-log space.

### 7.5.2 S-VECD Characterization Curves

Figure 7-3 presents the averaged damage characteristic curves for the KEC test mixtures. As shown, the corresponding curve for the ASTM mixture is slightly above that of the PMA mixture. It can be concluded that both the PMA and ASTM mixes follow the same behavior even though their dynamic modulus values are considerably different. This outcome could be related to the higher asphalt content in the ASTM mix compared to the PMA mix. Another reasonable explanation for this observation may be related to the physical nature of the base binder and SBS modifier used in the PMA mix. The other important point is that the curve for the BB1 mix is below the other curves, which could be due to its low asphalt content and large aggregate size.

Generally, a comparison of the damage curves cannot yield reliable information about different mixtures' fatigue behavior, because the energy that is input by mechanical force is consumed not only in creating and propagating the cracks, but also in deforming the material. Therefore, it is important to include both stiffness and damage characteristics of the material when determining a mixture's fatigue cracking resistance.

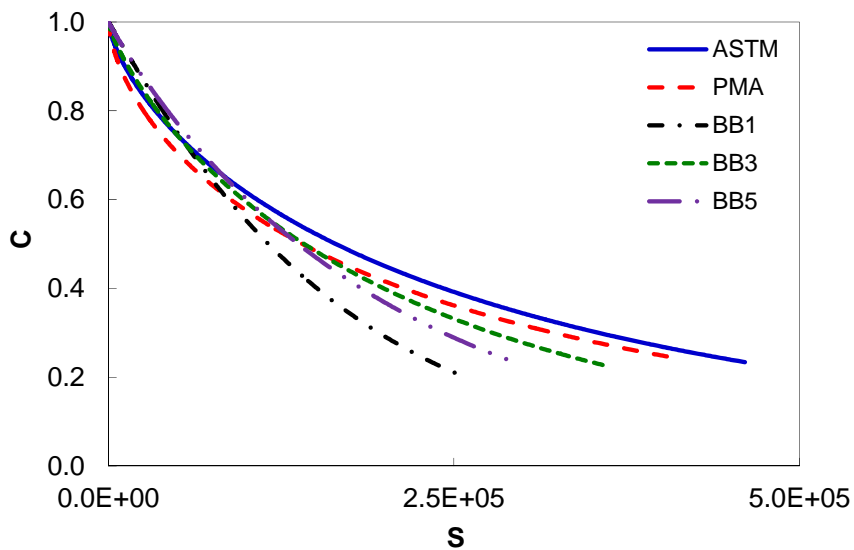


Figure 7-3. Averaged damage characteristic curves for KEC test road mixtures.

### 7.5.3 Fatigue Failure Criterion Lines

The S-VECD failure criterion was applied to all of the mixtures in this study, and the results are presented in Figure 7-4. The position of the failure criterion lines can be used to make a relative comparison of a mixture's expected fatigue resistance. Also, not only the position but also the slope of the failure criterion line plays an important role in the pavement system's fatigue behavior. As observed in Figure 7-4, the line for the PMA mix is parallel to that of the ASTM mix and is slightly above that of the control mixture. Because the two test mixtures follow the same gradation, the difference in the failure criterion lines, which was observed before in the characteristic curves, may be due to the modified binder that is used in the PMA mix. The BB5 mix curve is located over the BB3 mix curve, which indicates that the mixtures with smaller aggregate sizes perform better than the ones with larger aggregates.

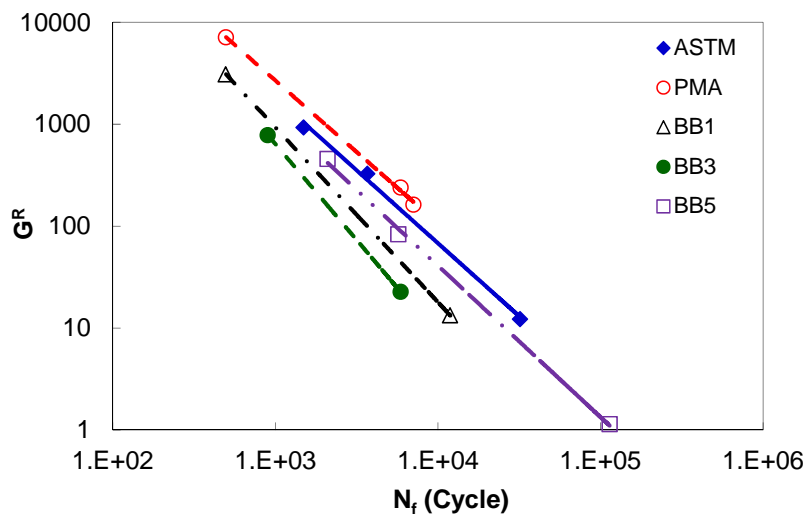


Figure 7-4. Fatigue failure criterion lines for the KEC mixture.

#### 7.5.4 Triaxial Stress Sweep Tests

The TSS test method requires four tests with two replicates for each test to calibrate the shift model. The TSS test temperatures for the KEC mixtures are specified as follows: 22°C as the low temperature ( $T_L$ ), 36°C as the intermediate temperature ( $T_I$ ), and 46°C as the high temperature ( $T_H$ ). Details regarding the temperature selection method can be found elsewhere (Choi et al. 2012). Figure 7-5 presents the results of the TSS tests. The dotted lines show the reference curves and the solid lines correspond to the averaged permanent strains of the MSS tests at each temperature. The first important observation regarding the surface mixtures is the difference in permanent strain levels between the ASTM and PMA mixtures. The corresponding curves for the ASTM mix indicate higher permanent deformation levels than the PMA mix because the PMA mix contains SBS-modified asphalt binder (PG 76-22), which provides strong evidence for the benefits of polymer modification for rutting resistance. For the base course (BB1 mix and BB3 mix) comparison, the BB1 mix exhibits lower permanent deformation levels than the BB3 mix due to the smaller aggregate particles (25 mm) and lower target air void content than the BB3 mix.

The averaged permanent strain levels presented in Figure 7-5 were used to characterize the shift model. The model coefficients were then applied to the LVECD program to evaluate rutting performance within a pavement structure.

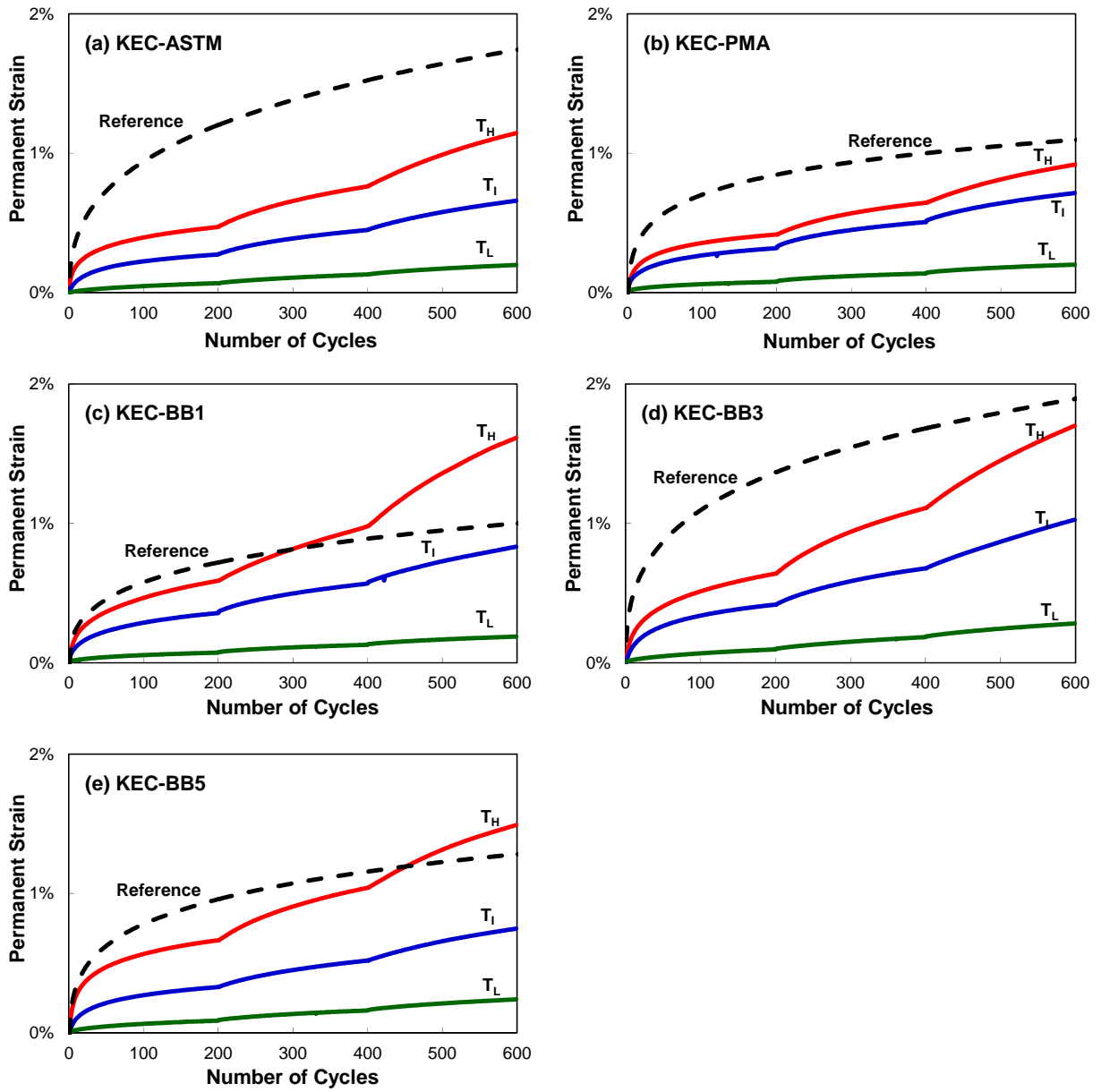


Figure 7-5. TSS test results of KEC mixtures: (a) ASTM, (b) PMA, (c) BB1, (d) BB3, and (e) BB5.

## 7.6 Pavement Analysis

In this study, LVECD program simulations were used to evaluate the effects of the pavement design parameters, i.e., the surface layer type, base layer thickness, base layer material, sub-base thickness, and the impact of an anti-frost layer on pavement performance. Eslaminia et al. (2012) developed the LVECD program to calculate the stresses and strains throughout the pavement depth. The LVECD program, by combining time-scale separation and layered viscoelastic analysis, uses fast-Fourier transforms to perform three-dimensional viscoelastic calculations under moving loads in a rapid manner. The assumption behind using the transforms is that loading occurs in the same repeated manner each time, so the behavior is cyclic and has a steady-state response.

The asphalt layer is modeled as viscoelastic material with damage. Therefore, the asphalt layer is represented by the Prony series of the dynamic modulus values, time-temperature shift factors, S-VECD model coefficients, and TSS model parameters. The aggregate base, anti-frost layer, and subgrade were modeled using linear elastic properties with modulus values of 350 MPa, 88 MPa, and 75 MPa, respectively. The other inputs required for the LVECD simulations are design time, pavement structure, traffic, and climate. The design time for this study was assumed to be twenty years. A single tire with standard loading of 80 kN at the center of the pavement was assumed. The average annual daily truck traffic (AADTT) was 935 based on the traffic data obtained from the site. Pavement temperatures were obtained from the Enhanced Integrated Climate Model (EICM) software. The EICM program provides hourly temperatures of asphalt pavements in terms of pavement depth.

### 7.6.1 Fatigue Performance

In order to evaluate fatigue resistance, the LVECD program calculates the damage growth and the damage factor using Equation (7.6) based on Miner's law. If the damage factor is equal to zero, the element does not experience any damage. A damage factor of one indicates failure of the element.

$$Damage\ Factor = \sum_{i=1}^T \frac{N_i}{N_{fi}} \quad (7.6)$$

where

$T$  = total number of periods,

$N_i$  = traffic for period  $i$ , and

$N_{fi}$  = allowable failure repetitions under the conditions that prevailed in period  $i$ .

The fatigue cracking simulation results for 24 pavement sections are presented in Figure 7-6. It should be noted that the fatigue performance predicted from the LVECD program has not yet been fully calibrated with the field performance data, and the transfer functions that convert the damage predicted from the LVECD software to the percentage of cracking areas are still in process. To compare the fatigue life of the mixtures, the numbers of failure points (elements with the damage factor of ‘1’) were counted and divided by the total number of points throughout the section, and the resultant value was specified as an index for the amount of damage (in percent, %) in the pavement section. To verify the cracking data obtained from the LVECD program, field distress data from Seo (2010) were used.

Figure 7-6 (a) shows the amounts of damage for the different base layers (BB1, BB3, and aggregate base mixtures). A comparison of the results clearly suggests better performance for the pavements that have an asphalt material base layer than the ones that have an aggregate base layer in terms of the different base layer thicknesses, which was expected. Between the pavements that have an asphalt layer base, it seems that the BB1 mix, which shows better fatigue resistance based on the failure criterion lines, exhibits less damage than the BB3 mix. This outcome is in strong agreement with the field cracking data, as presented in Figure 7-7 (a). Also, the difference in performance between the BB1 and BB3 mixes may be due to the lower air void content and smaller aggregate size of the BB1 mix, which led to better aggregate interlocking in the mixture.

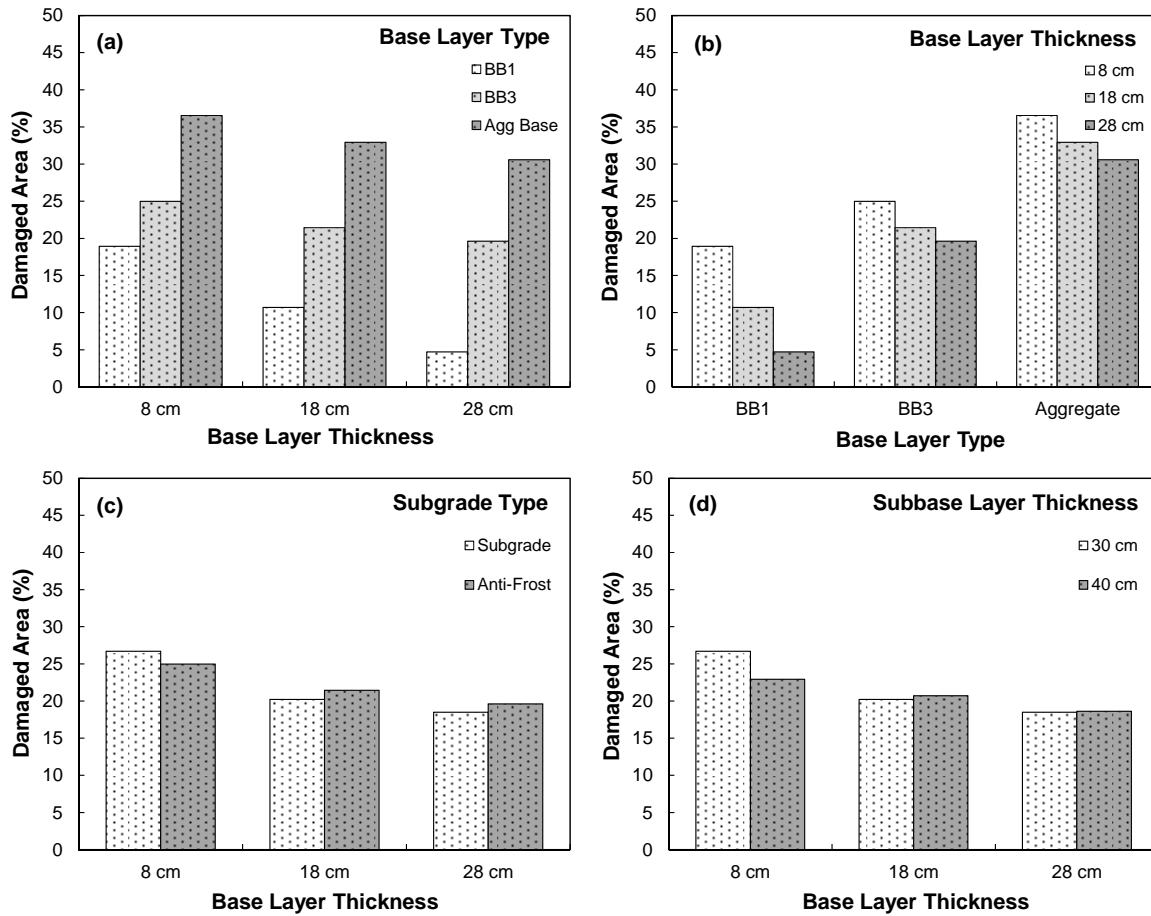


Figure 7-6. Effects of different parameters on fatigue cracking performance as obtained from LVECD simulations: (a) base layer material, (b) base layer thickness, (c) subgrade material, and (d) sub-base thickness.

Another interesting observation that can be made from Figure 7-6 (b) is the interaction between two factors: the base layer material type and the base layer thickness. For example, in the case of the aggregate base pavements, with an increase in the base layer thickness from 8 cm to 28 cm, the damage decreased from 36% to 30%, whereas the same increase in the BB1 mix layer led to a corresponding decrease in damage from 20% down to less than 5 percent. As expected, the BB3 mix was not as effective in resisting fatigue cracking as the BB1 mix because the BB3 mix performed the worst among all of the mixtures used in the KEC test road. However, a greater reduction in fatigue cracking was observed with an increase in the base layer thickness, especially for the aggregate base

structure in the field, which was not captured effectively by the LVECD program, as shown in Figure 7-7 (b).

The analysis results presented in Figure 7-6 (c) briefly indicate that the subgrade type (anti-frost or subgrade) does not appear to play an important role in the fatigue behavior of the entire pavement. In other words, similar pavement performance can be expected for pavements that have either anti-frost or subgrade material. The field observations presented in Figure 7-7 (c) also confirm this finding.

The effects of the sub-base layer thickness are demonstrated in Figure 7-6 (d). In general, the pavements with a 30-cm sub-base layer behave similarly to the ones with a 40-cm sub-base layer. It seems, unlike the base layer thickness that significantly alters fatigue resistance, that the sub-base layer has no major impact on the amount of cracking. Although this observed trend was not unexpected, the quantification of the changes in fatigue cracking can be useful for an optimal pavement design.

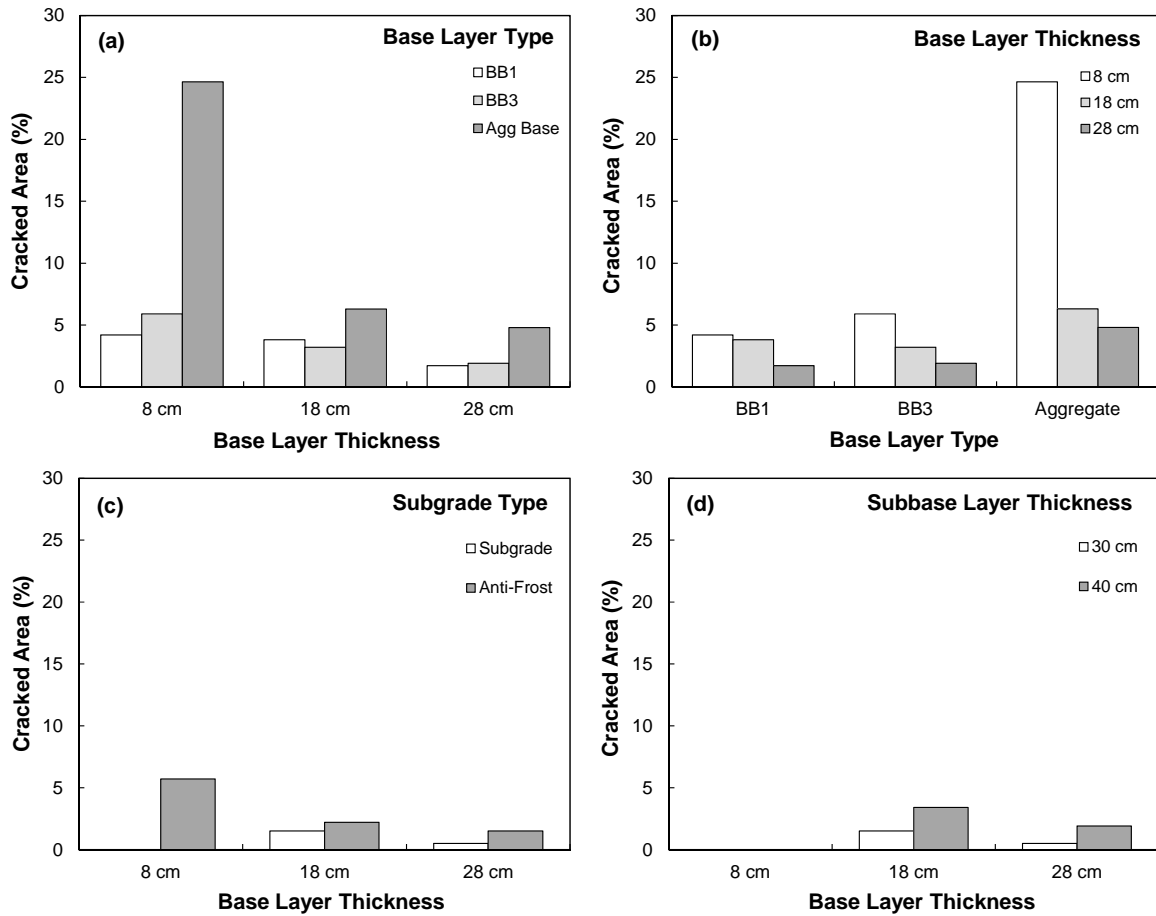


Figure 7-7. Effects of different parameters on pavement fatigue cracking in the field: (a) base layer type, (b) base layer thickness, (c) subgrade material, and (d) sub-base thickness.

### 7.6.2 Rutting Performance

In order to help determine rutting resistance, the deviatoric stress and load time underneath the pavement can be calculated using the LVECD program. The deviatoric stress changes throughout the depth of the pavement depending on the load applied. The permanent deformation is calculated for each layer based on the deviatoric stress.

The permanent deformation value that is the sum of the permanent deformation of all the layers is the total rut depth; therefore, the ultimate deformation in a given layer can be obtained by multiplying the permanent strain by the total thickness.

As for the fatigue performance analyses, the LVECD rutting simulation results also were compared to the measured rut depths in the field, as presented in Figure 7-8. Both the measured and predicted rut depths obviously show better rutting resistance of the polymer-modified mixture than the ASTM mixture, as shown in Figure 7-8 (a). Figure 7-8 (b) presents the comparison of the rut depths of the different base layer types (BB1, BB3, and aggregate base). As shown, the 8-cm aggregate base layer exhibits extreme rutting deformation, whereas an increase in the thickness up to 18 cm corresponds to a decrease in the rut depth. This outcome leads to the conclusion that a relatively thick aggregate base layer provides reasonable rutting resistance.

However, increasing the thickness up to 28 cm did not decrease (lessen) the rut depth compared to the 18-cm layer. The LVECD program was not able to simulate the poor prediction of the thinner aggregate base layer because the rutting coefficient inputs in the LVECD program were not accurate enough to capture the true performance of the aggregate base. The utilization of the asphalt base mixtures (BB1 and BB3) provided better rutting resistance than the aggregate base layers. Overall, the BB1 mix shows better rutting resistance than the BB3 section, as demonstrated in Figure 7-8 (b).

The subgrade and anti-frost layers constituted the sublayers of the asphalt sections. Three sections (1, 3, and 6) were selected among six sections that have no anti-frost layer (2, 4, and 8), and their rut depths were compared against those sections with an anti-frost layer. Figure 7-8 (c) illustrates the effects (or lack thereof) of an anti-frost layer on rutting performance. In general, no correlation between the anti-frost layers and rutting was found, even though slightly greater rut depths were apparent at sections that had an anti-frost layer. The LVECD prediction results show very close agreement with and without anti-frost layers.

Figure 7-8 (d) presents the effect of the sub-base layer thickness on the rutting performance of sections without an anti-frost layer. Although the rut depths in the 30-cm base layer are slightly greater than those in the 40-cm base layer, there is no significant relationship in terms of the sub-base layer thicknesses. The LVECD prediction results show that the rut depths of the 30-cm and 40-cm sub-base layers are exactly the same. The rut depths increase with an increase in base layer thickness because the deformation calculated in a given layer is the permanent strain multiplied by the thickness.

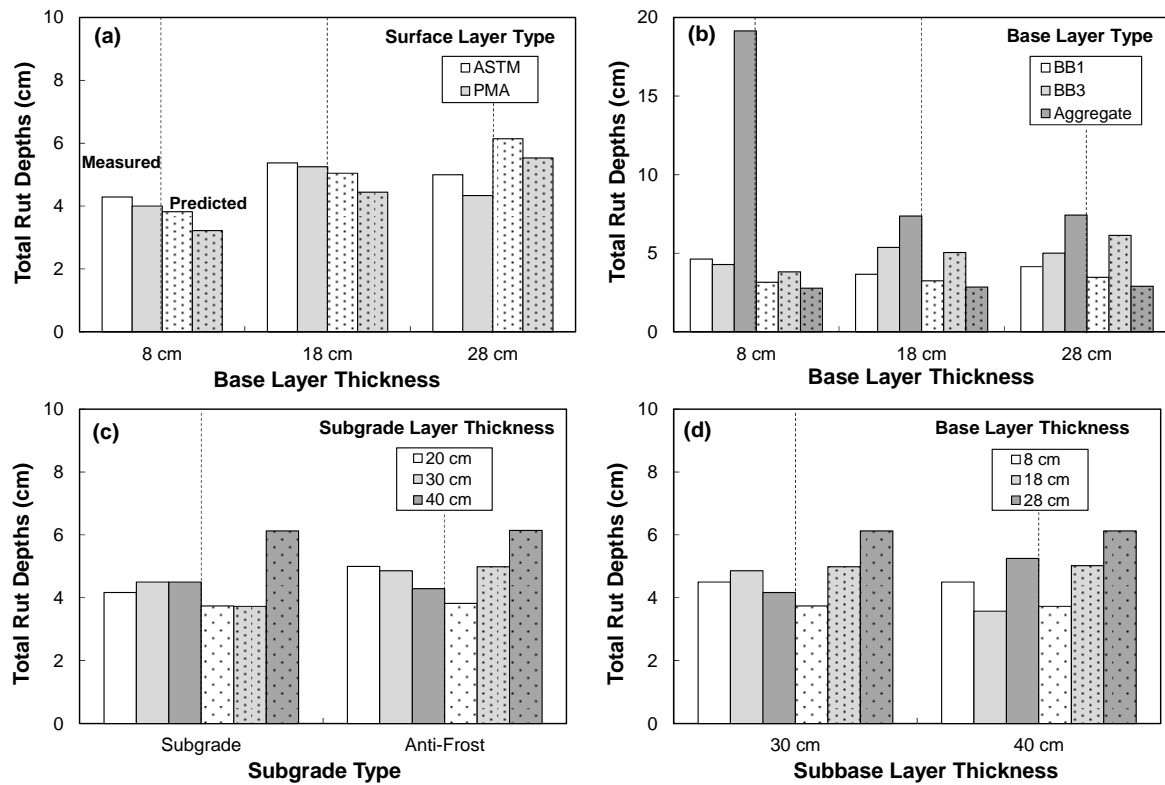


Figure 7-8. Effects of different parameters on rutting performance: (a) surface layer type, (b) base layer type, (c) subgrade type, and (d) sub-base thickness.

## 7.7 Conclusions

In this study, the effects of common pavement design parameters on asphalt pavement performance have been investigated through laboratory-produced asphalt mixture testing, numerical simulations, and field verification. The fatigue cracking and rutting performance of 24 asphalt pavement sections with different structures were evaluated using validated models. The S-VECD model was used to evaluate the fatigue properties of the mixtures, and TSS tests were performed to assess the rutting behavior of the mixtures. The results were then input in the LVECD pavement analysis program to predict the long-term performance of the test pavement sections. A summary of the findings and the conclusions that can be drawn from this study are as follows:

- As expected, the utilization of the mixtures that contained modified binders improved the pavement performance. As seen in Figure 7-8 (a), the sections with the PMA mix exhibited less permanent deformation than the ASTM sections due to the higher stiffness values of the PMA mix, especially at higher temperatures.
- One interesting observation is that the base layer material played the most important role in affecting both rutting and fatigue cracking in the KEC test road sections. The aggregate base layer exhibited greater rut depths and more cracking than the asphalt base layers, whereas the sections with an asphalt base layer (either the BB1 mix or BB3 mix) showed less distress than the aggregate base sections.
- The data obtained from the pavement analyses of the different base layer thicknesses briefly indicate that an increase in the base layer thickness reduces the pavement distresses, but the amount of improvement is dependent on the material type. According to the observations made from Figure 7-7 (b) and Figure 7-8 (b), increasing the aggregate base layer thickness from 8 cm to 28 cm can provide up to 70% reduction in pavement distress.

- The pavement simulations indicate no significant change in the fatigue resistance or permanent deformation when using an anti-frost layer or increasing the sub-base layer thickness. The field observations are in strong agreement with these findings, as shown in Figures 7 (c) and (d).
- The key point that has emerged from the field measurements versus the simulation predictions is that the magnitude of the damage area (%) index and the total rut depths do not directly correspond to the observed field data. This finding suggests the need for developing a simulation-to-field transfer function. The need for such a function is not unexpected for a simulation program such as the LVECD software.

# **CHAPTER 8 APPLICATION OF VISCOELASTIC CONTINUUM DAMAGE APPROACH TO PREDICT THE FATIGUE CRACKING PERFORMANCE OF BINZHOU PERPETUAL PAVEMENTS<sup>5</sup>**

## **8.1 Abstract**

Fatigue cracking in the asphalt pavements has been known as one of the complex distresses that is dependent of asphalt mixture properties, environmental conditions, and pavement structure. This phenomenon is still difficult to predict not only due to models, because it has not been well recognized. One way to improve the fatigue life is to increase the pavement thickness to decrease the tensile strain at the bottom of the asphalt layer. To reach this goal, perpetual pavements can be considered as a reasonable alternative. In this section, the Binzhou perpetual pavement test sections constructed in Shandong Province, China, have been simulated for the long term fatigue performance using the finite element package, LVECD (Layered Viscoelastic pavement analysis for Critical Distresses). In this framework, asphalt concrete is modeled in the context of linear viscoelastic continuum damage theory. A recently developed unified fatigue failure criterion is also incorporated to define the boundaries of the applicable region of the theory. All material models are characterized by dynamic modulus tests and direct tension cyclic fatigue tests with cylindrical specimens in the laboratory. The 15 year fatigue performance simulations recommend the use of Section 1 and 3 as the perpetual pavement design.

---

<sup>5</sup>This chapter was previously published as: Cao, Wei., **A. Norouzi**, and Y. R. Kim (2015). Application of Viscoelastic Continuum Damage Approach to Predict the Fatigue Cracking Performance of Binzhou Perpetual Pavements. *Journal of Traffic and Transportation Engineering*, in press.

## 8.2 Introduction

For the past decades, the most widely used pavement type in China has been the semi-rigid asphalt pavement, which is characterized by semi-rigid base layers, such as cement-stabilized aggregate and lime-fly ash treated soil, and overlays of asphalt concrete. This type of pavement structure is cost effective and environmentally friendly as it is able to consume a considerable amount of industry waste. On the other hand, the semi-rigid base also provides a stable support necessary for the high traffic volumes (and even overloading) typically seen in China. However, the semi-rigid materials are prone to fatigue cracking under repeated traffic loading. Once crack initiates in the base layer, it propagates upward into the flexible asphalt layers thereby leading to the reflective cracking and consequently the structural failure of the pavement. Hence, the design life of such pavements is usually limited to 10-15 years.

Inserting a stress-absorbing interlayer between the asphalt concrete and base materials has been one of the major remedies for reflective cracking. Nevertheless, it can at most help to delay the crack propagation when a high-quality material design and construction are guaranteed for the interlayer; the base may crack as well. At the end, the rehabilitation or even reconstruction is necessitated for the whole pavement structure involving all the layers. Considering these unavoidable defects with semi-rigid materials, another alternative, albeit expensive in the short term, would be the perpetual pavement. Perpetual pavement is commonly designed to last for 40-50 years without structural failure; only the surface asphalt layer requires rehabilitation or replacement when necessary. Therefore, in the long run perpetual pavement could be a choice of high cost effectiveness and sustainability (Amini et al 2011).

Traditionally, perpetual pavement is designed by invoking the concept of limiting critical pavement responses. It is generally believed that if the imposed traffic loads produce responses below certain threshold values then the structural damage does not accumulate. The critical pavement responses of interest are the vertical compressive strain at the top of subgrade and the horizontal tensile strain at the bottom of asphalt layers for structural rutting and bottom-up fatigue cracking, respectively (Behiry 2012).

In order to limit the rutting to upper few inches of the pavement, increase in the structure thickness or stiffness of materials is required so that the vertical load can be distributed to a greater extent before reaching the subgrade. Experimental evaluation tools for the material rutting resistance include Asphalt Pavement Analyzer, Hamburg Wheel-Tracking Device, and the Heavy Vehicle Simulator, to list a few. To simulate the material macroscopic behavior and understand the underlying deformation mechanisms, readers are encouraged to follow the work by Choi (2013), Cao (2015), and Darabi et al. (2012), for example.

On the fatigue side, one way to decrease the probability of bottom-up cracking is to increase the structure thickness as well, thereby reducing the maximum strain at the bottom of asphalt pavement. The bending beam test has been conventionally used in the laboratory to evaluate the fatigue resistance of asphalt mixtures and investigate the concept of fatigue endurance limit which is the aforementioned threshold level of tensile strain. More advanced explorations regarding the endurance limit are performed by Underwood and Kim (2009) and Bhattacharjee et al. (2009) within the context of viscoelastic continuum damage theory.

Despite the wide acceptance, the above described design methods for perpetual pavements are subject to questions. During the service life pavement experiences complex traffic and environmental conditions, and thus the consideration of effects of temperature, aging, and healing, for example, should be included in both material and structural design as they all lead to variations in material properties.

Obviously, it is less persuasive and lacks rigor to approve or disapprove a mix design by testing the material only at certain pre-specified conditions.

This chapter is focused on the material characterization and pavement performance evaluation on the aspect of bottom-up fatigue cracking. A comprehensive analysis system is presented and its applicability and versatility is demonstrated via simulations on the Binzhou perpetual pavement test sections in Shandong Province, China. In this framework the effects of temperature have been naturally incorporated through rigorous mechanistic modeling of asphalt materials. As for the other factors such as aging and healing, continuous efforts are being made in the on-going research.

### 8.3 Overview of Binzhou Test Sections

Six different asphalt mixes were designed for the Binzhou project. The material designations and descriptions are listed in Table 8-1. Five different sections were implemented, and the structure layout has been illustrated in Figure 8-1. As can be observed from Figure 8-1, Section 1 through Section 3 are categorized as the full-depth asphalt pavement which are the typical designs for perpetual pavement in Europe and North America. In the project Section 1 was designed by using  $70 \mu\epsilon$  as the critical value for the tensile strain at the bottom of pavement, while Section 2 and 3 used  $125 \mu\epsilon$ . Section 5 is the semi-rigid asphalt pavement extensively adopted in China as mentioned previously. Section 4 used a similar design to Section 5 whereas the thickness of asphalt layers is considerably increased by inserting a layer of large stone porous asphalt mixture (LSPM) right above the semi-rigid base. Note that for all the sections the top 30 cm of subgrade was treated with lime in field construction in order to increase the soil modulus.

As a relatively new type of asphalt mixture, LSPM is usually designed with a uniform gradation and large particle sizes with the nominal maximum aggregate size (NMAS) typically greater than 25 mm, which is intended for an interlocking aggregate structure. In the meanwhile, a small amount of fine aggregate is used to fill the aggregate void to increase the material's stiffness and durability.

The air void content is usually targeted at 13-18% which gives the mixture excellent draining capability (Zhao and Huang 2010). In addition, owing to the large particle size and high air void content, LSPM is also able to function as a stress-absorbing interlayer and thus possesses the potential to reduce the reflective cracking according to numerical simulations and field observations in China (Luo and Xu 2007, Yufeng et al. 2008, Yin 2011).

Table 8-1. Asphalt concrete materials used in the Binzhou test sections.

Designation	Description
SMA	Stone Matrix Asphalt (PG 76-22, MAC <sup>a</sup> modified)
Superpave-19	19-mm NMA Superpave (PG 76-22, MAC modified)
Superpave-25	25-mm NMA Superpave (PG 64-22)
LSPM	25-mm Large Stone Porous Mixture (PG 70-22, MAC modified)
F-1	12.5-mm NMA Superpave Fatigue Layer (PG 64-22)
F-2	12.5-mm NMA Superpave Fatigue Layer (PG 76-22, SBS <sup>b</sup> modified)

Note: <sup>a</sup>Multigrade Asphalt Cement, <sup>b</sup>Styrene-Butadiene-Styrene.

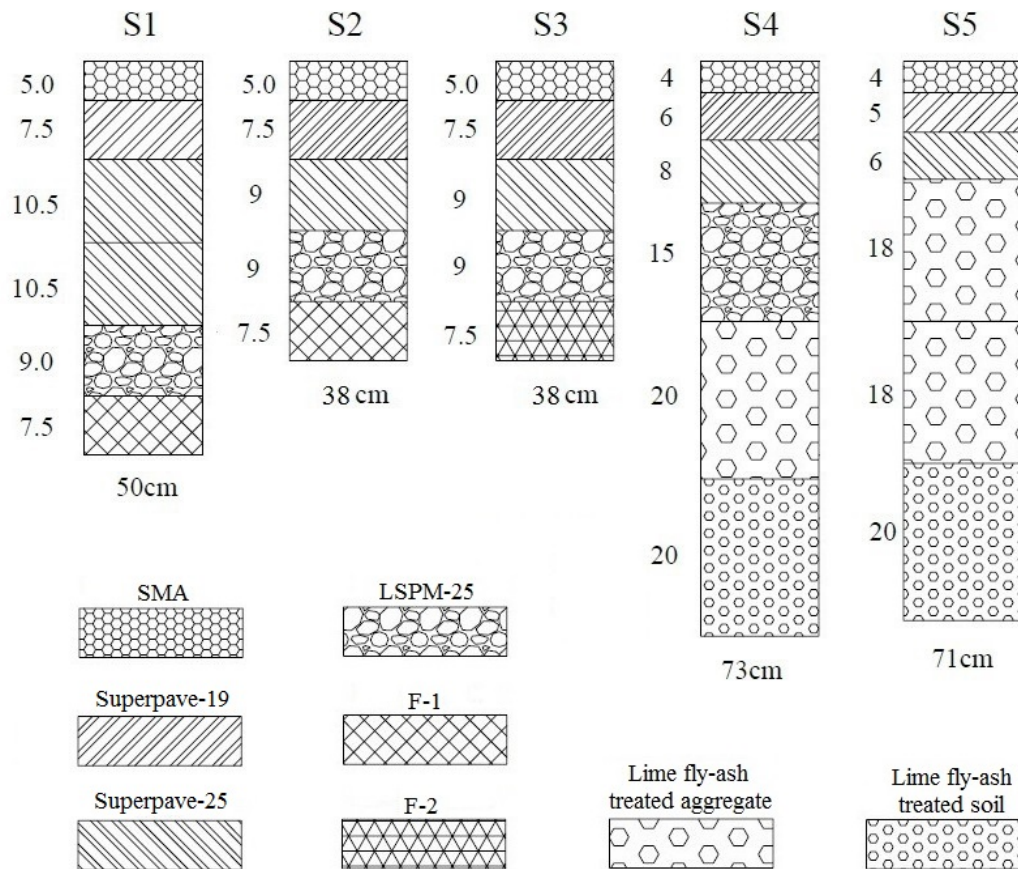


Figure 8-1. Structure layout of test sections in Binzhou perpetual pavement project.

## 8.4 Material Modeling

Strictly speaking, asphalt concrete is a viscoelastic-viscoplastic material; which mechanism dominates the material responses is dependent on the material intrinsic properties, temperature, and loading rate. Since fatigue cracking usually occurs at lower temperatures and the structure layer of interest is the bottom asphalt layer a few inches below the surface, it is reasonable to confine the study within the context of viscoelasticity. In the following the theory of linear viscoelasticity and continuum damage mechanics are briefly reviewed. In the next section, the coupled viscoelastic continuum damage (VECD) theory is then applied to laboratory testing to characterize the material stiffness and fatigue resistance.

### 8.4.1 Linear Viscoelastic Continuum Damage Theory

As just mentioned in the above, an intact linear viscoelastic material would demonstrate a linear relationship between stress and pseudo strain in a monotonic loading. When the microcrack damage initiates, this relation will evolve into nonlinear regions resulting in a reduction in the instantaneous secant modulus, which is named as the secant pseudo stiffness ( $C$ ). As analogous to elastic cases, this pseudo stiffness is used to characterize the material deterioration due to damage. Material is treated as a continuum with microcracks being assumed as uniformly distributed within the body without coalescence. By ignoring the effects of anisotropy, nonlinear viscoelasticity, and plasticity, if any, the VECD framework hypothesizes that any reduction in the pseudo stiffness is caused by the material's internal damage ( $S$ ), exclusively:

$$C(S) = \frac{\sigma}{\varepsilon^R} \quad (8.1)$$

where  $C$  is the secant pseudo stiffness, and  $S$  is the internal variable quantifying the material damage status. It is assumed that between  $C$  and  $S$  there exists a single-valued monotonically decreasing function, referred to as the *damage characteristic relationship*.

The pseudo stiffness can be directly calculated using Equation (8.1). Note that for the intact state free of damage, the  $C$ -value is 1, equal to  $E^R$ , as obtained by substituting Equation (8.4) into Equation (8.1). Yet, the damage state variable can usually be approached only

through experimental investigations and theoretical hypotheses. In this case, Schapery's work potential theory, which is derived based upon thermodynamic principles, is employed to characterize the damage evolution process:

$$\frac{dS}{dt} = \left( -\frac{\partial W^R}{\partial S} \right)^\alpha \quad (8.2)$$

where  $\alpha$  is a material constant denoting the damage evolution rate, and  $W^R$  is the pseudo strain energy density function, which is given by analogy with linear elastic cases as

$$W^R = \frac{1}{2} C(S) (\varepsilon^R)^2 \quad (8.3)$$

Initially developed for material constitutive modeling under monotonic loading conditions (Kim and Little 1990, Park et al. 1996), the VECD theory and its algorithms were later on extended and improved to accommodate the cyclic loading scenarios (Daniel and Kim 2002, Underwood et al. 2010, 2012), and it is then that the theory begins to see its prosperity in modeling the fatigue characteristics in asphalt materials. In the laboratory, the  $C$ - $S$  curve is usually determined by running cyclic direct tension fatigue test with the displacement controlled mode in a closed-loop servo-hydraulic test system. Afterwards, an exponential function is usually used to fit the experimental curves in order for further manipulations:

$$C = \exp(aS^b) \quad (8.4)$$

where  $a$  and  $b$  are the fitting coefficients.

It is worth mentioning that the resulting damage characteristic relationship is a material intrinsic property that is independent of temperature, loading type (monotonic or cyclic), mode (stress, strain, or displacement controlled), and other conditions such as loading amplitude and rate, as long as viscoelasticity is maintained as the dominating mechanism in the material. Also note that the time-temperature superposition principle for the intact state is still applicable to the material despite of a significant presence of damage (Chehab et al. 2002, Underwood et al. 2006), and therefore the same time/frequency-temperature equivalence relation can be used in the VECD framework.

### 8.4.2 Failure Criterion

By now, the damage characteristic relationship has been obtained. It prescribes the path that the damage evolution of each material point in asphalt layers should follow. However, the VECD theory does not provide a definition of the applicable region for the damage curves as the fundamental assumption of the continuum would be violated as soon as microcracks start to coalesce causing damage localization. Hence, a separate failure criterion is called for to complete the VECD system.

Early explorations (Hou et al. 2010, Underwood et al. 2012) are focused on the pseudo stiffness ( $C$ ) by seeking a relationship to express the critical  $C$ -value at failure as a function of mixture type (i.e., whether contains reclaimed asphalt pavement or not), NMAS, and test conditions (e.g., temperature and load frequency). Such criteria are proved to be unreliable because of high variability and dependence on the loading mode. The energy based failure criterion developed by Sabouri and Kim (2014) presents a consistent and unified approach to failure characterization that has been verified successfully for non-RAP and RAP materials (Norouzi et al.,2014) . In the following the model is reviewed in a slightly different way than the original presentation.

As shown in Figure 8-2, attention is placed on the space of stress and pseudo strain. To construct the damage characteristic curves, the values of  $C$  and  $S$  are computed in a cyclic manner in the VECD theory. Starting immediately after the stress peak in the first cycle,  $C$  is redefined as the peak-to-peak pseudo stiffness, designated as  $F$ . Since the pseudo strain energy dissipates slowly in the cyclic test, which is evidenced by the small area enclosed by the hysteresis loops before failure,  $F$  is deemed as a good indicator of material damage status or degree of integrity.

Material deterioration is exhibited via a progressive decline in the  $F$ -value, which is accompanied with the loss in material's ability to store the pseudo strain energy. For the specific stress and (pseudo) strain history in a cycle  $i$ , the amount of the maximum pseudo strain energy that could be stored if the material is intact is indicated by the triangular area ADC, as shown in Figure 8-2, where the AC line has a slope of one,  $\varepsilon_s^R$  denotes the permanent pseudo strain, and  $\varepsilon_{0,ta}^R$  denotes the tensile amplitude of the pseudo strain in this

cycle. Meanwhile, the actual amount of the maximum pseudo strain energy that can be stored in the material for this particular cycle is indicated by the area ADB.

The difference between the two energy, indicated by ABC and denoted as  $W_C^R$ , is the pseudo strain energy that would have to dissipate for the material to degrade from the intact state to the specific damage state in that cycle. Therefore, for a given fatigue test,  $W_C^R$  can be considered as another damage state variable, and is named as the *total released pseudo strain energy* in the original presentation. However, it should be noted that this energy is not physically released or dissipated in the fatigue test, and therefore in this chapter it is referred to as the *characteristic dissipated pseudo strain energy* (CDPSE). Nevertheless, it provides an effective and convenient approach to tracking material status by comparing the damaged to the virgin state in a cyclic manner. Lastly, it is also worth noting that in the above discussion the reverse loading and the potential healing effects are neglected.

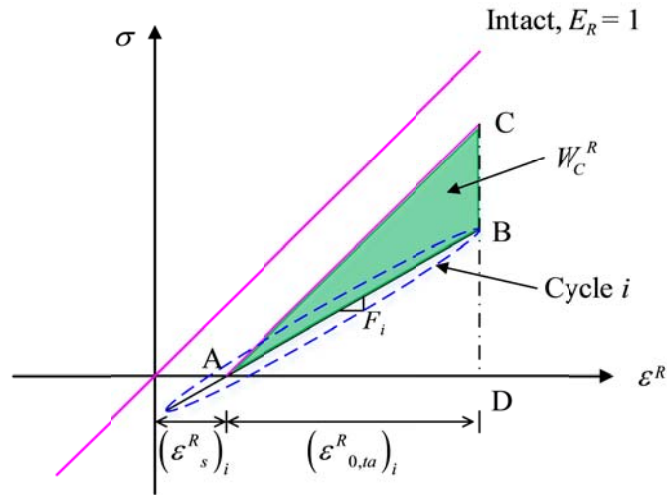


Figure 8-2. Schematic representation of the characteristic dissipated pseudo strain energy.

According to Figure 8-2, the CDPSE for cycle  $i$  is given by

$$(W_C^R)_i = \frac{1}{2} (\varepsilon_{0,ta}^R)_i^2 (1 - F_i) \quad (8.5)$$

When plotted with cycle number until the cycle at failure  $N_f$ , the CDPSE exhibits different profiles in terms of shape and magnitude depending on the test temperature and loading mode. However, it is discovered that the following quantity  $G^R$ , as defined in (8.6), is consistently related to the fatigue life  $N_f$ :

$$G^R \equiv \frac{\overline{W_C^R}}{N_f} = \frac{\int_0^{N_f} W_C^R(N) dN}{N_f^2} \quad (8.6)$$

where  $\overline{W_C^R}$  is the averaged characteristic dissipated pseudo strain energy (ACDPSE) in a fatigue test, and  $G^R$  is named as the “rate of change of the average released pseudo strain energy (per cycle)” throughout the entire history of the test (Sabouri and Kim, 2014). The relationship found between  $G^R$  and  $N_f$  from experimental data is well expressed via a power function, or presented as a straight line in the logarithmic scales:

$$G^R = \lambda \cdot N_f^\kappa \quad (8.7)$$

where  $\lambda$  and  $\kappa$  are fitting parameters.

Some inappropriateness, however, is sensed regarding the physical significance assigned to  $G^R$  in the original model presentation as described above. Basically, according to (8.6)  $G^R$  is simply equal to the accumulated CDPSE that is averaged twice over the entire fatigue life. It is difficult for the authors to relate the ratio of  $\overline{W_C^R}$  to  $N_f$  with the rate of change of ACDPSE. Instead, ACDPSE itself has a well-defined physical meaning and it may be reasonably related to the total amount of pseudo strain energy that should be dissipated in an intact material before reaching failure. Substituting (8.6) into (8.7) yields

$$\overline{W_C^R} = \lambda \cdot N_f^\gamma \quad \text{with} \quad \gamma = \kappa + 1 \quad (8.8)$$

In this study, the unified failure criterion expressed in (8.8) is employed.

## 8.5 Experimental Characterization

### 8.5.1 Dynamic Modulus Test

To identify the relaxation modulus function, in the laboratory the dynamic modulus test is often chosen preferably over the relaxation test given the concerns related to machine compliance, capacity, and the accuracy in observing instantaneous responses. In this study, for the dynamic modulus test the plant-mixed loose mixtures acquired from the project site were compacted using a Servopac Superpave gyratory compactor and then cored and cut to obtain cylindrical specimens for each mix with 100 mm in diameter and 150 mm in height. All tests were conducted in accordance with AASHTO TP 62-10 testing protocol (AASHTO, 2010) using the Asphalt Mixture Performance Tester (AMPT). By virtue of the time-temperature superposition principle, the resulting modulus data points at different temperatures were then horizontally shifted in the space of modulus versus frequency to construct a continuous and smooth master curve at a pre-specified reference temperature. The amount of shift for each temperature is termed as the shift factor. The dynamic modulus master curve is commonly expressed as a sigmoidal function:

$$\log |E^*| = \delta + \frac{\alpha}{1 + \exp[\beta + \gamma \log(f_r)]} \quad (8.9)$$

$$f_r = f / a_T \quad (8.10)$$

$$\log a_T = \alpha_1 T^2 + \alpha_2 T + \alpha_3 \quad (8.11)$$

where  $|E^*|$  is the dynamic modulus,  $f_r$  is the reduced frequency,  $f$  is the physical loading frequency,  $a_T$  is the shift factor at temperature  $T$ , and  $\delta, \alpha, \beta, \gamma, \alpha_1, \alpha_2, \alpha_3$  are parameters that can be identified in an optimization process in practice.

In the laboratory test, a minimum of three replicates were employed and the averaged dynamic modulus master curves are now presented in Figure 8-3, together with the phase angle master curves and the shift factor functions. A few observations can be made as follows. The LSPM mix shows the lowest stiffness at higher reduced frequencies (physically representing lower temperatures and/or higher loading frequencies) and a relatively high stiffness at lower reduced frequencies (physically representing higher temperatures and/or lower loading frequencies), which is presumably due to the high air void content and the interlocking aggregate structure formed by large particles, respectively. Conversely, the Superpave-25 mix demonstrates the highest stiffness at higher reduced frequencies and a relatively low stiffness at higher reduced frequencies. The F-1 and F-2 mixes are asphalt-rich mixtures primarily designed to mitigate the fatigue and reflective cracking. They have the same aggregate structure design but it can be seen that the master curve of F-2 consistently lies above that of F-1 due to the use of SBS modified binder with a higher PG grade.

With the dynamic modulus test results at hand, the coefficients in the relaxation modulus function, can be conveniently calculated by following the algorithms described in Park and Schapery (1999). Basically, the dynamic modulus is converted into the relaxation modulus by solving a system of linear algebraic equations for unknown Prony coefficients ( $E_i$ ), while the time constants ( $\tau_i$ ) are specified a priori, usually a decade apart. The time-temperature shift factor function, Equation (8.7), is applied to shift the obtained relaxation modulus function from the reference temperature to the actual test temperature of each fatigue test. Afterwards, the pseudo strain is calculated.

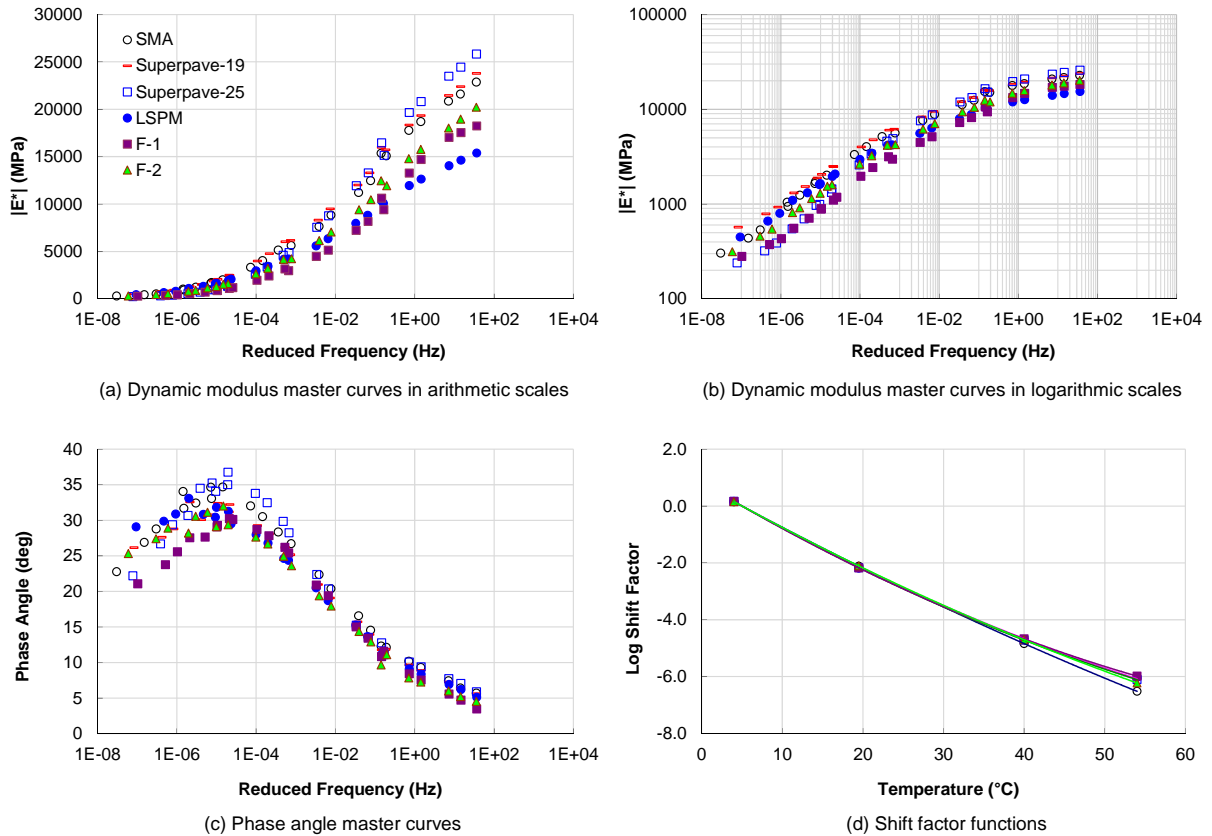


Figure 8-3. Dynamic modulus test results for the asphalt mixes in Binzhou sections.

### 8.5.2 Direct Tension Cyclic Fatigue Test

The fatigue resistance of asphalt mixtures is typically assessed by subjecting cylindrical specimens in direct tension cyclic tests in accordance with AASHTO TP 107-14 testing protocol (AASHTO, 2014). The experiment is usually conducted in the displacement controlled mode given the practical difficulties associated with other modes and the purpose of minimizing the accumulation of plastic deformation. Each test is continued until the specimen is pulled apart, and material failure and thus the fatigue life are determined as when the calculated phase angle begins to drop (Reese, 1997). Obviously, extension of the VECD theory to the material status with presence of macrocracks is invalidated.

In the early practices the specimen geometry of 75 mm in diameter and 150 mm in height was used with a strain-measuring gauge length of 100 mm in the middle along the axis of the specimen. However, it has been observed that chances are good that specimens fail in the proximity of ends beyond the gauge points. Such end failures may cause an inaccurate measure of deformation, and more importantly the true fatigue life is not able to be determined. Besides, the damage characteristic curves generated from tests with end failures are usually terminated at lower  $S$ -values as higher levels of damage occur at locations beyond the measurable range. Hence, for a complete material characterization the middle failure is required in which case the material macroscopic status from intactness through failure is fully captured. In order to raise the probability of middle failure, a comprehensive exploration is accomplished on the study of various geometric dimensions and gauge lengths by Lee et al. (2015) and it is recommended from finite element simulations and experimental investigations that the geometry with 100 mm in diameter and 130 mm in height be used along with a 70 mm gauge length. Nevertheless, it is worthwhile to point out that experimental evidences also show an excellent overlap between damage characteristic curves from both middle and end failures.

In this study, the above mentioned geometry is used for all fatigue tests. For each mix, a minimum of two or three replicates were tested, depending on the material availability. All tests ended with middle failures. In order to characterize the failure criterion, Equation (8.8), three levels of fatigue life were targeted:  $N_f < 5,000$ ,  $5,000 < N_f < 25,000$ , and  $N_f > 25,000$ , by properly choosing the displacement amplitude based on trial tests or experience on similar mixes. All fatigue tests were performed at 19°C and 10 Hz. The resulting damage characteristic curves were then fitted using Equation (8.4), and the relations are presented in Figure 8-4.

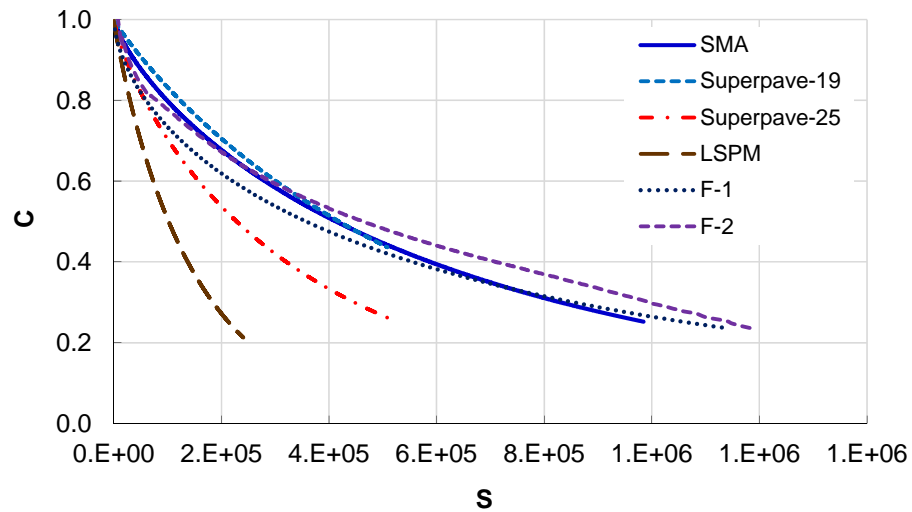


Figure 8-4. Damage characteristic curves for the asphalt mixes in Binzhou sections.

As previously stated,  $C$  is an indicator of material integrity while  $S$  quantifies the internal damage in the material. It is shown in Figure 8-4 that the material integrity of LSPM deteriorates quickly with damage, which is attributable to the high air void content and the open gradation. Conversely, for the F-2 mix, material maintains its integrity even when a significant amount of damage is experienced, and this can be explained by the high asphalt content and the use of SBS modified binder. In addition, a general observation can be made by comparing all six mixes that fatigue resistance can usually be enhanced by the use of smaller aggregate and modified asphalt binder. However, a better material property is not always a guarantee of a better performance in the pavement since the pavement structure and the material property in other layers should also be taken into consideration. Therefore, a fair and rigorous comparison should be achieved by carrying the damage characteristic relations obtained on the material level into a finite element structural analysis program, as will be presented in the next section.

For each fatigue test, the  $G^R$  was calculated via Equations (8.5) and (8.6), and is plotted with respect to its fatigue life as shown in Figure 8-5. Also illustrated in the figure are the best fits for each material using Equation (8.8). As can be observed from Figure 8-5, when a given amount of energy is to be consumed, LSPM would fail at early cycles, whereas the F-2 mix is able to dissipate the energy in a slower pace so that the material can stand a lot more cycles of loading before failure. The other four mixes demonstrate roughly the same fatigue resistance with F-1 and SMA being slightly superior to Superpave-19 and 25. Note that the line of Superpave-25 lies immediately above the line for Superpave-19 indicating a marginal advantage in fatigue resistance, which is contrary to what is observed in Figure 8-4. This inconsistency is presumably related to the variability in specimens, testing, and the process of finding the turning point in phase angle to determine  $N_f$ . After all, the ranking of fatigue resistance is expected to be the same using either the damage characteristic curves or the failure criterion lines. Nevertheless, the material fatigue performance should be finally assessed in the structural simulation.

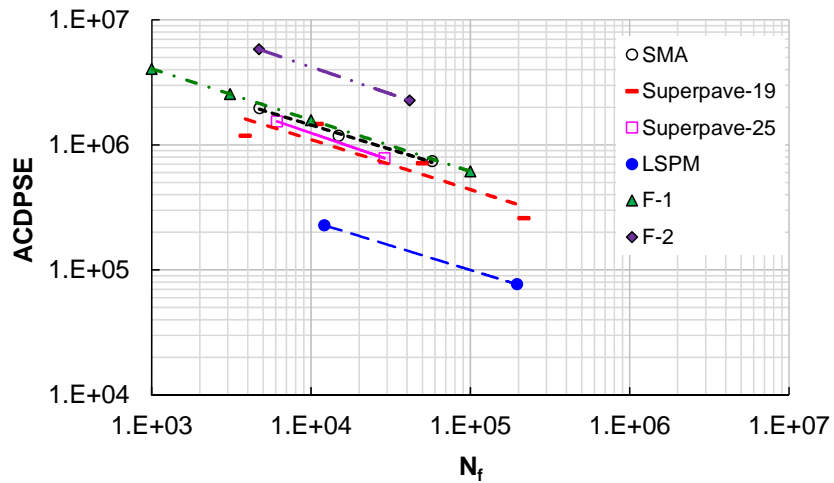


Figure 8-5. Relations between ACDPSE and fatigue life for each mix in Binzhou sections.

## **8.6 Fatigue Performance Predictions**

### **8.6.1 The Finite Element Package - LVECD**

The finite element structural analysis package has been developed and improved for pavement response and performance simulations along with the evolution of the VECD theory at NC State University (Underwood et al. 2012, Cao et al. 2012, Norouzi and Kim 2015). The latest version is called the Layered ViscoElastic pavement analysis for Critical Distresses (LVECD). In the following, the program input of material properties, traffic, and climate data are explained, and some critical assumptions and simplifications are briefly reviewed. For details in the algorithm, refer to Eslaminia et al. (2012).

All asphalt materials are treated in the framework of linear viscoelastic continuum damage theory. The Prony coefficients are required for material stiffness, and the parameters in Equation (8.4) and (8.8) are needed for predicting fatigue performance. The unbound materials are considered in the linear elastic domain. The elastic modulus is assumed as 1,500 MPa for the lime fly-ash treated aggregate, 500 MPa for the lime fly-ash treated soil, 85 MPa for the 30 cm lime stabilized subgrade, and 35 MPa for the natural subgrade. For all materials, Poisson's ratio is deemed as a constant irrelevant to temperature and loading conditions.

Traffic in LVECD is dealt with in a number of ways. Either a wheel (single/dual), an axle (single/tandem/tridem), or a vehicle can be defined with each tire having its own load and geometric characteristics. The traffic volume per day on the design lane is then given as the total number of passes of the wheel, axle, or vehicle, whichever is defined in the previous step. In the present simulation, a single axle with dual tires is employed as the unit for traffic. To accommodate the potential overloading, the axle load is set as 100 kN with tire pressure of 1.0 MPa. The number of passes of this traffic unit per day on the design lane is set at 10,000.

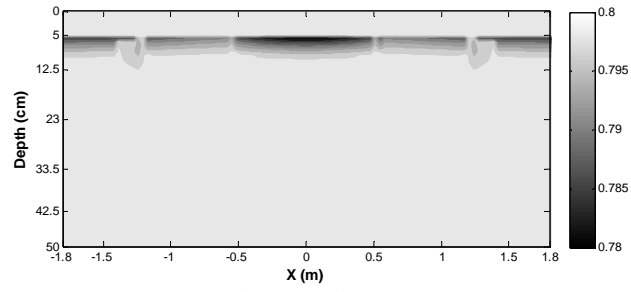
Temperature profile for the pavement structure is input on the hourly basis, and can be prepared using the climate information in the Enhanced Integrated Climate Model (EICM). For simplicity, only one year temperature data are required in LVECD; this history is then repeated for the remaining years of the whole design life. In this study, the climate information for the pavement site in Shandong Province is approximated by the averaged data over the state of Virginia in United States considering the geographic similarities.

In LVECD, adjacent layers are assumed as fully bound at the interface. The default setting for the meshing gives 11 and 101 nodes for the vertical and transverse directions, respectively, for each asphalt layer, which yields a total number of 1,111. The mesh size for the unbound elastic materials is relatively coarse. The responses of stress, strain, and displacement at each node under the moving loading of the traffic unit are conveniently solved via the Fourier transform techniques in both time and space domains.

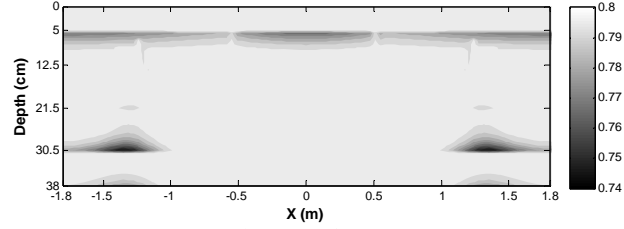
### **8.6.2 Simulation of Fatigue Performance and Discussions**

The fatigue performance of each section is predicted with a 15 year analysis period. As previously explained, the pseudo stiffness  $C$  is an indicator of material integrity, and thus the  $C$ -contour can be utilized to examine and compare the performances of all sections, as presented in Figure 8-6. Note that the Section Control shown in Figure 8-6 (e) is a virtual section which is designed as the same with Section 4 except for the use of the 15 cm Superpave-25 layer in place of the LSPM layer. The Section Control is added in the simulation only to make a parallel and thus fair comparison with Section 4 to assess the potential of LSPM in resisting fatigue cracking. Also note that in all contours, the maximum  $C$  value is set at 0.8 instead of 1.0 considering inherent defects in virgin materials and certain adverse effects due to compaction and aging during pavement construction.

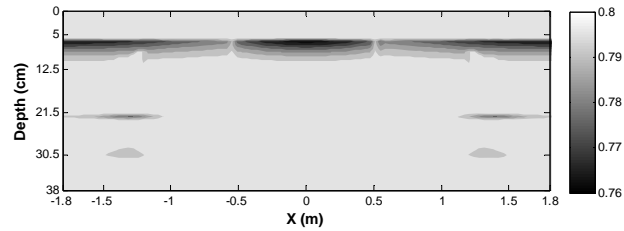
The fatigue performance can be compared by examining the lowest *C*-value shown beside the color bar in each section. The ranking among all Binzhou sections from superior to inferior is Section 1, 3, 2, Control, 4, and lastly Section 5. As expected, this sequence follows the general ranking of the thickness of asphalt pavement. Section 1 has the largest thickness and thus demonstrates the best fatigue performance at the end of the 15 year simulation. The material damage is seen to concentrate in the layer of Superpave-19 as shown in Figure 8-6 (a). Owing to the use of SBS modified binder in the bottom asphalt layer, Section 3 exhibits a slightly better performance than Section 2. Another noticeable difference between the two is that the use of better materials also helps to shift the location of fatigue damage to upper layers. In Section 2, fatigue damage is concentrated at the bottom of the fourth layer, whereas in Section 3 the location of major damage has shifted to the second layer. This finding is illuminating in the perpetual pavement design which is aimed to avoid structural failure at lower pavement layers.



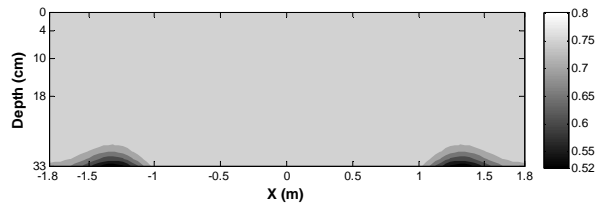
(a) C-contour for Section 1



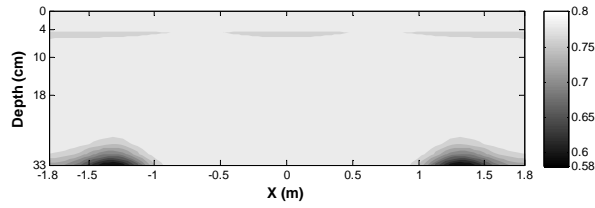
(b) C-contour for Section 2



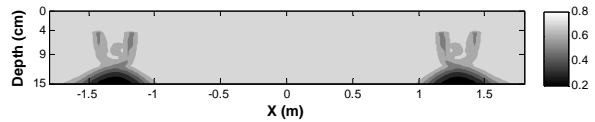
(c) C-contour for Section 3



(d) C-contour for Section 4



(e) C-contour for Section Control



(f) C-contour for Section 5

Figure 8-6. C-contour of the Binzhou sections after 15 year simulations.

For Section 4 and Control, fatigue cracking would initiate at the bottom of asphalt pavement according to Figure 8-6 (d) and (e). In comparing the lowest  $C$ -value in these two sections, it appears that the utilization of LSPM at the bottom of asphalt layer would make a poor design compared to Superpave-25 in the sense of fatigue cracking. Recall in Figure 8-5 and 6 that on the material level LSPM shows the least desired fatigue resistance due to its special aggregate gradation. Therefore, the above observation in the parallel structural comparison should be expected. However, Section 4 may actually perform better than Section Control because the placement of LSPM immediately above the semi-rigid base may potentially reduce the distresses caused by reflective cracking. Therefore, the previous conclusion between the two sections is deemed valid only as far as bottom-up fatigue cracking is concerned. In the current LVECD framework the mechanisms underlying reflective cracking which initiates in unbound materials are not incorporated and thus a fair comparison would require more advanced and comprehensive tools.

Section 5 is the conventional design of semi-rigid asphalt pavement that presents the worst fatigue performance at the end of 15 year. As shown in Figure 8-6 (f), damage is concentrated at the bottom of this thin asphalt pavement. The minimum  $C$ -value suggests that Section 5 may not be able to maintain structural integrity up to 15 years due to fatigue cracking, even if reflective cracking is not considered.

An alternative approach to fatigue performance inspection is to investigate the percentage of material points with failure in the pavement cross section. The failure percentage is simply calculated as the ratio of the number of material nodes with failure to the total number of nodes in the cross section. The evolution of failure percentage with respect to the number of axle passes is plotted in Figure 8-7 for each section.

The ranking of fatigue performance according to Figure 8-7 from superior to inferior is Section 1, Control, 3, 2, 4 and Section 5, which is the same with the  $C$ -based ranking except for the position of Section Control. This inconsistency is attributed to the fact that a pavement having a lower minimum  $C$ -value may possibly show a smaller area of material failure. In fact, a lower  $C$ -value may not necessarily represent a worse fatigue performance. Recall that the process of material deterioration follows the damage characteristic curve, and

the *C*-contours shown in Figure 8-6 are generated based on this principle without considering when failure would occur. Hence, the predicted *C*-values for the material nodes in the cross section can be asymptotically decreasing to zero under repeated fatigue loading. Yet, beyond failure the VECD theory is no longer applicable, which means that any further calculation of the pseudo stiffness is actually invalid for any material point that has already failed. Given these considerations, it is deemed that the comparison from the perspective of failure percentage is more reasonable in ranking different structural designs.

Again, it should be emphasized that all the above simulations and conclusions are conducted without involving the role of reflective cracking and other complexities such as aging, healing and shearing. Judging purely from the fatigue performance, it is recommended that Section 1 and 3 be the ideal candidates for perpetual pavement design. All other sections are ruled out because of either severe damage or initiation of damage at lower structural layers.

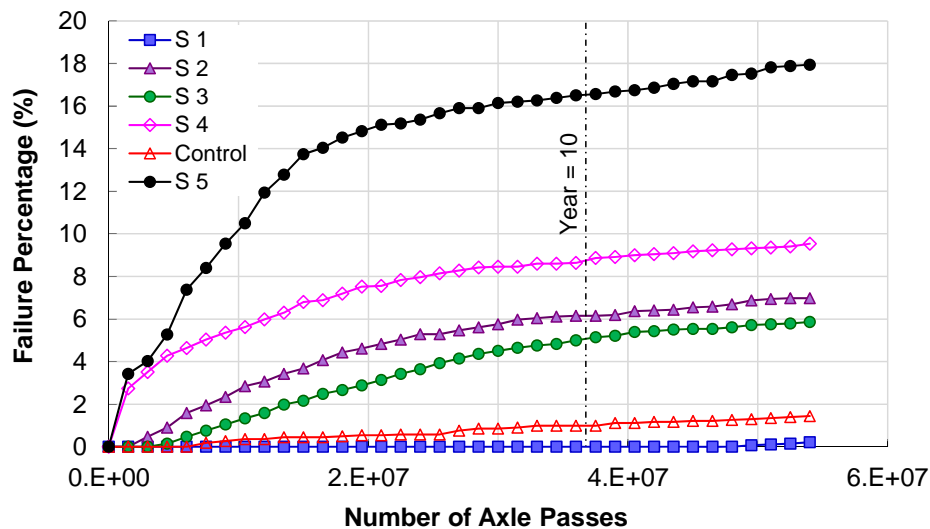


Figure 8-7. The evolution of failure percentages for Binzhou sections after 15 year simulations.

## **8.7 Conclusions**

This section presents a systematic VECD framework of evaluating fatigue performance for asphalt pavement. Asphalt mixture is treated as a linear viscoelastic material, while the constitutive modeling of fatigue damage under repeated loading is fulfilled by identifying the damage characteristic curve for each mix. The VECD framework is then completed with the unified failure criterion which defines the applicable domain of the theories. The model parameters are determined through dynamic modulus tests and direct tension cyclic fatigue tests. All the material models are integrated in the finite element package LVECD, which is used for fatigue performance predictions on Binzhou perpetual pavement sections. The 15 year fatigue simulations suggest that Section 1 and 3 should be used as the perpetual pavement design.

# **CHAPTER 9 CALIBRATION OF FATIGUE CRACKING MODEL FOR LVECD PROGRAM**

## **9.1 Introduction**

Fatigue cracking that is due to repeated wheel loads is one of the major distress types that can occur in flexible pavement systems. The action of repeated traffic loading induces both tensile and shear stresses in all the asphalt layers and leads to a reduction in the structural integrity of the pavement. Fatigue cracks initiate at the points where critical tensile strains and stresses occur. Depending on the dominant mechanism, the development and propagation of fatigue cracks inside a pavement structure can be categorized into two major phases: pre-localization and post-localization. In general, pre-localization is manifested by the initiation and propagation of microcracks, and post-localization is manifested by the formation and propagation of macrocracks.

The location of the critical strain/stress is dependent upon several factors. The most important one is the stiffness of the asphalt layer. In addition, it should be recognized that the maximum tensile strain that develops within the pavement system might not be the most critical or damaging factor, because the critical strain is a function of the stiffness of the mix and the material's integrity. Because the properties of asphalt mixes in a layered pavement system change throughout the depth of the pavement, these variations will eventually affect the location of the critical strain that causes fatigue damage.

It is commonly assumed that fatigue cracking typically initiates at the bottom of the asphalt layer and propagates to the surface. This so-called 'bottom-up' cracking is due to the bending action of the pavement layer that results in flexural stress developing at the bottom of the bound layer. However, various studies have also clearly demonstrated that fatigue cracking may also initiate from the top and propagate downward (top-down cracking).

The aforementioned common understanding of fatigue failure due to bottom-up cracking has been challenged in recent years as more and more agencies have begun to report another form of failure, top-down fatigue cracking (Myers et al. 1998, Pellinen 2002, Myers and Roque 2001, Uhlmeier 2000). At the time of this study, universal agreement has not yet been reached as to the exact causes of this type of distress (Al-Qadi and Yoo 2007). Nevertheless, it can still be stated with certainty that the overall driving conditions for top-down fatigue appear to differ from those that cause the more common bottom-up fatigue cracking. Thus, the material characteristics that are tied most closely to pavement performance in terms of bottom-up and top-down fatigue cracking also may differ. For example, pavements constructed with materials that exhibit a strong propensity for aging may be significantly more sensitive to the top-down cracking phenomenon than pavements constructed with materials that have a relatively weak propensity to age. However, because aging is a top-down process, the bottom-up cracking phenomenon may be affected only slightly.

Layered Viscoelastic pavement analysis for Critical Distresses (LVECD) computer program that has been developed in North Carolina State University is capable of predicting the fatigue cracking in both bottom-up and top-down modes using the Simplified Viscoelastic Continuum Damage (S-VECD) model. However, this software has not been fully calibrated with the field observations yet and the LVECD damage-to-field cracking transfer function needs to be developed to truly predict the amount of cracking in the field. Therefore, this chapter focuses on the calibration of the fatigue cracking model that is used in the LVECD software. This section consists of an overview of traditional and energy-based fatigue failure criteria, the field data collection procedure, the LVECD program simulation process, and the transfer function development that is based on the field data and simulation results.

## 9.2 Fatigue Cracking Prediction Models

### 9.2.1 Traditional Tensile Strain-Based Fatigue Cracking Model

The MEPDG utilizes the incremental damage concept in predicting alligator cracking. The incremental damage concept simulates ways that pavement distresses in the field develop incrementally over time. The Asphalt Institute's (AI's) fatigue cracking model is employed in the MEPDG to predict alligator cracking, as shown in Equation (9.1). In addition to the AI model, the MEPDG employs Miner's law, as presented in Equation (9.2), to convert the predicted number of cycles to failure ( $N_f$ ) to the equivalent damage for different combinations of traffic loading and environmental conditions.

$$N_f = 0.00432C\beta_{f1}k_{f1}\left(\frac{1}{\varepsilon_t}\right)^{\beta_{f2}k_{f2}}\left(\frac{1}{|E^*|}\right)^{\beta_{f3}k_{f3}} \quad (9.1)$$

where

$$C = 10^M,$$

$$M = 4.84\left(\frac{V_b}{V_a + V_b} - 0.69\right),$$

$\beta_{f1}, \beta_{f2}, \beta_{f3}$  = local calibration factors, and

$k_{f1}, k_{f2}, k_{f3}$  = model calibration factors.

$$Damage = \sum_{i=1}^T \frac{n_i}{N_{fi}} \quad (9.2)$$

For a particular pavement structure with a HMA bottom layer, the pavement response prediction models within the MEPDG employ linear elastic theory to predict the critical tensile strain ( $\varepsilon_t$ ) at the bottom of the asphalt layer for a given combination of traffic loading and environmental conditions. Knowing the dynamic modulus ( $|E^*|$ ) value for the bottom HMA layer, the critical tensile strain value, and some mixture volumetric information, the  $N_f$  model shown in Equation (9.1) calculates the number of cycles that is required to fail the pavement under specific combinations of traffic loading and environmental conditions.

To calculate the amount of damage that the pavement has experienced, Miner's law, shown in Equation (9.2), is used to sum up all similar combinations of traffic loading and environmental conditions and divide the summation by the  $N_f$  to calculate the percentage of damage.

### 9.2.2 Energy-Based Fatigue Cracking Model

One of the primary material functions that can be determined from the S-VECD model is the energy-based failure criterion. During cyclic fatigue testing, the maximum stored pseudo strain energy can be determined at the stress peak points in each cycle. The amount of energy at each cycle can be calculated using Equation (2.21).

The maximum stored pseudo strain energy at each cycle represents the material's ability to store energy at that particular time. The material loses its stored energy as the damage grows for the same magnitude of applied pseudo strain due to the reduction in pseudo stiffness. The difference between the maximum stored pseudo strain energy and the corresponding undamaged state is referred to as the *total released pseudo strain energy* and is denoted as  $W^R_C$ . Therefore, a term,  $G^R$ , is defined as the rate of change of the averaged released pseudo strain energy (per cycle) throughout the entire history of the test and can be defined as Equation (2.24). Details regarding the  $G^R$  method and its corresponding calculations can be found in Section 2.4.

### 9.3 Calibration of Energy-Based Fatigue Criterion

In order to provide credibility to the new LVECD-based performance prediction methodology, the theoretically predicted distress models must be calibrated to be applicable to real asphalt pavements. The following steps were taken in this study to calibrate the fatigue cracking model in the LVECD program.

- Field performance data, including the percentage of the fatigue cracking/length of longitudinal cracks, were collected from the site projects and converted to the percentage of cracking (% cracking) using the LTPP procedure.

- Materials were acquired based on the accuracy of the field data and binder/aggregate availability. More than 33 pavement sections with different characteristics (e.g., modified binder, RAP content, structure, warm mix additive) from different locations in the United States, Canada, South Korea, and China were selected for study.
- Samples were fabricated based on the field air void content of the asphalt layer. Mechanical testing (dynamic modulus testing, S-VECD cyclic testing, and TSS testing) characterization was performed to obtain the required parameters for LVECD program analysis.
- Simulations were run using the experimental data, environmental conditions, pavement structures, and traffic level. The climatic data were collected directly from the EICM database.
- As a first step for verification, the predicted damage results obtained from each simulation were compared to the measured cracking that was observed in the field.
- The predicted damage was correlated to the measured cracking in the field using the sigmoidal function (as presented by many researchers as the best indicator of fatigue cracking growth in real pavements).

The calibration data were collected at the same time for all types of fatigue cracking, as the same sections were used for both bottom-up and top-down cracking calibration. In the following sections, each step of the calibration process is discussed in detail.

#### **9.4 Field Cracking Data Collection**

The first step in the calibration process was to identify potential test sites. As part of the FHWA's HMA-PRS project, 33 pavement sections that are known to have experienced sufficient cracking for the study were selected. These test sections cover a diverse range of site features, including climate, traffic level, subgrade soil, and pavement structural cross-section characteristics. All the data required for executing the models, including measurements of fatigue distress, were extracted directly from the site, reviewed for accuracy and completeness, and incorporated into the project database.

These data elements include performance observations, material properties, traffic and climatic characteristics, pavement cross-sections, and foundation information. The crack measurement procedure is discussed in the following paragraphs.

#### **9.4.1 Long Term Pavement Performance (LTPP)**

For this study, fatigue cracking within a single site was divided into different categories (i.e., low, medium, and high levels) in accordance with the procedure proposed by the LTPP project. The recorded amounts of alligator and longitudinal cracking in the wheel paths as obtained from the field surveys were converted to percentages based on the total area of the site. In order to obtain the *% cracking* value, the crack length was converted to a unit area by applying a standard width of wheel path (0.3 m or 1 ft) to the crack length, as suggested by Jackson and Puccinelli (2006). The crack lengths were summed arithmetically, regardless of the severity of the distresses, for the LVECD program fatigue cracking calibration.

#### **9.4.2 National Center for Asphalt Technology (NCAT)**

The amount of cracking measured by the NCAT is reported in three separate categories for each pavement section: right wheel path (RWP), left wheel path (LWP), and percentage of the cracked area in a lane. According to the procedure adopted by the NCAT, each crack exhibits influence for six inches. When multiple cracks are present, the connected cracks have zones of influence that overlap, and simple cracking then becomes referred to as *cracking areas*. For this study, simple and complex cracking patterns were converted to cracking areas either by calculating the length of simple cracks and multiplying by 1 foot or by directly calculating the area of influence of complex cracking, respectively.

The wheel paths at the NCAT test track are 3 feet wide and lie 1.5 feet from the edge/centerline of the lane. Therefore, *percent wheel path cracking* is defined as the distressed area over the total wheel path area. *Percent lane* also is specified as the total cracked area by the total lane area in the section (150-ft length by 12-ft width) as presented in Figure 9-1.

### 9.4.3 Manitoba Infrastructure and Transportation (MIT)

The crack length is reported in three different categories (low, medium, and high) for the MIT pavement sections (500-ft length and 12-ft width). For this study, the LTPP program procedure was employed to convert the crack length to the percent cracked area without considering any weight for different crack types.

### 9.4.4 Federal Highway Administration Accelerated Loading Facility (FHWA-ALF)

All of the fatigue cracking distresses were measured and reported in terms of percent cracked area for the FHWA-ALF pavement sections in accordance with the LTPP specifications.

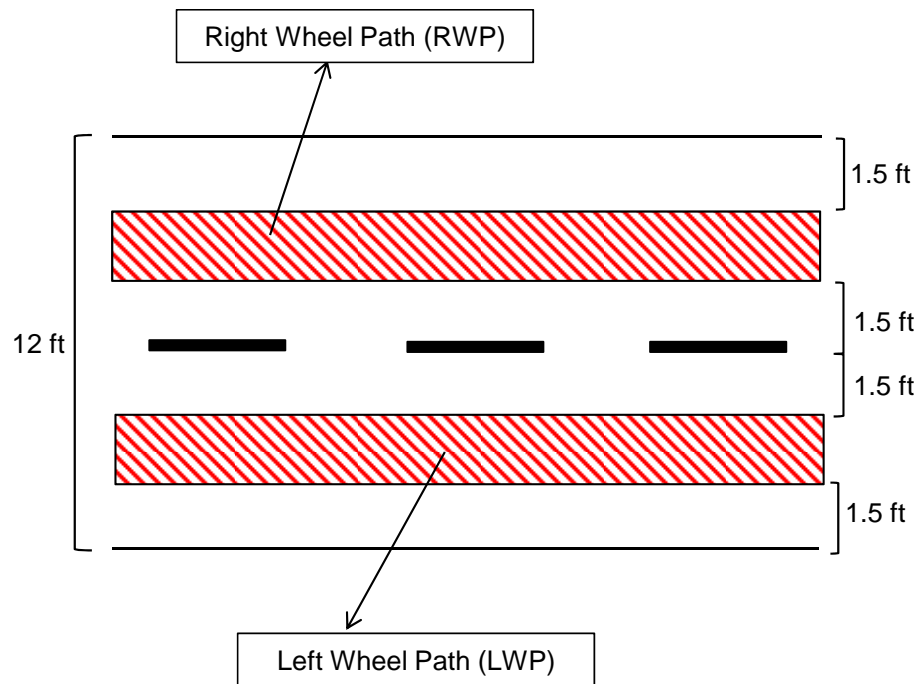


Figure 9-1. NCAT test track section area.

#### **9.4.5 Korea Expressway Corporation (KEC)**

Similar to the FHWA-ALF project, the KEC defines fatigue cracking in terms of percent cracked area according to the procedure proposed by the LTPP program.

### **9.5 LVECD Program Simulation Process**

#### **9.5.1 Stress-Strain Calculation Method in LVECD Program**

Reasonable stress-strain analysis is a key component in pavement design and for pavement life predictions. Given the complexity of variables such as pavement life, traffic loading, and temperature variations, various approximate methods can be used to predict pavement performance. Despite differences in their assumptions, all of these prediction methods aim to reduce analysis that can take millions of cycles over several years to a few hundred analyses for a single cycle of loading.

The most basic method that is used in the Pavement ME program is layered elastic analysis (LEA), where the pavement is idealized as a layered elastic system under a stationary axisymmetric load. In this method, the normal and radial stresses/strains often are computed using a Fourier-Bessel transform (Huang 2003). However, LEA can lead to inaccurate responses because (1) traffic loading (i.e., tire pressure) is neither stationary nor circular in reality, and (2) asphalt concrete exhibits significant viscoelastic behavior, especially under moving loads.

Layered viscoelastic moving-load analysis (LVEMA) is an improvement over LEA in that the viscoelasticity and the moving load effects are handled efficiently with the help of Fourier transforms. LVEMA is thus more appealing than LEA for pavement stress analysis, although the stress redistribution effects due to damage still are not captured. Taking LVEMA into consideration, the NCSU research team has developed a three-dimensional layered viscoelastic FEM tool with moving loads to calculate the responses and performance of asphalt pavements. The advantages of this analysis tool, i.e., the LVECD program, can be summarized as follows:

- Asphalt concrete shows a significant amount of viscoelasticity, and thus, the behavior of asphalt concrete depends on both loading frequency and temperature. Pavements undergo wheel loading at a vast range of frequencies as well as different temperature distributions throughout the depth of the pavement over the lifetime of the pavement, such that the whole structural behavior of the pavement changes significantly over time. The LVECD program is able to account for this loading frequency and temperature dependency of asphalt concrete at different depths of the pavement.
- Each pavement layer in the analysis tool can be assigned its own material and structural properties. For example, for granular material, the LVECD program can assume anisotropic elasticity with the axis of symmetry in the depth direction.
- The LVECD program takes advantage of the assumptions of Fourier transform and time-scale separation to reduce computational costs. This three-dimensional moving load layer analysis considers damage (rutting and fatigue) and can still complete a simulation within a relatively short time compared to other viscoelastic analysis programs.

### 9.5.2 Damage Calculation in the LVECD Program

The LVECD program can evaluate fatigue cracking using the VECD model (Kim et al. 2009) where asphalt concrete is modeled as a viscoelastic material with microcrack-induced damage. The 3D-Move program also is capable of fatigue performance analysis, but its framework is based on the conventional tensile strain-based model.

The VECD model (Kim et al. 2009) can be used to represent the effect of damage on the material's stiffness, where  $S$  is the damage parameter and  $\varepsilon^R$  is the pseudo strain. Then, the damage characteristic curve can be obtained through laboratory cyclic testing. The damage evolution law is given by

$$\frac{ds}{dt} = \left( -\frac{\partial W^R}{\partial S} \right)^\alpha = \left( -\frac{1}{2} \frac{\partial c}{\partial S} E_R (\varepsilon^R)^2 \right)^\alpha \quad (9.3)$$

where  $\alpha$  is a material model parameter.

Equation (9.3) can be extended to the multiaxial case using the definition for a pseudo strain energy density function.

$$W^R = \frac{1}{2} \left[ A_{11} e_v^2 + A_{22} e_d^2 + 2A_{12} e_d e_v + A_{44} (\gamma_{13}^R + \gamma_{23}^R) + A_{44} (\gamma_{13}^R + e_s) \right] \quad (9.4)$$

where

$$e_v = \varepsilon_{11}^R + \varepsilon_{22}^R + \varepsilon_{33}^R,$$

$$e_d = \varepsilon_{33}^R - \frac{e_v}{3}, \text{ and}$$

$$e_s = \varepsilon_{11}^R - \varepsilon_{22}^R.$$

For the multiaxial state of stress, the damage evolution law can be written as

$$\frac{\partial s}{\partial t} = \frac{1}{2^\alpha} \frac{\partial c}{\partial s} \left( -\frac{\partial c}{\partial s} \right)^\alpha \left( \frac{1}{3} e_v^R + e_d^R \right)^{2\alpha} \quad (9.5)$$

Using the chain rule and integrating with respect to time, the change in the normalized stiffness value in a single cycle can be obtained easily, which becomes Equation (9.6).

$$\Delta c = \frac{1}{2^\alpha} \frac{\partial c}{\partial s} \left( -\frac{\partial c}{\partial s} \right)^\alpha \int_0^{T_{cycle}} \left( \frac{1}{3} e_v^R + e_d^R \right)^{2\alpha} dt \quad (9.6)$$

where  $T_{cycle}$  is the time period of the cyclic moving load. The LVECD program calculates the damage increment for each segment assuming constant pseudo stiffness at the beginning of each life stage. Then, nonlinear extrapolation is conducted by solving the following ordinary differential equation to calculate the damage during each stage.

$$\Delta c = \sum_{i=1}^{N_{segments}} \left( \frac{dc}{ds} \right) \left( \frac{ds}{dt} \right), \quad (9.7)$$

$$\frac{\partial c}{\partial n} = \Delta c \left( \frac{c}{c_0} \right)^{1+\alpha} \left( \frac{\log(c)}{\log(c_0)} \right)^{(1+\alpha) \left( 1 - \frac{1}{b} \right)},$$

where  $C_0$  is the pseudo stiffness at the start of each life stage,  $n$  is a cycle in each analysis segment, and  $N$  is the total number of cycles at the end of each analysis segment.

The LVECD program can calculate damage  $C$  for a large  $N$  and then calculates the  $W_R^c$ .

$$W_R^c = \frac{1}{2}(1-c)W^R \quad (9.8)$$

At the end of each stage, the total damage increment that is due to traffic and thermal loading is calculated. The LVECD program uses weighted averages of the damage increments of all the segments in each stage using Equation (9.9)

$$\Delta C_{comb} = \frac{\sum_i^{Segments} N_i \Delta C_i(C_0)}{\sum_i^{Segments} N_i} \quad (9.9)$$

Using the nonlinear extrapolation formula, the final damage value for each point can be calculated using Equation (9.10). Note that there is no need to extrapolate  $C$ ; the  $C$  value needs to be found only at the end of the last cycle of loading. The LVECD program finds the final  $C$  value for the mesh points. Because all the output data should be shown for the evaluation points, the LVECD program uses interpolation to find the damage values.

$$\frac{\partial c}{\partial n} = \Delta C_{comb} \left( \frac{c}{c_0} \right)^{1+\alpha} \left( \frac{\log(c)}{\log(c_0)} \right)^{(1+\alpha)(1-\frac{1}{b})} \quad (9.10)$$

Damage increases as the number of cycles increases according to the damage characteristic curve. As the damage increases, an asphalt element will fail when the element reaches the ultimate state, which is defined by the  $G^R$  versus  $N_f$  relationship. The LVECD program finds the number of cycles to failure ( $N_f$ ) in each element for a segment of applied traffic and thermal loading condition by calculating the  $G^R$  value for the given loading conditions in the segment and by finding the corresponding  $N_f$  value to the  $G^R$  value using the  $G^R$  versus  $N_f$  relationship. Then damage index value is calculated as the ratio between the actual experienced numbers of cycles in that loading segment to the  $N_f$  value calculated for that loading segment.

The damage index values are cumulative and are added up at the end of each life stage according to Miner's law. The damage index is calculated for each nodal point and varies between 0 (no damage) and 1 (failure).

## 9.6 Analysis of Measured Fatigue Cracking in LTPP Database

To find the true parameters that are involved in the transfer function, the field data must be checked for general reasonableness, and any trends observed from these data should be examined. The Pavement ME design guide provides information about the measured data obtained from the LTPP database.

As a first step, the thickness values of all the asphalt concrete layers for each section were extracted from the database and then added together to obtain the total thickness of the asphalt concrete layers for each section. Figure 9-2 shows the plots of the total fatigue cracking percentages from the 640 LTPP sections that were evaluated as a function of asphalt thickness. This figure clearly indicates that maximum cracking generally occurs at an asphalt layer thickness between four inches and six inches. It also shows that the amount of cracking dramatically decreases when the asphalt layer thickness is more than six inches.

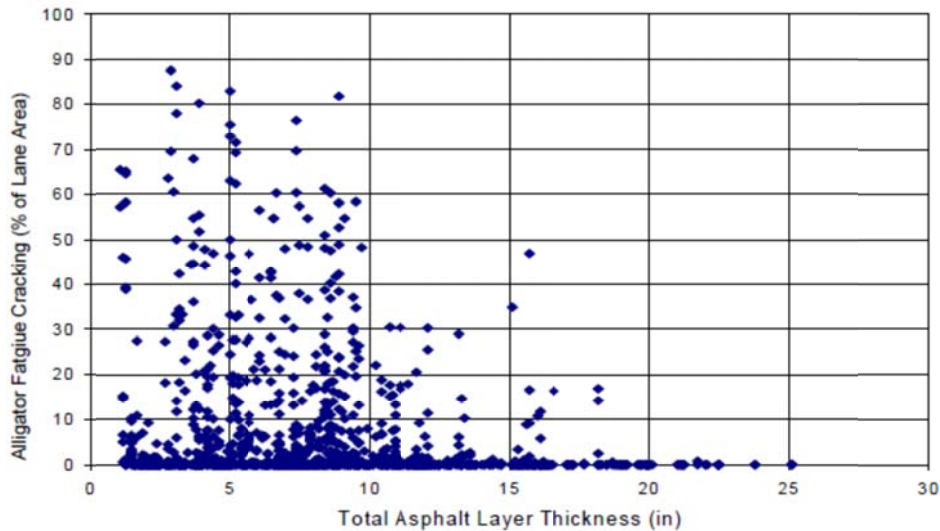
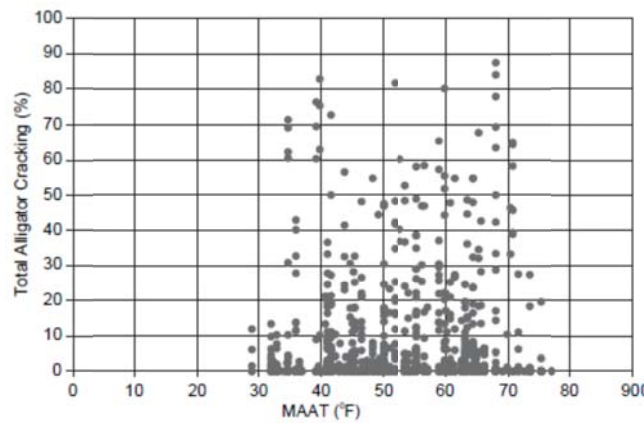
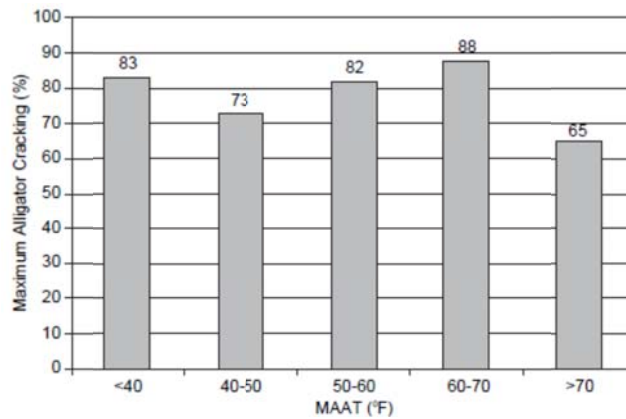


Figure 9-2. LTPP alligator cracking vs. asphalt layer thickness.

Another major factor that can affect fatigue cracking is the mean annual air temperature (MAAT). As shown in Figure 9-3 (a) and (b), the MAATs for the LTPP sections evaluated ranged from approximately 29°F to approximately 77°F. An initial expectation of the alligator cracking results was that more cracking would occur in cold regions and less cracking would occur in hot regions. However, the plots indicate that the occurrence and amount of alligator cracking are very close for all regions and independent of the MAAT (site environment). Thus, the MAAT appears to have little to no significant effect on the measured alligator cracking reported in the LTPP database.



(a)



(b)

Figure 9-3. (a) Alligator cracking vs. MAAT ranges and (b) maximum alligator cracking.

## 9.7 Fatigue Cracking Transfer Function

The next step of the calibration process is to derive an appropriate transfer function that relates the predicted damage to the measured fatigue cracking. The performance index used in the LVECD program is the so-called *damage area* (%), which is the number of nodes where the asphalt mixture fails under the wheels ( $N/N_f = 1$ , as discussed in Section 10.5.2) over the total number of nodes throughout all the asphalt layers expressed in percentage. Each layer has 101 nodes in length and 11 nodes in depth, for a total of 1,111 nodes for each layer.

To specify the appropriate procedure to define damage in LVECD program and to introduce indices for the top-down and bottom-up cracking in the pavement sections, two methods were adopted to check the fatigue cracking behavior in the LVECD simulations: (1) the failure points in the area of 40 cm of right and left side of each wheel with the pavement depth was counted and divided by the total points for the top and bottom halves of the layer thickness as demonstrated in Figure 9-4, and (2) the averaged  $N/N_f$  values through the asphalt layer was calculated and presented as percentage for both top and bottom halves of the asphalt layer. Figure 9-5 to Figure 9-12 present the comparison of fatigue behavior trends obtained from the aforementioned procedures for both halves of the pavement layer with the field performance data.

According to the results obtained from the analysis, considering only top or bottom of the asphalt layer cannot lead to the true performance prediction and it is necessary to consider the whole asphalt layer to define the damage in LVECD. However, these two methods can be identified as two different indices to predict the top-down or bottom-up cracking within the asphalt layer.

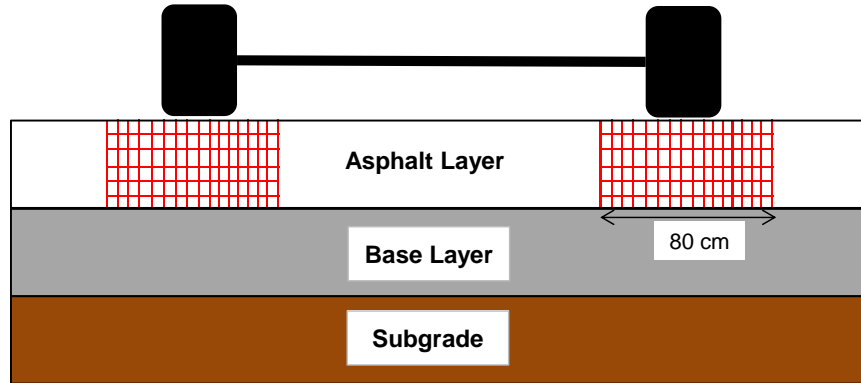


Figure 9-4. Schematic definition of damage area in LVECD.

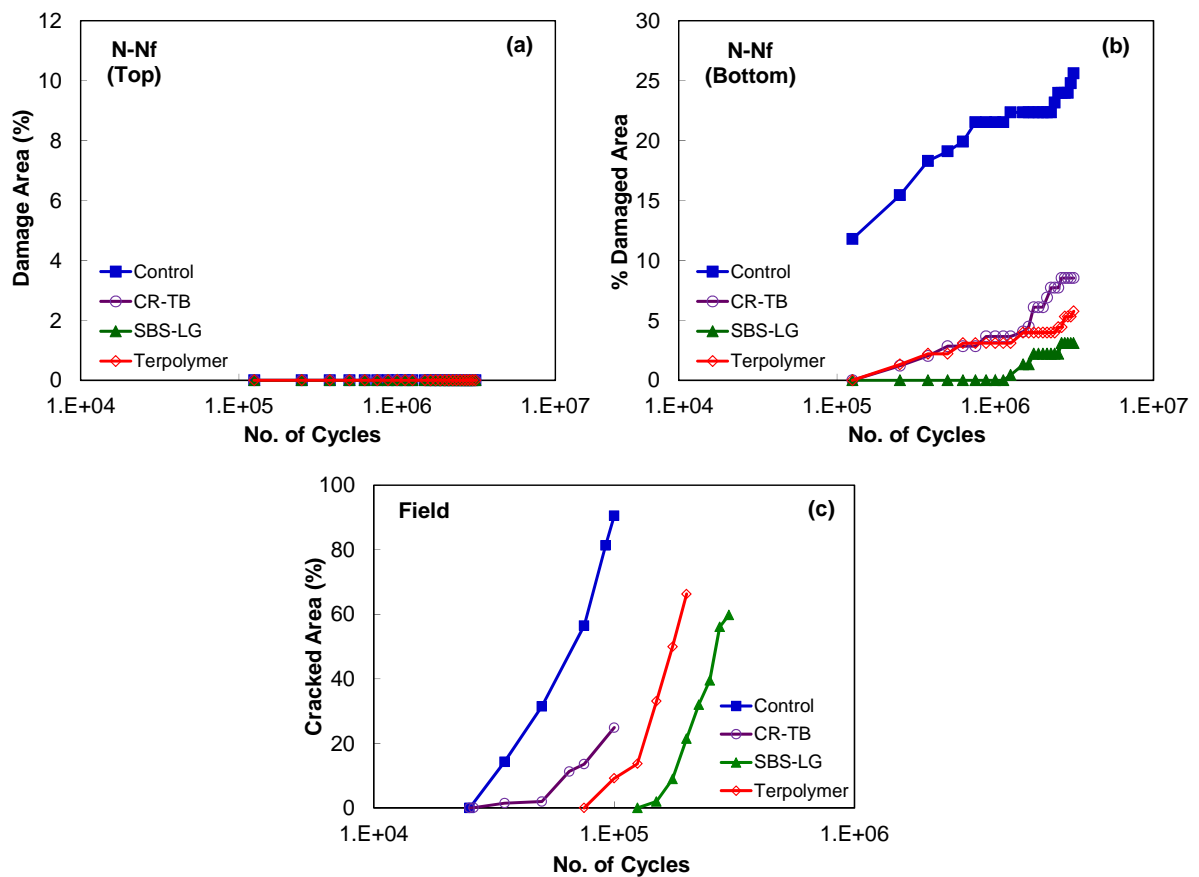


Figure 9-5. Damage definition obtained from method 1 for FHWA-ALF: (a) top half of asphalt layer, (b) bottom half of asphalt layer, and (c) field measurements.

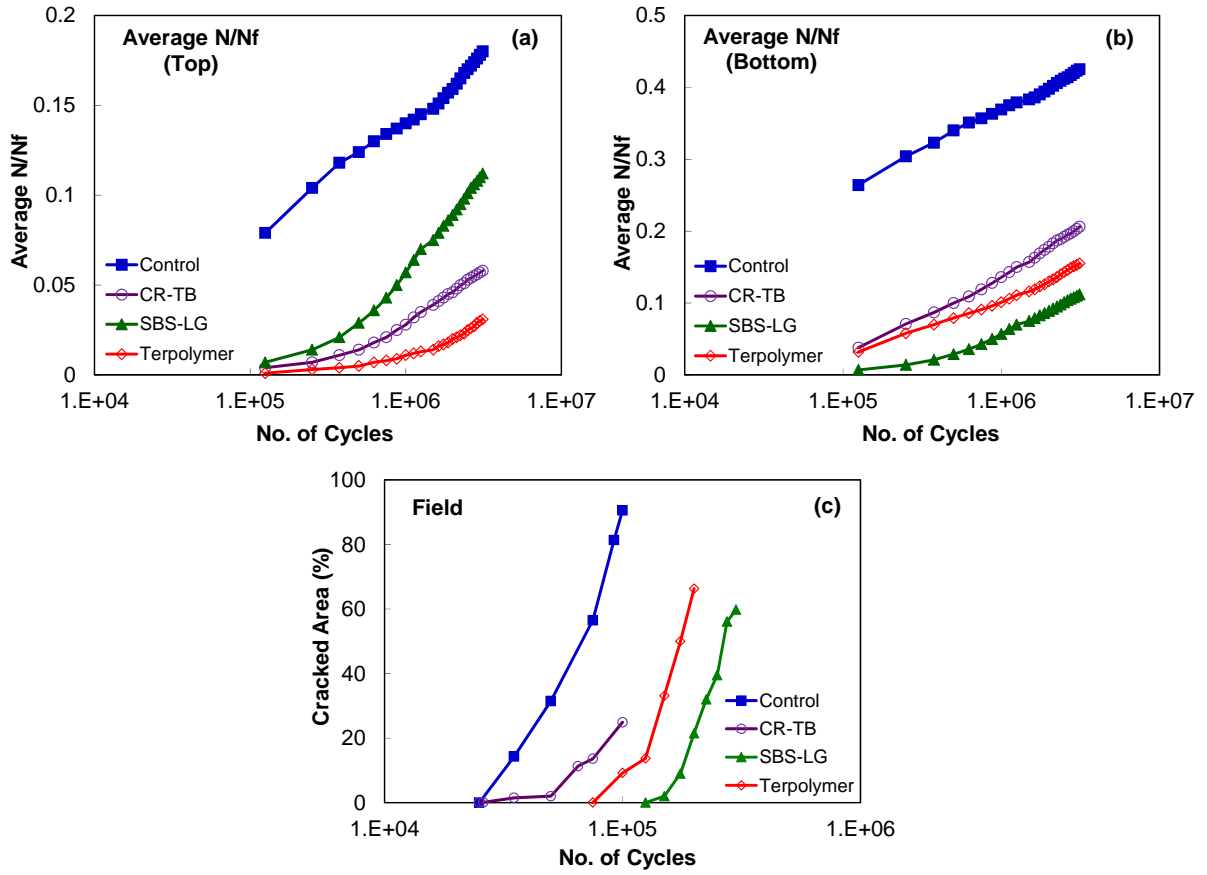


Figure 9-6. Damage definition obtained from method 2 for FHWA-ALF: (a) top half of asphalt layer, (b) bottom half of asphalt layer, and (c) field measurements.

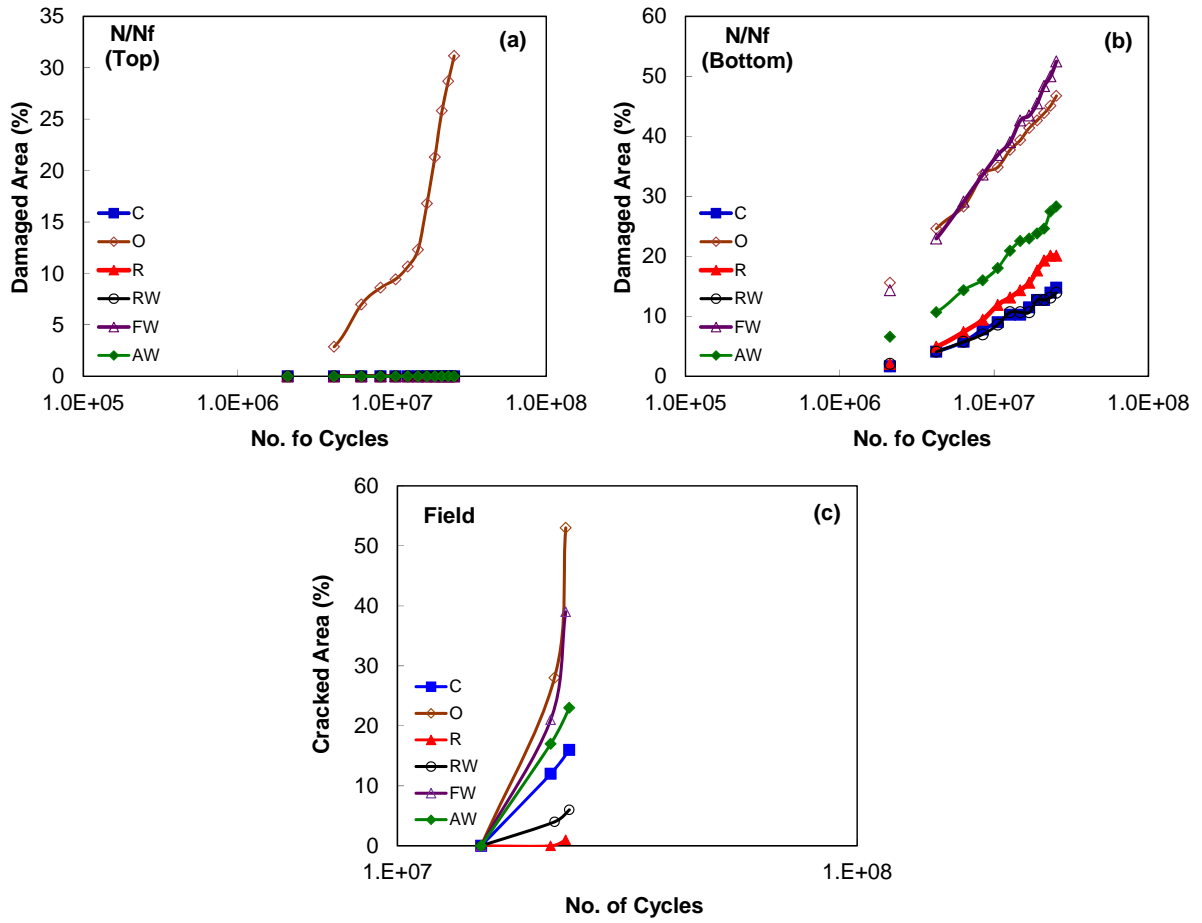


Figure 9-7. Damage definition obtained from method 1 for NCAT: (a) top half of asphalt layer, (b) bottom half of asphalt layer, and (c) field measurements.

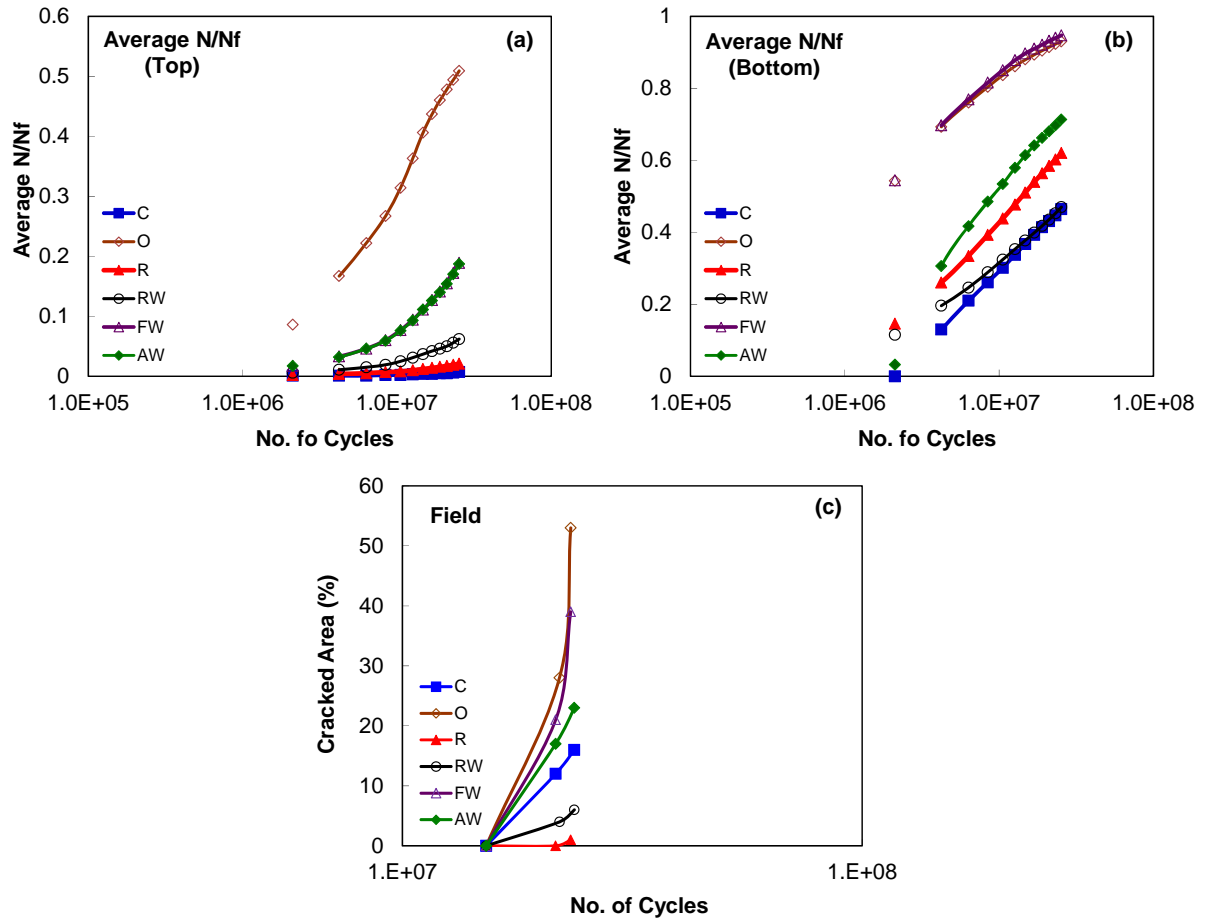


Figure 9-8. Damage definition obtained from method 2 for NCAT: (a) top half of asphalt layer, (b) bottom half of asphalt layer, and (c) field measurements.

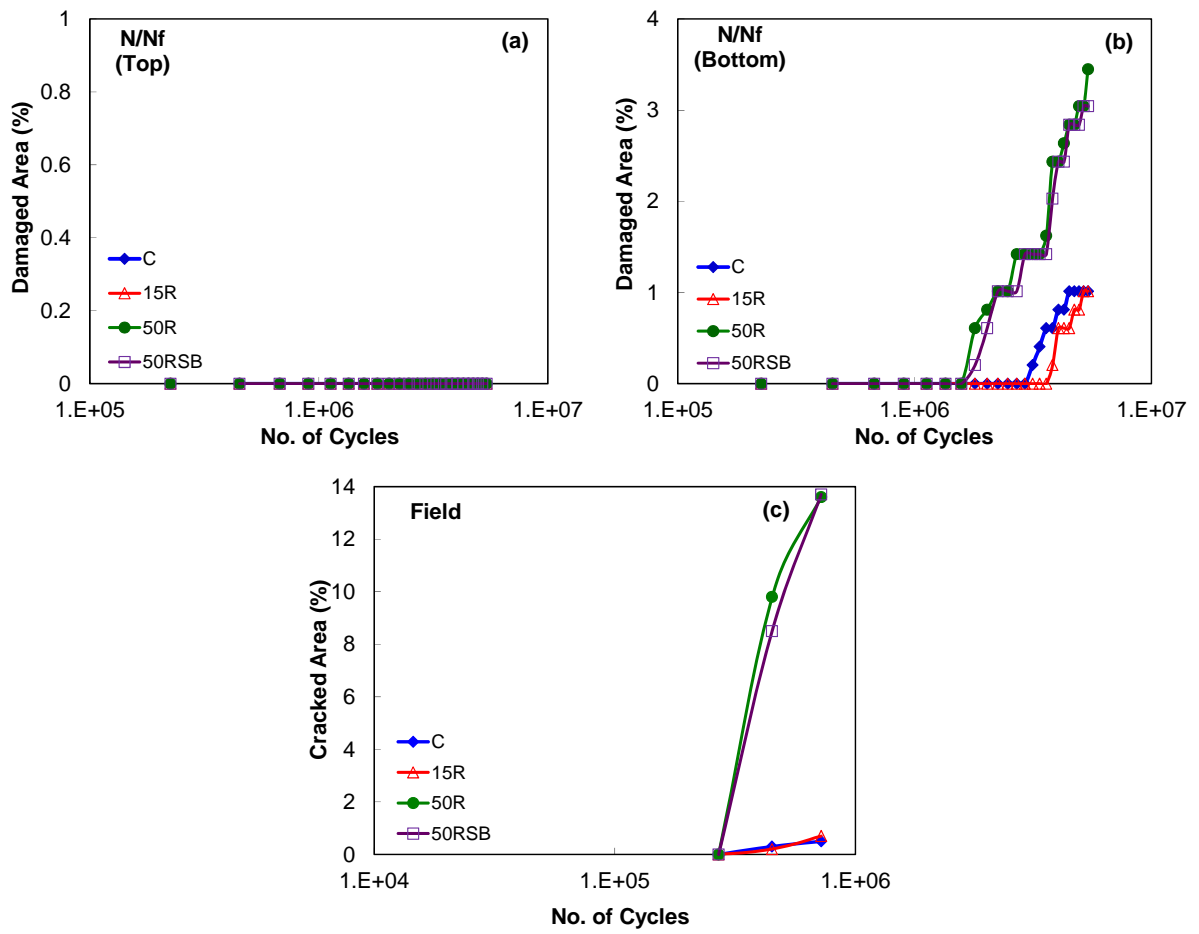


Figure 9-9. Damage definition obtained from method 1 for MIT-RAP: (a) top half of asphalt layer, (b) bottom half of asphalt layer, and (c) field measurements.

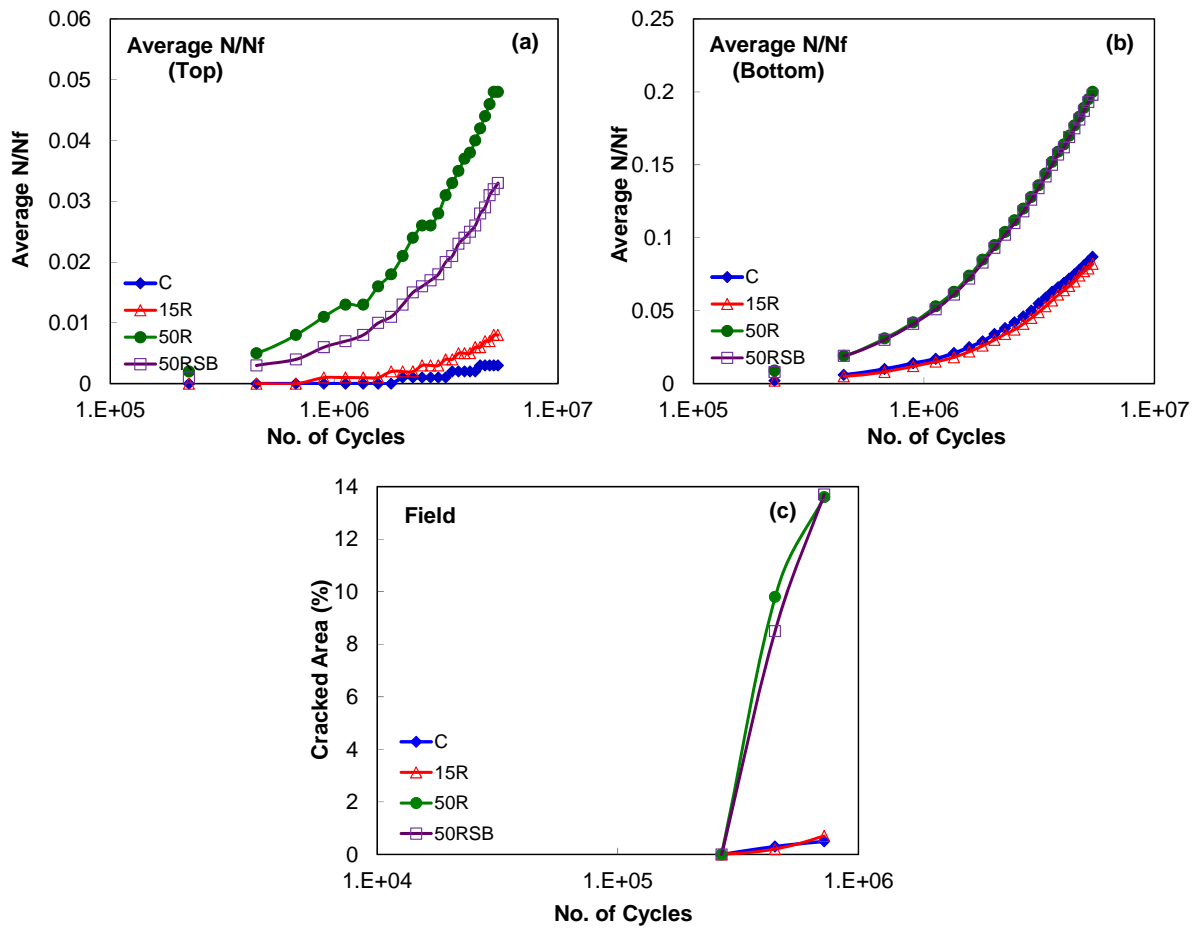


Figure 9-10. Damage definition obtained from method 2 for MIT-RAP: (a) top half of asphalt layer, (b) bottom half of asphalt layer, and (c) field measurements.

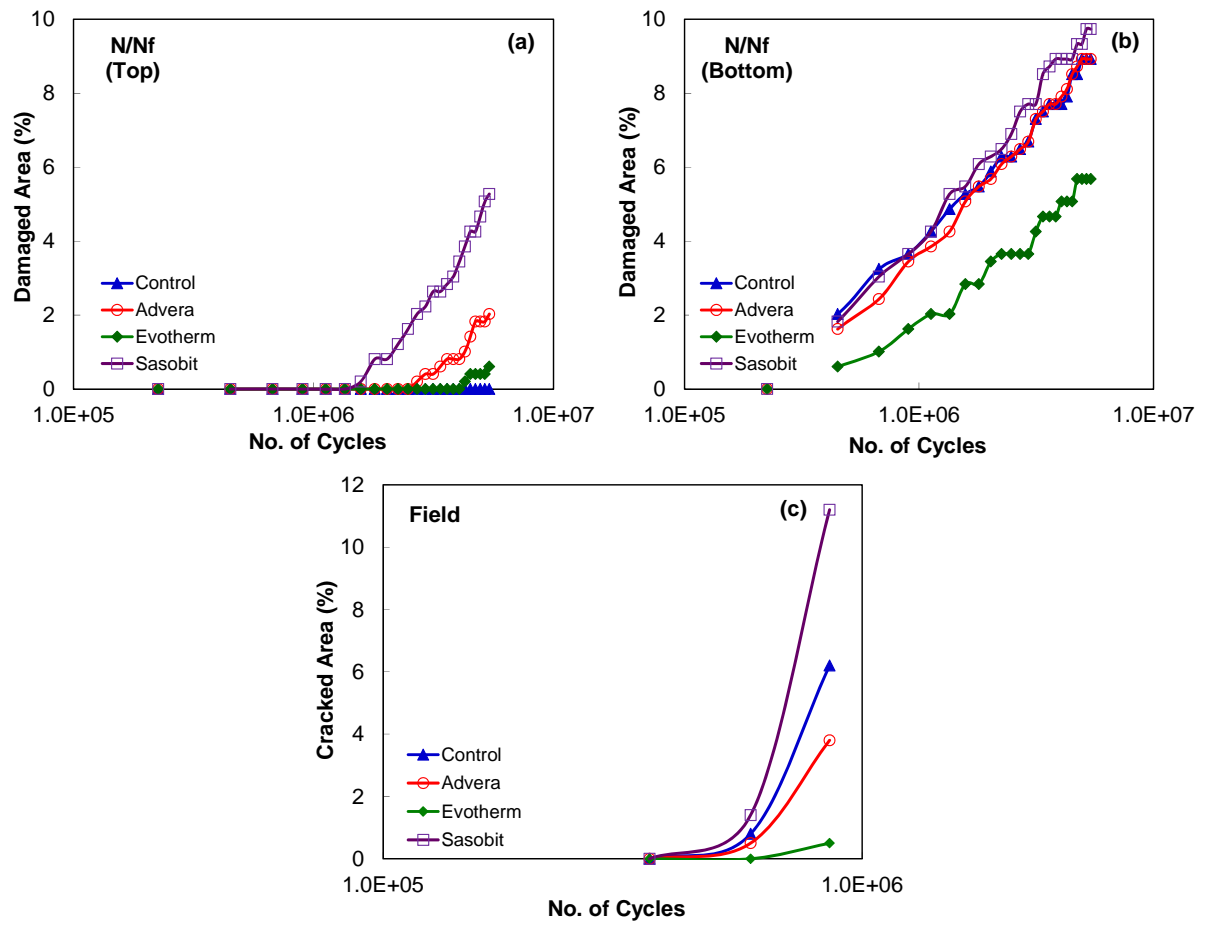


Figure 9-11. Damage definition obtained from method 1 for MIT-WMA: (a) top half of asphalt layer, (b) bottom half of asphalt layer, and (c) field measurements.

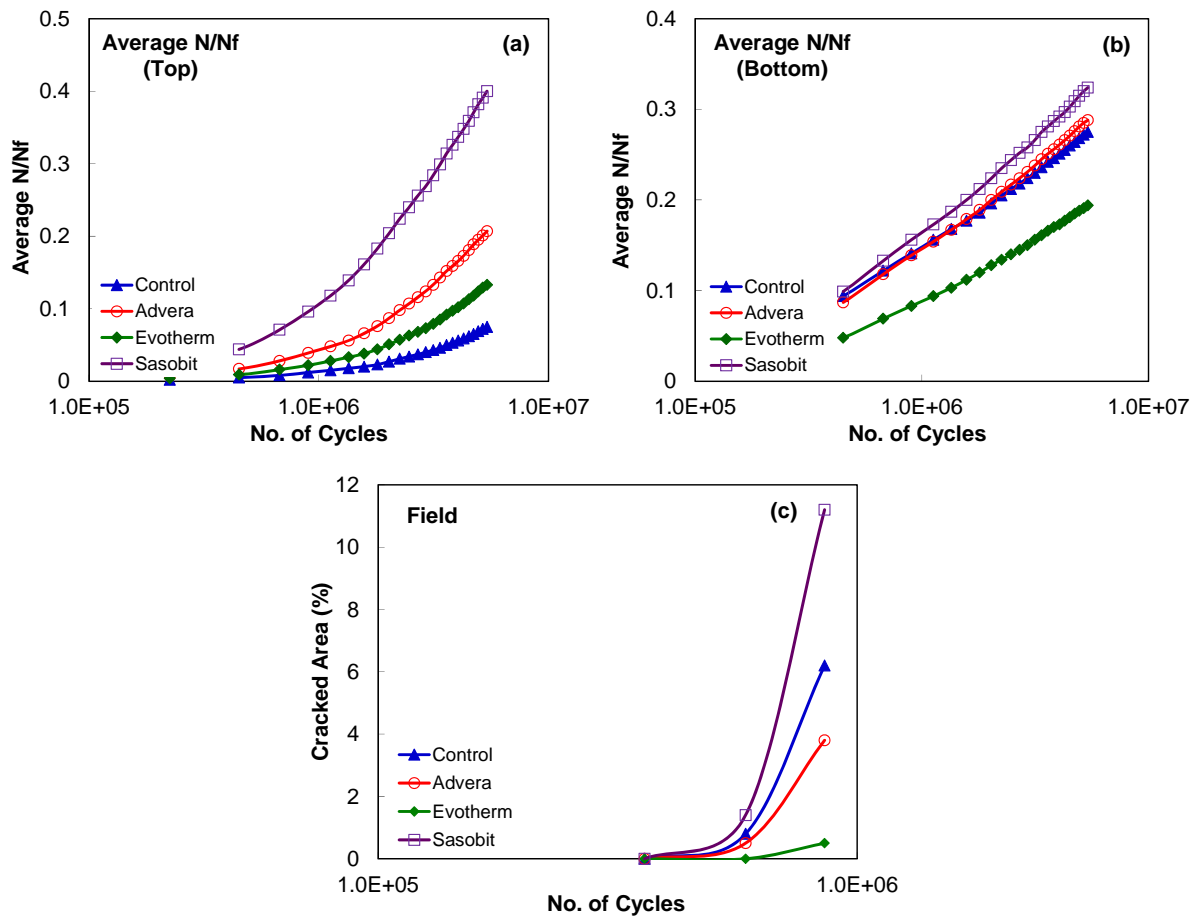


Figure 9-12. Damage definition obtained from method 2 for MIT-WMA: (a) top half of asphalt layer, (b) bottom half of asphalt layer, and (c) field measurements.

Figure 9-13 (a) and (b) present the field measurements versus the predicted damage obtained from the Pavement ME and LVECD programs, respectively. It seems that the same trend is observed in both cases where there is a shift to the left with an increase in pavement thickness. Therefore, it can be assumed that the same functional form that is in the Pavement ME can be used to represent the field crack growth in the LVECD program. Figure 9-14 presents the fitted curves for predicting the field cracking using the sigmoidal function. According to the observations made from Figure 9-13 (b) and Figure 9-14 (b), the following assumptions can be made for the LVECD program transfer function:

- A sigmoidal function is the best representation of the relationship between cracking and damage.
- The fatigue cracking value of 50 percent of the total area of the lane occurs at a damage percentage of 40 percent in the LVECD program.

The fatigue cracking predicted damage transfer function is assumed to take the form of a mathematical sigmoidal function that is similar to the Pavement ME transfer function. The transfer function can be presented as Equation (9.11).

$$\%FC = \frac{100}{1 + e^{C_1 + C_2 \log 2.5D}} \quad (9.11)$$

where

FC = fatigue cracking percentage in the field,

D = LVECD program-predicted fatigue damage in terms of percentage,

C<sub>1</sub>, C<sub>2</sub> = regression coefficients.

To satisfy the second assumption, the C<sub>1</sub> value must be equal to twice the negative value of C<sub>2</sub>, as shown below:

$$C_1 = -2C_2 \quad (9.12)$$

Following the aforementioned assumption, Equation (9.11) can be simplified as Equation (9.16):

$$\%FC = \frac{100}{1 + e^{C_2(-2 + \log 2.5D)}} \quad (9.13)$$

$$\%FC = \frac{100}{1 + e^{\log\left(\frac{2.5D}{100}\right)^{C_2}}} \quad (9.14)$$

$$\%FC = \frac{100}{1 + e^{\left(\log_e\left(\frac{2.5D}{100}\right)^{C_2} \cdot \log_{10}^e\right)}} \quad (9.15)$$

$$\%FC = \frac{100}{1 + \left(\frac{2.5D}{100}\right)^{0.43C_2}} \quad (9.16)$$

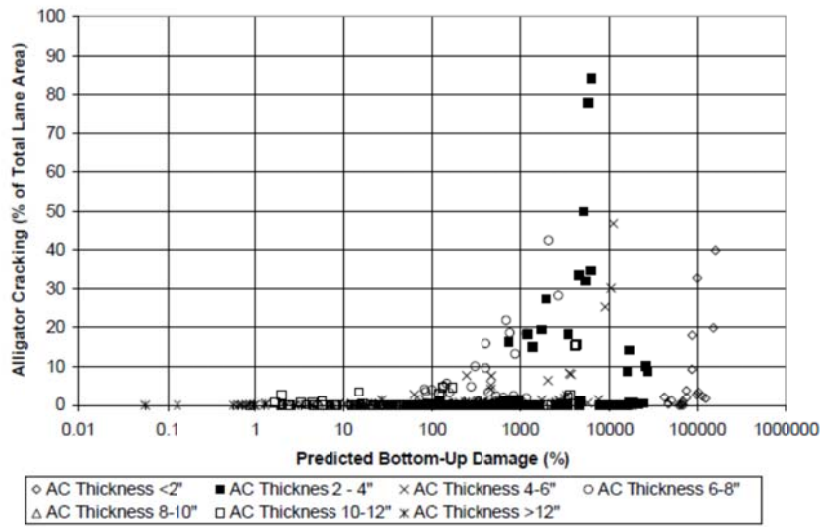
By considering  $0.43C_2 = K$ , Equation (9.16) can be written as:

$$\%FC = \frac{100}{1 + \left(\frac{2.5D}{100}\right)^K} \quad (9.17)$$

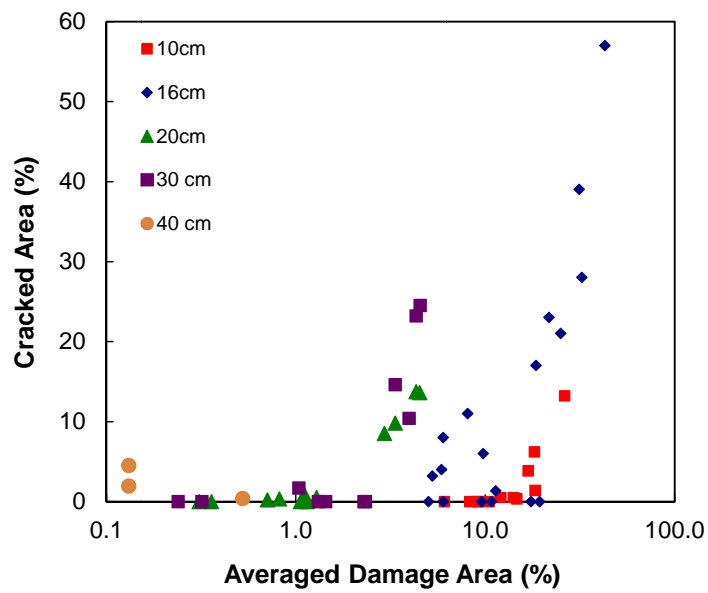
With more simplification of Equation (9.17), it will be found that there is a linear correlation between the two logarithmic terms as presented in Equation (9.18). Figure 9-15 presents the plot of  $\left(\frac{100}{FC} - 1\right)$  versus  $\left(\frac{2.5D}{100}\right)$  for different pavement sections.

$$\left(\frac{100}{FC} - 1\right) = \left(\frac{2.5D}{100}\right)^K \quad (9.18)$$

$$\log\left(\frac{100}{FC} - 1\right) = K \cdot \log\left(\frac{2.5D}{100}\right) \quad (9.19)$$



(a)



(b)

Figure 9-13. Predicted damage vs. measured fatigue cracking: (a) Pavement ME design guide and (b) LVECD program.

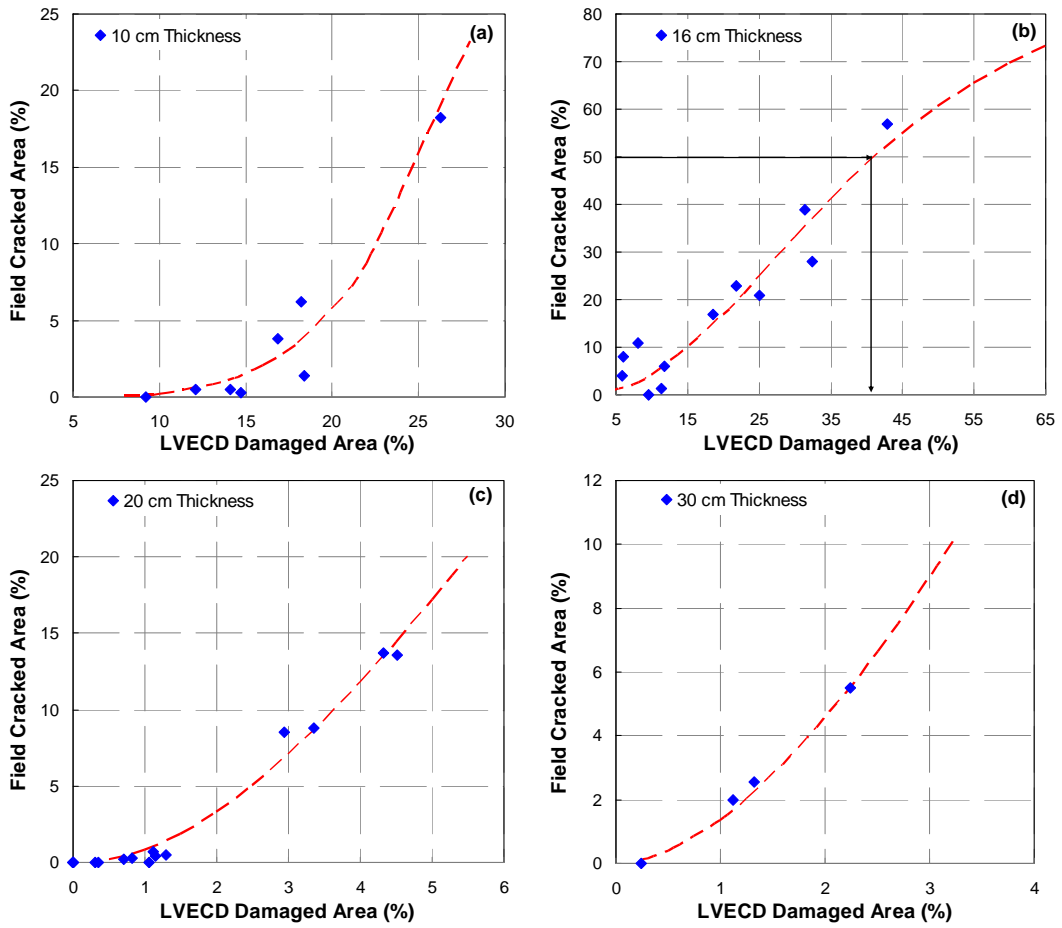


Figure 9-14. Measured field cracking vs. LVECD program-predicted cracking at different pavement thicknesses: (a) 10 cm, (b) 16 cm, (c) 20 cm, and (d) 30 cm.

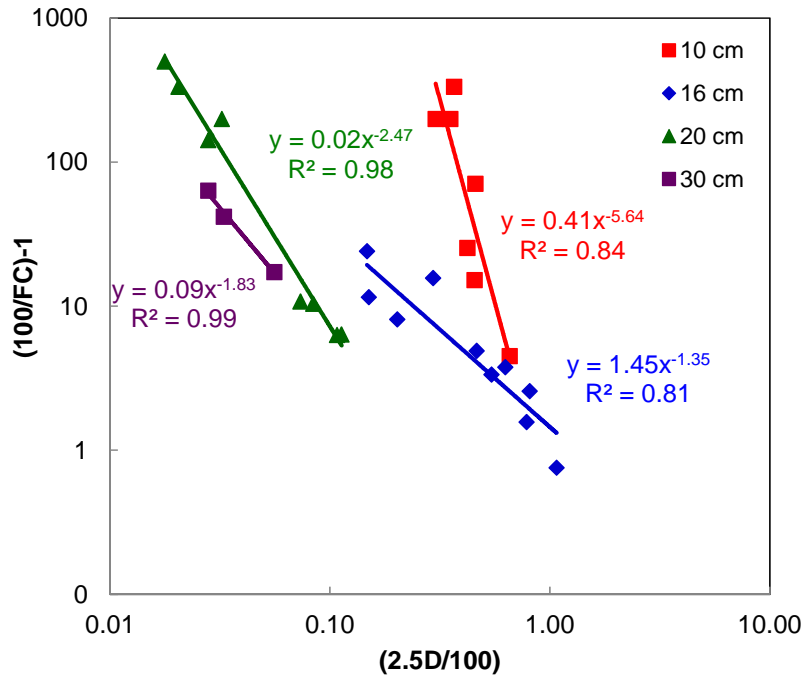


Figure 9-15. Plot of correlation between  $((100/FC)-1)$  and  $(2.5D/100)$  for different pavement sections.

The rate at which cracks initiate and propagate in a pavement structure depends mainly on the asphalt layer thickness. Therefore, the relationship that correlates fatigue cracking to the damage in a pavement should include the effect of the rate of cracking that is a function of the asphalt concrete layer thickness. To find the relationship between the  $C_2$  (or the so-called  $K$  value) and the pavement thickness, the absolute values of  $K$  were plotted versus the total section thickness, as shown in Figure 9-16. As shown, the exponential function seems to be a suitable form to represent this relationship. However, it is still necessary to modify the relationship between  $K$  and pavement thickness in a way that limits the maximum and minimum values of  $K$  based on the pavement thickness.

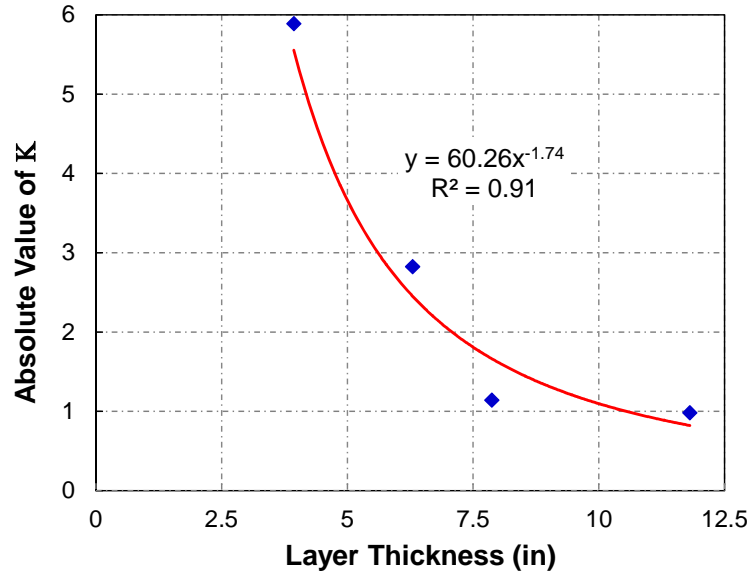


Figure 9-16. Variation of absolute values of  $K$  vs. pavement thickness.

Given all the aspects mentioned thus far, the most reasonable form that is able to demonstrate the variations of  $K$  in terms of pavement thickness can be presented as Equation (9.20).

$$K = \alpha + \beta(1 + h_{ac})^\gamma \quad (9.20)$$

After fitting the calculated data using Equation (9.21), the final equation is as follows:

$$K = -0.83 - 724(1 + h_{ac})^{-3.103} \quad (9.21)$$

where  $h_{ac}$  is the asphalt layer thickness.

Figure 9-17 demonstrates the plots of measured versus predicted cracking for different pavement sections. The prediction capabilities presented in Figure 9-17 (R-square of 0.81) are considered good for modeling the pavement fatigue cracking. The NCHRP report 457 presents a synthesis of the AASHTO MEPDG implementation in the United States, where R-square values above 0.65 are considered to have reasonable prediction capabilities. The same report mentions that the fatigue cracking prediction capability of the AASHTO MEPDG (United States national calibration) is poor, as it presents an  $R$ -square of 0.27.

Figure 9-18 shows the comparison of the damage trends before and after fatigue cracking calibration for the PRS pavement sections.

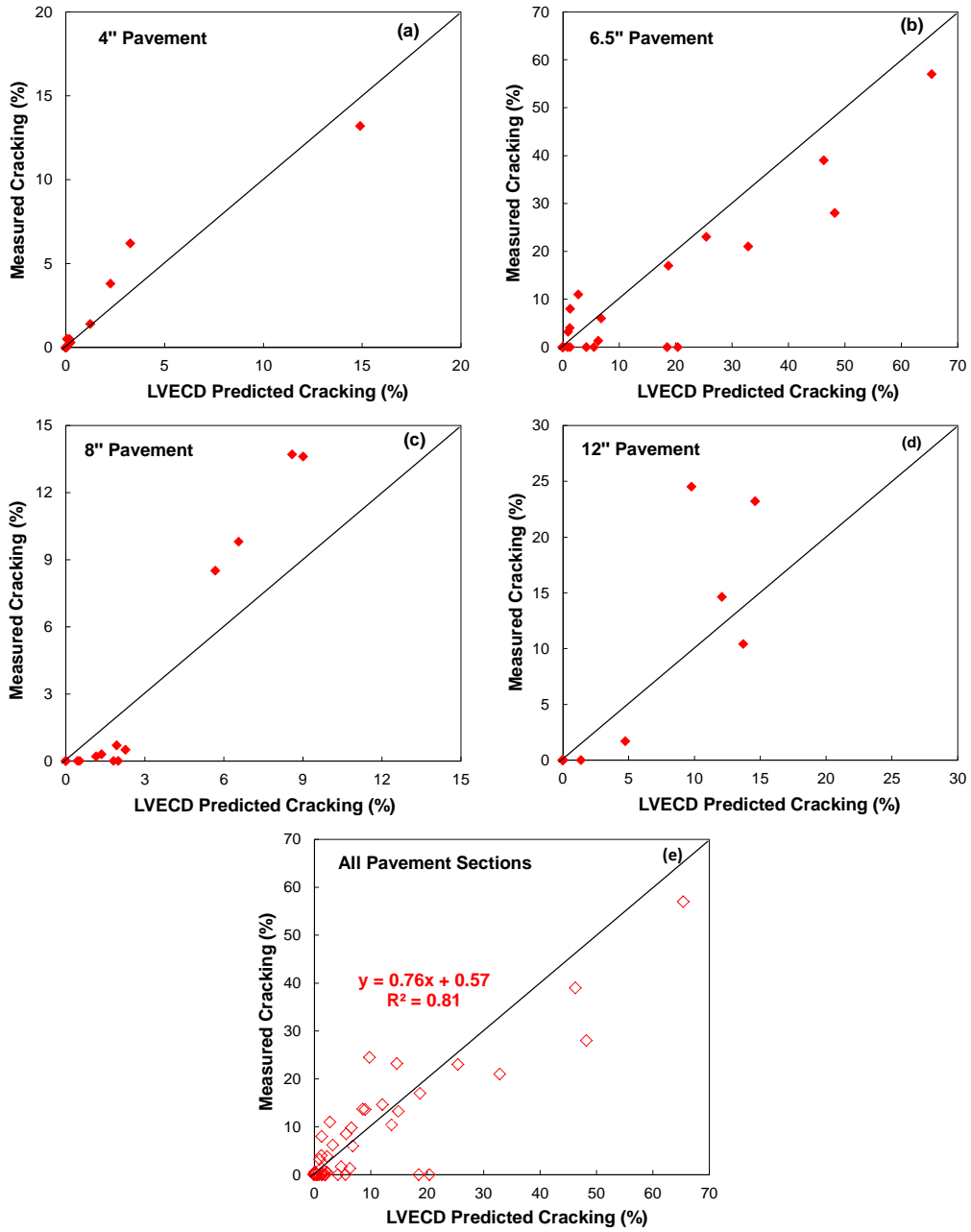


Figure 9-17. Comparison of observed versus predicted cracking with the LVECD transfer function.

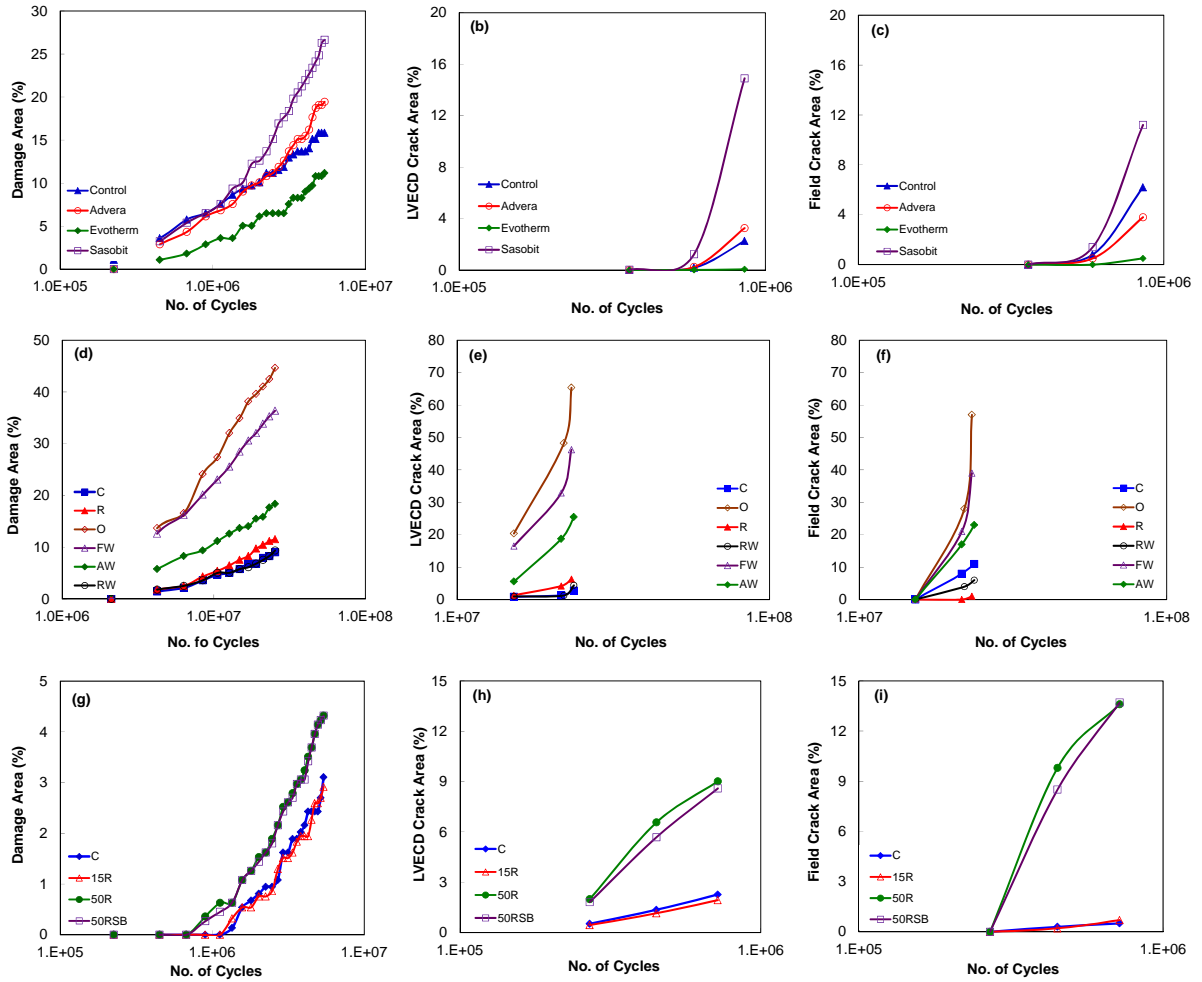


Figure 9-18. (a) non-calibrated damage trends for MIT-WMA, (b) measured cracks for MIT-WMA, (c) calibrated predicted damage for MIT-WMA, (d) non-calibrated damage trends for NCAT, (e) measured cracks for NCAT, (f) calibrated predicted damage for NCAT, (g) non-calibrated damage trends for MIT-RAP, (h) measured cracks for MIT-RAP, and (i) calibrated predicted damage for MIT-RAP.

# CHAPTER 10 COMPARISON OF FATIGUE CRACKING PERFORMANCE PREDICTIONS IN ASPHALT PAVEMENTS USING PAVEMENT ME AND LVECD PROGRAMS<sup>6</sup>

## 10.1 Abstract

The performance-based design of asphalt pavements has been ongoing since 2000. Currently available software for pavement performance design includes the program, the AASHTOware Pavement ME program that was known as *Mechanistic Empirical Pavement Design Guide* (MEPDG). The Pavement ME program allows users to predict pavement distresses by applying layered elastic theory for the mechanical responses and using empirical models for the distress predictions. In addition to the Pavement ME program, the ‘layered viscoelastic pavement design for critical distresses’ (LVECD) program, which was developed recently at North Carolina State University, can be used to predict the fatigue and rutting performance of pavements using three-dimensional viscoelastic finite element analysis with moving loads. The LVECD program employs the well-known simplified viscoelastic continuum damage (S-VECD) model as an effective tool for the fatigue performance prediction of asphalt mixtures under complex loading and environmental conditions, in conjunction with a newly developed energy-based fatigue failure criterion. This failure criterion can predict the fatigue life of asphalt mixtures independent of loading mode, frequency, strain amplitude, and temperature.

This study investigates and compares the performance of 33 pavement sections from five different research projects located in the United States, Canada, and South Korea using both the Pavement ME and LVECD programs. To verify the results obtained from these two

---

<sup>6</sup> This chapter was previously published as: Wang, Yizhuang., **A. Norouzi**, and Y. R. Kim (2015). Comparison of Fatigue Cracking Performance Predictions in Asphalt Pavements Using Pavement ME and LVECD Programs. *Journal of Transportation Research Records*, in press.

programs, the simulations were compared to the field performance data. In terms of ranking, the LVECD simulations provided better agreement with the field performance data than the Pavement ME simulations. For multilayer pavement sections, the LVECD program captured the properties of all the layers for fatigue performance, whereas the Pavement ME program considers only the bottom layer.

## **10.2 Introduction**

It is now well accepted that fatigue cracking due to repeated traffic loading is one of the most significant distresses found in the asphalt pavements. To determine the optimal pavement design or management strategies, the origin of cracks that appear within the pavement section needs to be identified. For achieving this goal, effective models and design procedures that can reliably represent the fatigue damage growth are in demand to predict the asphalt pavement performance (Nishizawa et al. 1997, Tayebali et al. 1992, Norouzi et al. 2015).

Performance-based design is applied by most state highway agencies for pavement construction, thereby replacing the empirical design procedures that were based on the AASHTO test road data from the 1950s (Hveem 1955). Unlike empirical design, performance-based design allows designers to see the predicted performance of a pavement at the end of the design period and to select the most suitable pavement design accordingly (NCHRP 2004). Designers can now predict the performance of a pavement using computer programs such as AASHTOWare Pavement ME and the newer ‘layered viscoelastic pavement design for critical distresses’ (LVECD) software.

The Pavement ME program was developed in 1996 based on the existing state-of-the-practice mechanistic-based models and became available in 2004 in the form of software called the Mechanistic-Empirical Pavement Design Guide (MEPDG) (El-Basyouny and Witczak 2004, Guo 2013).

It applies layered elastic theory for the flexible pavements to calculate the required stress and strain responses under traffic loading, and the responses are utilized in the empirical models to link laboratory test results to field performance, including fatigue damage and permanent deformation. However, it has been common to assume that fatigue cracking normally initiates at the bottom of asphalt layer and propagates to the surface (bottom-up cracking) due to the bending action of the pavement layer, which results in flexural stresses to develop at the bottom of the bound layer (Myers and Rouqe 2001). Consequently, top-down cracking cannot be explained by the traditional fatigue mechanisms that are used to explain load-associated fatigue cracking that initiates at the bottom of the pavement (Park et al. 2014). Furthermore, commonly used multi-layered elastic pavement analysis is not capable of modeling the time dependent nature of asphalt concrete appropriately (Park and Kim 2013).

The LVECD program was developed recently at North Carolina State University. This program applies three-dimensional (3-D) finite element analysis with moving loads to obtain the mechanical responses and uses mechanics-based models for the distress predictions. For example, the simplified viscoelastic continuum damage (S-VECD) model is employed for fatigue performance predictions (Guddati 2012, Guddati et al. 2013). The S-VECD model is built on three concepts: (1) the elastic-viscoelastic correspondence principle based on pseudo strain, (2) the continuum damage mechanics-based work potential theory, and (3) the time-temperature superposition principle with growing damage to include the combined effects of time/rate and temperature (Chehab et al. 2002, Park et al. 1996, Underwood et al. 2012, Gibson et al. 2012). The model also includes a newly developed energy-based failure criterion, referred to as  $G^R$ , which is independent of temperature and loading mode, to determine the failure of the mixture (Zhang et al. 2013, Sabouri and Kim 2014, Norouzi and Kim 2015). Therefore, LVECD does not require the assumption of crack initiation a priori since the flexibility of S-VECD model allows cracks to initiate and propagate wherever the fundamental law suggests, so that a realistic cracking condition can be conducted through the simulation (Norouzi et al. 2014). As is the case with using the Pavement ME program, designers who use the LVECD program are able to see the

performance of a pavement during the entire design period predicted from the mechanistic models.

For this study, both the Pavement ME and LVECD programs were used to predict fatigue cracking in 33 different pavement test sections from five different research projects. The fatigue prediction results from the two programs are presented and compared in this chapter. The chapter also includes descriptions of the tests conducted and the input information needed for the two programs.

### **10.3 Background**

Both the Pavement ME and the LVECD programs allow users to predict the long-term performance of a pavement's trial structure. Although similar input information is required for both programs, the mechanisms of the two programs are very different. For example, computational cost is an important factor for the long-term simulation of pavement performance, and the two programs apply very different mechanisms to address the issue of cost-effectiveness.

In the Pavement ME program, a multilayer elastic analysis program, JULEA, is used to calculate the mechanical responses in order to reduce computational expenses. This elastic analysis program is employed although the asphalt materials used in flexible pavements are viscoelastic materials. To predict fatigue performance, the Pavement ME program applies the Asphalt Institute Model, Equation (10.1), which is an empirical model that links the number of cycles at failure and the applied strain. In this study, the fatigue properties of the different mixtures used in the different pavement sections are taken into account through the material-specific coefficients,  $k_{f1}$ ,  $k_{f2}$ , and  $k_{f3}$ . These material-specific coefficients were obtained from cyclic direct tension fatigue tests performed on each mixture and the regression based on further derivation (Equation (10.2)) from the S-VECD model.

Using this equation, the number of cycles to failure under different loading strains and temperatures can be calculated, and therefore, the exponential relationship between the number of cycles to failure and the loading strain can be obtained through linear regression in logarithmic scale. In this way,  $k_{f1}$ ,  $k_{f2}$ , and  $k_{f3}$  for the different materials are computed. Pavement ME program applies Miner's law (Equation (10.3)) to accumulate the fatigue damage. The calculated fatigue damage results are then converted to field performance data by employing the transfer function presented in Equation (10.4). In this study, the local calibration factors for North Carolina (Jadoun, 2011) is applied for all the pavement sections regardless of the location of the projects.

$$N_f = \beta_{f1} k_{f1} \left( \frac{1}{\varepsilon_t} \right)^{\beta_{f2} k_{f2}} \left( \frac{1}{E} \right)^{\beta_{f3} k_{f3}} \quad (10.1)$$

where

$N_f$  = number of repetitions to fatigue cracking,

$\varepsilon_t$  = tensile strain at the critical location,

$E$  = material stiffness,

$k_{f1}, k_{f2}, k_{f3}$  = material-specific coefficients, and

$\beta_{f1}, \beta_{f2}, \beta_{f3}$  = local calibration factors.

$$N_f = \left[ \frac{\alpha - C_{12}\alpha + 1}{\alpha - C_{12}\alpha + 1 + C_{12}} \frac{C_{11}}{2\gamma} (\varepsilon_{0,ta}^R)^2 \left( \frac{(\alpha - C_{12}\alpha + 1)(C_{11}C_{12})^\alpha (\varepsilon_{0,ta}^R)^{2\alpha} K_1}{f_R \times 2^\alpha} \right)^{\frac{C_{12}}{\alpha - C_{12}\alpha + 1}} \right]^{\frac{\alpha - C_{12}\alpha + 1}{(\alpha + 1)(\delta + 1) - C_{12}(\alpha + \delta\alpha + 1)}} \quad (10.2)$$

where

$\varepsilon_{0,ta}^R$  = pseudo strain

$f_R$  = reduced frequency

$K_1$  = loading shape function

$$\sum_{i=1}^T D_i = \frac{N_i}{N_{fi}} \quad (10.3)$$

where

$D$  = damage,

$T$  = total number of periods,

$N_i$  = traffic for period  $i$ , and

$N_{fi}$  = allowable failure repetitions under the conditions that prevail in period  $i$ .

$$\text{Alligator Cracking} = \left( \frac{6000}{1 + e^{(C_1 \cdot C_1' + C_2 \cdot C_2' \cdot \log(\% \text{Damage}))}} \right) \cdot \left( \frac{1}{60} \right) \quad (10.4)$$

where

$$C_1' = -2C_2'$$

$$C_2' = -2.40874 - 39.748(1 + h_{ac})^{-2.856}$$

The LVECD program computes the amount of pavement distress from the beginning to the end of the design period. In terms of the calculation of the mechanical responses, 3-D finite-element viscoelastic analysis with moving loads is performed by the LVECD program. In this analysis, fast Fourier transform is conducted twice to reduce the computational cost. In terms of the computation of the fatigue damage, the S-VECD model (presented in Equations (10.5) and (10.6)) is applied. Equations (10.5) and (10.6) characterize the damage evolution in the asphalt mixtures where damage is a combination of microcrack initiation and propagation. Equation (10.7) is the energy-based failure criterion ( $G^R$ ), which has been proven to be able to determine the failure of mixtures; the  $G^R$  versus  $N_f$  (number of cycles to failure) curves among different types of mixtures (i.e., modified binder mixtures, high RAP mixtures, and WMA mixtures) differ significantly. The S-VECD model is able to describe the comprehensive constitutive fatigue behavior of an asphalt mixture. Each asphalt layer in the cross-section of the pavement is divided into 1000 ( $100 \times 10$ ) elements with 11,111 ( $101 \times 11$ ) nodes, and the elements and nodes are used in the finite elements analysis for the mechanical response and damage calculations. The whole design period also is divided into a large number of life-stages (i.e., 240 life-stages for 20 years). At the end of each life-stage,

the damage state of the mixtures is updated. During the simulation, the LVECD program applies Miner's law, Equation (10.3), in order to accumulate the fatigue damage that is due to different loading conditions. The performance index used in the LVECD program is the so-called *damage area* (%), which is the number of nodes where the asphalt mixture fails ( $\frac{N}{N_f} = 1$ ) over the total number of nodes throughout all the asphalt layers.

Note that, even though the transfer function, which converts the 'damage area' into the scale of the 'cracking area' in the field, has not been fully developed and thus has not yet been applied in the LVECD program, the predicted results nonetheless match the field measurements quite well, and the ranking of the fatigue performance of the pavement sections is not affected by the inclusion of a transfer function. Therefore, with the lack of the application of transfer function in LVECD and the local calibration factors for each section in Pavement ME, this chapter focuses only on the ranking instead of the absolute values of the prediction results. Furthermore, at the end of the computation process in the LVECD program, the damage contours can be plotted to show the state of the fatigue damage of the pavement and cracking location at any time in the design period; for example, see Figure 10-3.

$$\text{Damage Function: } \frac{\partial S}{\partial t} = \left( -\frac{\partial W^R}{\partial S} \right)^\alpha \quad (10.5)$$

$$\text{Damage Curve: } 1 - C_{11} (S^{C_{12}}) \quad (10.6)$$

$$\text{Failure Criteria: } G^R = \gamma N_f^\delta \quad (10.7)$$

where

- $S$  = damage parameter,
- $C$  = pseudo stiffness,
- $W^R$  = work potential function,
- $C_{11}, C_{12}, \alpha, \gamma, \delta$  = model parameters,
- $G^R$  = energy release rate.

## 10.4 Data Collection and Field Sections

Experiments were performed and data were collected based on the input requirements of the two programs. Several sections of input data are incorporated in both programs; these data include general information (i.e., design period), traffic data, climate data, structural data (i.e., layer thickness, flexible material properties, and unbound layer material properties), and other information (i.e., local calibration factors). The traffic information in the Pavement ME program is comprised of basic information (i.e., average annual daily truck traffic (AADTT), vehicle speed), traffic volume adjustment (i.e., vehicle class distribution, hourly truck traffic, and traffic growth factors), axle load distribution factors, and general traffic input (i.e., mean wheel location, wander standard deviation). In the LVECD program, all the traffic data are converted into the number of passes of a standard axle (two single tires with 80-kN axle load) with constant speed (27 m/s) based on the design equivalent single-axle loads (ESALs). For the climate data, both the Pavement ME and LVECD programs employ the Enhanced Integrated Climate Model (EICM) database. Using this database, temperatures can be extracted that are applicable throughout the pavement depth and design life. In addition, the Pavement ME software extracts other information from the database, including moisture profiles, frost depth, annual freezing index values, and mean annual number of wet days.

The structural data, including material properties, are the most important information in the performance-based design process. For this study, the material properties of the asphalt mixtures were obtained by performing dynamic modulus and fatigue tests, the results of which are needed to run both Pavement ME Level I and the LVECD program. For both programs, dynamic modulus tests were conducted, because material stiffness is important to the simulations. In the Pavement ME program, the modulus values of the asphalt mixtures at specific temperatures and frequencies are utilized directly by the program as the elastic modulus of the mixtures under different conditions because no historical loading effects are taken into account. However, in the LVECD program, the dynamic modulus test results were analyzed based on the time-temperature superposition (Equation (10.8) and (10.9)).

Coefficients of the Prony series (in Equation (10.10)) were calculated based on the test results and input into the LVECD program in order to apply viscoelastic theory. In terms of the inputs for the fatigue model, for the LVECD program, direct tension fatigue tests were conducted based on AASHTO TP 107, and the required parameters of the S-VECD model were computed and used in the program. For the Pavement ME program, the material-specific fatigue coefficients  $k_{f1}$ ,  $k_{f2}$ , and  $k_{f3}$  in Equation (10.1) were obtained from the same tests. However, unlike the LVECD program, the Pavement ME program considers the fatigue coefficients only for the bottom layer asphalt material. In addition to the mechanical properties of the mixtures, the volumetric properties of the mixtures and shear modulus values of the binders in the mixtures were input to the Pavement ME program. The material properties of the unbound layers, i.e., the aggregate base and subgrade soil, also are needed. Both programs take the mechanical properties of the unbound layer material, i.e., the modulus values and Poisson's ratio, into account. In addition to the mechanical properties, other properties, such as soil type and gradation, also were input to the Pavement ME software.

$$\log |E^*| = a + \frac{b}{1 + \frac{1}{e^{d+g \times \log(f_R)}}} \quad (10.8)$$

$$\log(a_T) = \alpha_1 T^2 + \alpha_2 T + \alpha_3 \quad (10.9)$$

$$E(t) = E_\infty + \sum_{i=1}^m E_i \cdot e^{-t/\rho_i} \quad (10.10)$$

where

$f_R$  = reduced frequency,

$e$  = exponential function,

$a, b, d, g$  = fitting coefficients of sigmoidal function,

$a_T$  = time-temperature shift factor,

$\alpha_1, \alpha_2, \alpha_3$  = fitting coefficients of time-temperature shift factor function,

$T$	=	temperature,
$E_{\infty}$	=	long-term equilibrium modulus,
$i$	=	index of summation,
$m$	=	number of Prony terms,
$E_i$	=	modulus of Prony term number $i$ ,
$t$	=	time, and
$\rho_i$	=	relaxation time of Prony term $i$ .

The performance prediction results from the two programs, Pavement ME and LVECD, were compared with the field performance measurements of the different pavement sections. Thirty-three pavement sections from five different research projects located in the United States, Canada, and South Korea were used, and 38 different asphalt mixtures were tested. The sections used in this study are from the National Center for Asphalt Technology (NCAT) Test Track, the Federal Highway Administration Accelerated Loading Facility (FHWA-ALF), the Manitoba Infrastructure and Transportation warm mix asphalt (MIT-WMA) project, the MIT reclaimed asphalt pavement (MIT-RAP) project, and the Korean Expressway Corporation (KEC) Test Road.

Six sections were selected from the NCAT Test Track: S9, S8, S10, S11, N10, and N11. For this study, these section designations were abbreviated to C (control), O (open-graded friction course surface with control intermediate/base), FW (control mixture with foamed asphalt WMA), AW (control mixture with Advera additive WMA), R (50 percent RAP mixture), and RW (50 percent RAP mixture with foamed asphalt WMA), respectively. The structures of the NCAT pavement sections are all three-layer systems, and the schematics are presented in Figure 10-1 (a).

From the FHWA-ALF project, Lane 2, Lane 4, Lane 5, and Lane 6 were selected; similarly to the NCAT sections, the ALF sections were renamed as control, SBS-LG (styrene butadiene styrene with linear grafting), CR-TB (crumb rubber terminal blend), and terpolymer (ethylene terpolymer), respectively, based on the materials used in the sections. The structures of the ALF sections are presented in Figure 10-1 (b). For the MIT-WMA project sections, three different types of WMA mixtures were compared to a hot mix asphalt (HMA) control mixture. For the MIT-RAP project sections, four mixtures with different contents of RAP were compared: control (zero percent RAP), 15%-R (fifteen percent RAP), 50%-R (fifty percent RAP), and 50%-RSB (fifty percent RAP with a soft binder). The structural schematics for the MIT-WMA and MIT-RAP sections are shown in Figure 10-1 (c) and (d), respectively. The KEC test road was built to evaluate the effects of the type of base layer material, base layer thickness, an anti-frost layer, and the sub-base layer thickness. The structural layout of the KEC project is presented in Figure 10-1 (e).

Among the selected projects, the NCAT and FHWA sections are full-scale accelerated test sections, whereas the MIT and KEC projects are test roads. For the subgrade inputs for the MIT and KEC sections, the soil properties were obtained from field core falling weight deflectometer (FWD) backcalculations. Because the MIT and KEC projects are not in the United States, their actual climate stations were not available in the EICM database. Grand Forks, ND was selected to represent Manitoba, Canada, and Washington D.C. was selected to represent South Korea, because the climate data are very similar to the locations of the test roads in these two regions. The input traffic data are based on actual traffic measurements. To determine the mixture properties, dynamic modulus tests and fatigue tests were conducted for each mixture used in this study. For the Pavement ME program, only the fatigue coefficients of the bottom layer material were input to predict the fatigue performance. The loads applied in the full-scale test sections, i.e., the NCAT and ALF sections, were converted into Pavement ME and LVECD program inputs. Details regarding the traffic inputs, as well as other information, are presented in Table 10-1.

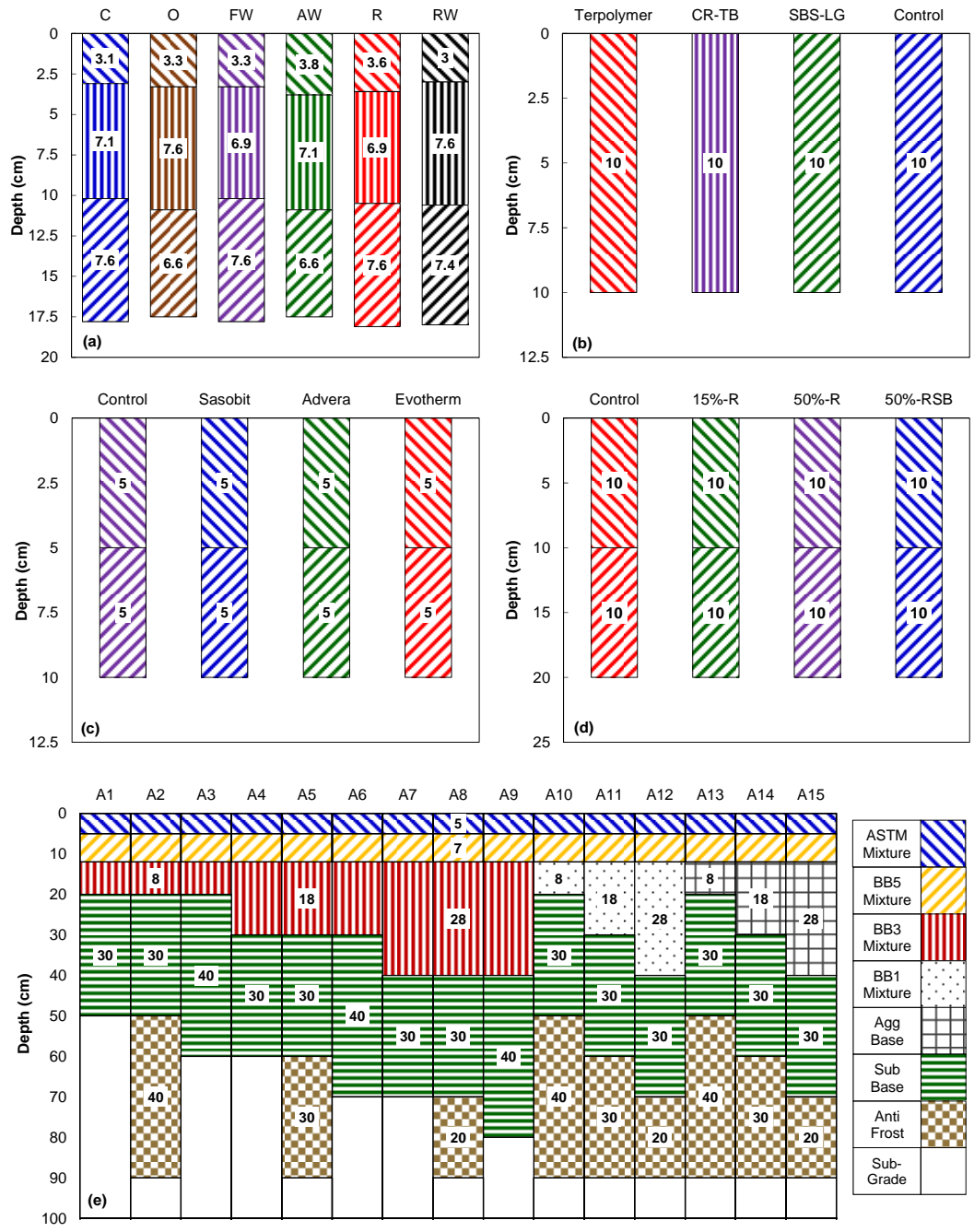


Figure 10-1. Schematics of asphalt pavement structures for the test sections: (a) NCAT (asphalt layers), (b) FHWA-ALF (asphalt layers), (c) MIT-WMA (asphalt layers), (d) MIT-RAP (asphalt layers), and (e) KEC (whole pavement structure).

Table 10-1. Input Information for LVECD and Pavement ME Programs for Performance Analysis of NCAT and ALF Test Sections

	LVECD			Pavement ME						
		NCAT	ALF	NCAT			ALF			
<b>Traffic</b>	AADT	14083	835	Basic Information	AADTT	3082	Tire Load	16000 lb.		
					Vehicle Speed	45 mph	Tire Pressure	120 psi		
				Traffic Volume Adjustment	Vehicle Class Distribution	50% Class 12+ 50% Class 13	Standard Deviation of Wheel Wander	5.25 in.		
					Hourly Truck Traffic	As distributed in the field based on shift changes, truck refueling, driver breaks, and maintenance stops	Monthly Repetitions	5208		
					Monthly Adjustment Factors	1 for all months	Annual Growth	0		
					Traffic Growth Factors	No growth	Tire Location	Single Tire		
	Growth	No Growth	No Growth	Axle Load Distribution Factors	single axle + tandem axle + 5 single axles					
				General Traffic Input	Axle Configuration	width: 8.5 ft. dual tire space: 13.5 in. tire pressure: 100 psi				
					Mean Wheel Location	Default value				
					Wander Standard Deviation	Default value				
<b>Climate</b>	EICM Station: Montgomery AL	Isotherma 1 19 °C	Longitude	-86.394			19 °C			
			Latitude	32.301						
			Station	Montgomery, Alabama						
<b>Asphalt Material</b>	Dynamic Modulus	Prony series coefficients for all asphalt mixtures	Dynamic Modulus	Tested results for all the mixtures, 4 temperatures and 6 frequencies						
	Fatigue Properties	S-VECD Model Coefficients for all asphalt mixtures	Fatigue Properties	Regressed material-specific coefficients k1, k2, and k3 for only bottom layer mixture						
<b>Unbound Layers</b>	Mechanical Properties	Resilient Modulus or Young's Modulus; Poisson's Ratio								
	Other Information	Soil Type, Gradation								

## 10.5 Results and Discussion

After the data were collected, the Pavement ME and LVECD programs were used to calculate the performance prediction results for each pavement section. The prediction results were compared between the two programs, and the predicted results were compared with the measured ‘cracking areas’ in the field.

Comparisons between the prediction results and the field measurements of the NCAT test track sections are presented in Figure 10-2 (a) – (f). According to the field measurements, the open-graded friction course (OGFC) section and the foamed WMA section exhibited the worst fatigue cracking performance (i.e., the least resistance to cracking), and the ‘cracking areas’ of the control section and the two sections with RAP material are seen to be relatively small. The LVECD program was able to capture the ranking of the ‘cracking areas’, according to Figure 10-2 (d), and (e); however, the Pavement ME program could not, according to Figure 10-2 (f) and (c). In the Pavement ME predictions, the OGFC section has the same damage level as the control section, which is not the case in the field. This outcome is due to the fact that the Pavement ME program considers only the bottom asphalt layer to be critical for fatigue cracking, so only the fatigue cracking coefficients of the bottom layer mixture were required by the program. However, the intermediate and bottom layer mixtures in the OGFC section are the same materials as those used in the control section. The only difference between the two sections is the application of the OGFC mixture in the surface layer; however, because the OGFC is open-graded and has a high air void content, cracking is more likely to occur using this mixture. By contrast, the LVECD program accounts for the whole cross-section of the pavement, and so, damage is computed throughout the pavement. In addition, the damage contours (presented in Figure 10-3) also are provided by the LVECD program. From the damage contours of the cross-section, top-down cracking is clearly critical in the OGFC section – not just bottom-up cracking.

In short, all the mixtures in a pavement must be taken into account, not just the bottom layer material. Also, in this case, the damage contours can help the designer to consider explicitly the ‘cracking area’ and severity of damage.

Figure 10-2 (g) – (l) presents the comparison between the predicted cracking damage and the measured ‘cracking area’ in the field for the FHWA ALF sections. According to Figure 10-2 (g) and (j), which present the cracks measured in the field, the control section shows the worst fatigue performance (resistance to fatigue cracking), and the SBS-modified section shows the best performance. The Pavement ME program generally was able to predict the ranking of the ‘% crack area’ in the field, except that the rankings of the terpolymer section and the SBS section are reversed. This ranking was better captured by the LVECD program, as the shape of the damage area versus ESAL curve is very similar to the curve in the plots for the field measurements when comparing Figure 10-2 (g) and (h) on a semi-log scale.

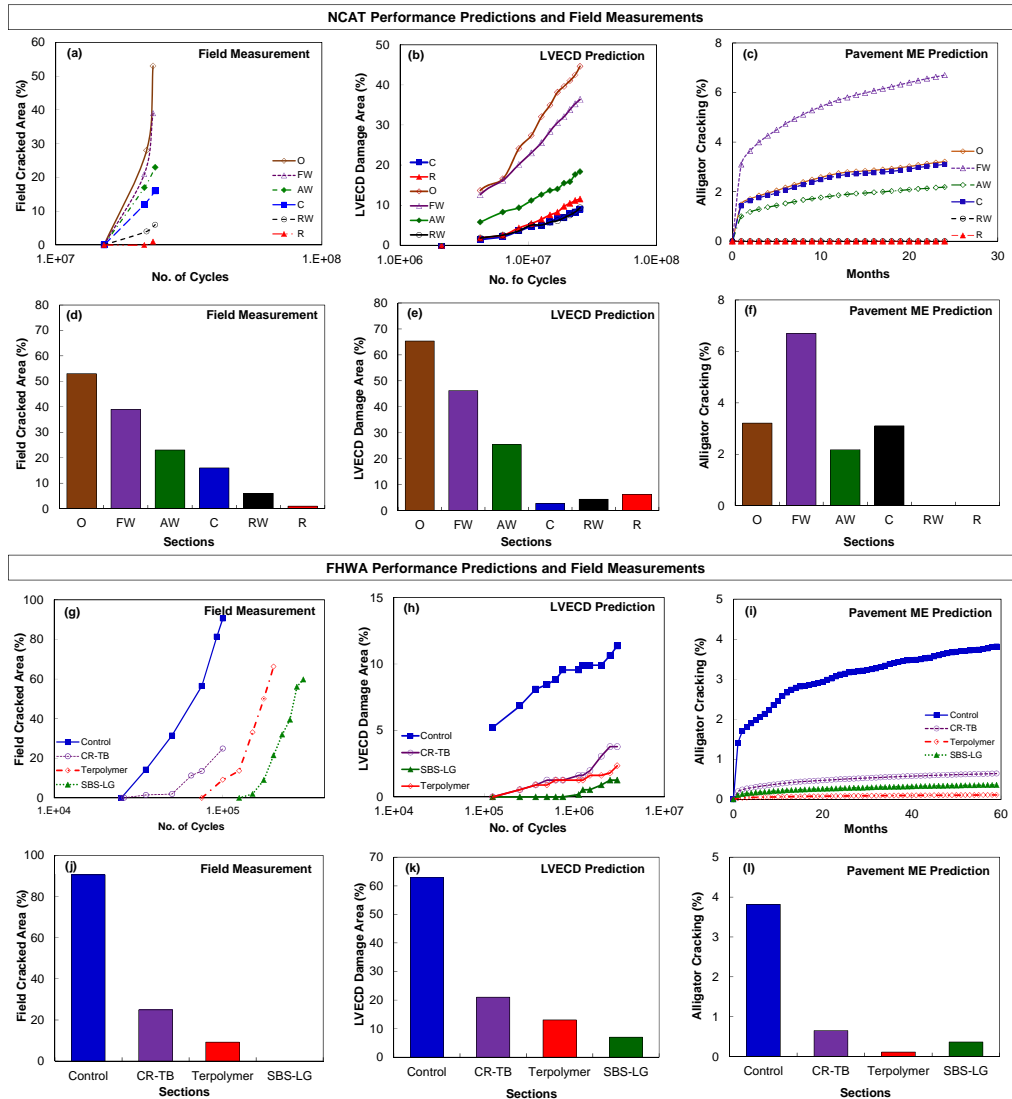


Figure 10-2. Measured and predicted fatigue cracking amount for NCAT and FHWA test sections: (a) amount of cracking in the field (NCAT), (b) predicted damage area in LVECD (NCAT), (c) predicted damage area in Pavement ME (NCAT), (d) maximum amount of cracking at the end period of study (NCAT), (e) maximum predicted damage area at the end of analysis with LVECD (NCAT), (f) maximum predicted damage area at the end of analysis with Pavement ME (NCAT), (g) amount of cracking in the field (FHWA), (h) predicted damage area in LVECD (FHWA), (i) predicted damage area in Pavement ME (FHWA), (j) maximum amount of cracking at the end period of study (FHWA), (k) maximum predicted damage area at the end of analysis with LVECD (FHWA), and (l) maximum predicted damage area at the end of analysis with Pavement ME (FHWA).

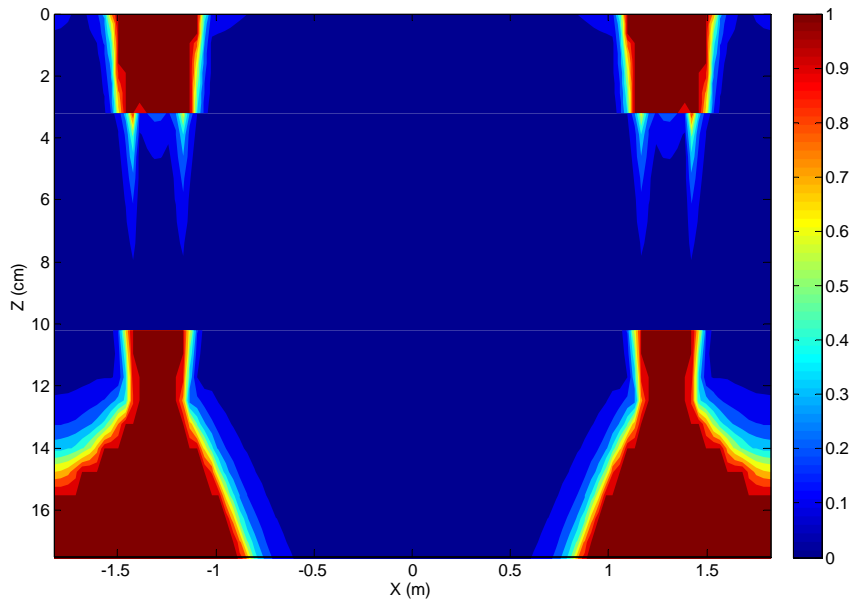


Figure 10-3. Damage factor (N/Nf) distribution of NCAT Test Track OGFC section at the end of analysis period.

The predicted and field-measured fatigue damage results for the MIT-WMA project are presented in Figure 10-4. In this case, while the rankings of the prediction results from the Pavement ME program matched the measured results in the field, the rankings of the Control and Advera sections were flipped in the LVECD program results. This outcome could be due to the properties of the WMA mixtures. Previous studies have shown that, under the same aging conditions, the stiffness of WMA mixtures increases more than that of HMA mixtures, and in the LVECD program, the aging model has not been developed yet. However, the aging effect of the WMA mixtures can be taken into account in the Pavement ME program simulations using the Global Aging System (GAS) model.

The predicted and field-measured performance results for the MIT RAP project sections are presented in Figure 10-4 (a) – (f). According to Figure 10-4 (g), the sections with materials with high RAP contents have significantly higher cracking damage values than those with low RAP contents; however, the section paved with 15% RAP mixture does not differ significantly from the control section. This finding confirms that it is reasonable to allow about 20 percent RAP in asphalt mixtures, which most state highway agencies suggest. The difference in performance between the high RAP mixtures and the low RAP mixtures is captured in the LVECD program predictions. However, the Pavement ME program prediction results indicate no significant difference among all the MIT RAP sections. Again, this outcome is due to the fact that the Pavement ME program considers the fatigue properties of only the bottom layer material, and all four sections have the same bottom layer material. It is worth noting that though not much difference can be observed in the MIT RAP sections based on the alligator crack curves predicted by the Pavement ME program, the four sections have slightly different absolute crack percentage values at the end of the design period. It can be observed that the ranking of the performance prediction results of the four sections is the reverse ranking of the modulus values of the surface mixtures (which are 8694 MPa, 8680 MPa, 6801 MPa, and 6283 MPa for 50RSB, 50R, 15R, and Control mixtures respectively at 20°C and 10 Hz). Therefore, with identical base mixtures, the Pavement ME program's fatigue cracking predictions were affected strongly by the modulus values of the mixtures rather than by their fatigue properties.

In brief, based on the prediction results and field measurements of the MIT RAP section, the effects of the different RAP contents in this project can be characterized by the LVECD program; in contrast, the Pavement ME program did not produce good results due to the limited input information and mechanism of fatigue damage calculation.

The KEC test road was constructed to evaluate ways that different factors affect pavement. The factors used in this study include the base layer material, the thickness of the base layer, the application of an anti-frost layer, and the thickness of the sub-base layer. The evaluation results are presented in Figure 10-4. The effects of the base layer material are presented in Figure 10-5 (a), (b), and (c). According to Figure 10-5 (a), aggregate base pavements have a significantly higher cracking damage percentage than full-depth pavements when the pavements have the same thickness of base layer. This effect was captured by both the Pavement ME and LVECD programs. The effects of the thickness of the base layer are shown in Figure 10-5 (d) to (f) where, for a given base layer material, a thicker base layer results in less fatigue damage. This trend is matched in both programs, and the prediction results of the two programs are also very similar to each other in this case. In terms of the effect of an anti-frost layer and the effect of the thickness of the sub-base layer, according to Figure 10-5 (g) to (i) and (j) to (l), respectively, the effects are not significant based on the measurements in the field and the prediction results from the Pavement ME and LVECD programs. In addition, according to Figure 10-5 (a) and (d), when the aggregate base is very thin (8 cm), the crack damage percentage of the pavement section is very high; however, this trend was not predicted by the Pavement ME and LVECD programs due to the application of linear theory to the aggregate base. When the base layer is very thin, the strain and deformation in the base layer are relatively high and exceed the linear elastic domain. When the base layer response is in the domain of nonlinear elasticity, the crack damage propagation is accelerated throughout the whole pavement. In short, based on the predictions and field results, these changes in the base and sub-base layers can be predicted by both the LVECD and Pavement ME programs. To improve the prediction programs, nonlinear elastic theory should be applied for the aggregate base layers when the bases are thin or the strain level in the base is relatively high.

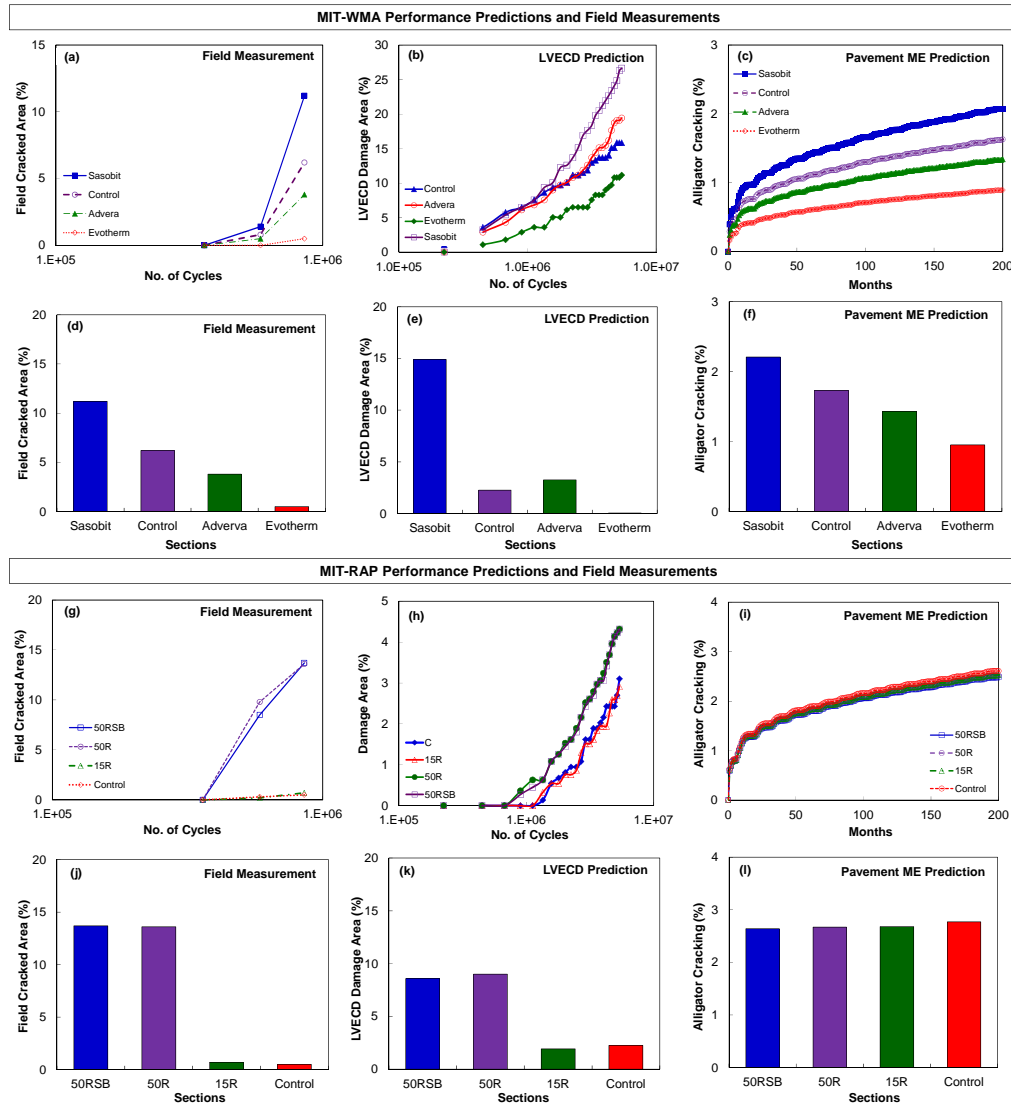


Figure 10-4. Measured and predicted fatigue cracking amount for MIT-WMA and MIT-RAP test sections: (a) amount of cracking in the field (MIT-W), (b) predicted damage area in LVECD (MIT-W), (c) predicted damage area in Pavement ME (MIT-W), (d) maximum amount of cracking at the end period of study (MIT-W), (e) maximum predicted damage area at the end of analysis with LVECD (MIT-W), (f) maximum predicted damage area at the end of analysis with Pavement ME (MIT-W), (g) amount of cracking in the field (MIT-R), (h) predicted damage area in LVECD (MIT-R), (i) predicted damage area in Pavement ME (MIT-R), (j) maximum amount of cracking at the end period of study (MIT-R), (k) maximum predicted damage area at the end of analysis with LVECD (MIT-R), and (l) maximum predicted damage area at the end of analysis with Pavement ME (MIT-R).

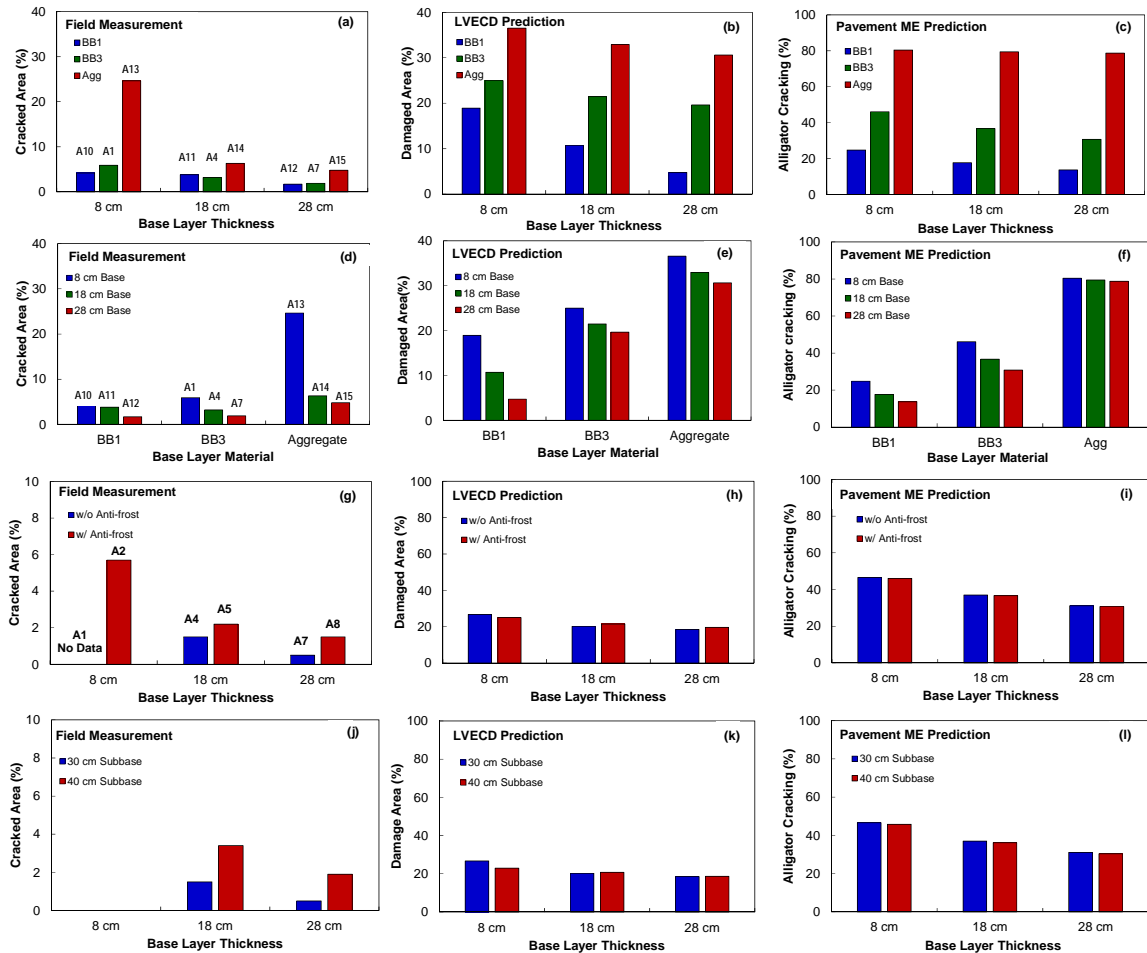


Figure 10-5. Effects of different parameters of fatigue cracking performance for KEC test sections: (a)-(c) base layer material, (d)-(f) base layer thickness, (h)-(j) application of anti-frost layer, and (k)-(m) sub-base thickness.

The overall trends of the prediction results from the LVECD and Pavement ME programs are plotted against the field measurements in Figure 10-6; these results include those of the NCAT, FHWA ALF, and MIT WMA and RAP projects. In terms of absolute values of the prediction results and the field measurements, due to the lack of the application of the transfer function and local calibration factors, the predicted damage values are not on the same scale as the field measurements.

However, the LVECD program results agree well with the results measured in the field. In contrast, when the Pavement ME program prediction results are plotted against the field measurements, the data are scattered and do not show good agreement, as seen in Figure 10-6 (b).

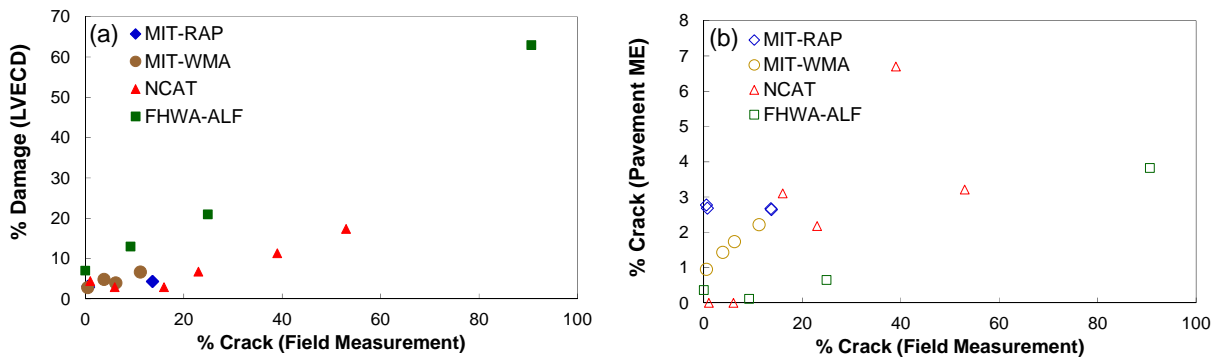


Figure 10-6. Overall trends of predicted fatigue cracking vs. field measurements: (a) LVECD program predictions and (b) Pavement ME program predictions.

## 10.6 Conclusions

This study presents the fatigue performance prediction results for selected field test sections using two programs, the LVECD and Pavement ME, and compares the prediction results with the field measurements. Thirty-three pavement test sections from five research projects were used in this study. The two programs apply different mechanisms to compute the fatigue damage in the pavement sections. The following conclusions can be drawn based on the comparison of the prediction results to the ‘cracking areas’ measured in the field:

- To obtain the mechanical responses of the pavements, the LVECD program employed 3-D finite element analysis with moving loads, and the Pavement ME program employed multilayer elastic analysis. To predict fatigue cracking, the S-VECD model, a constitutive damage model, was adopted in the LVECD program. The prediction results were affected more by the stiffness of the asphalt mixtures in the Pavement ME.

- Regarding the prediction results, in terms of ranking, the LVECD program provided better agreement with the field measurements than the Pavement ME program.
- For the multilayer pavement sections, the properties of the surface and intermediate layer materials, not just the bottom layer materials, are taken into account in the LVECD program.
- The damage contours of the cross-sections provided by the LVECD program can be useful in the design process.
- The analyses performed in both programs did not capture the effects of the properties of the aggregate base well. Nonlinear elastic analysis will be considered for inclusion in the LVECD program in the future.
- Although the LVECD program focuses on the analysis of asphalt layers, the Pavement ME program considers more information in terms of traffic and climate. Similar features will be added to the LVECD program in the future.

## CHAPTER 11 CONCLUSIONS AND FUTURE WORK

### 11.1 Conclusions

This research is divided into five main steps: (i) statistical analysis of effective parameters in dynamic modulus testing in indirect tension mode and development of testing specification for the field cores, (ii) geometry and gauge length study for the cyclic direct tension testing to obtain the specimen failure in the middle, (iii) implementation of the simplified viscoelastic continuum damage (S-VECD) model coupled with the  $G^R$  failure criterion for asphalt mixture characterization, (iv) validation of the LVECD design tool for pavement analysis based on field performance observations, and (v) defining simulated damaged area-to-field cracked area transfer function for the PRS pavement test sections.

A summary of the findings and the conclusions drawn are as follows:

- According to the ruggedness analysis of dynamic modulus in indirect tension mode, air void content was found to be statistically significant, especially at  $-10^{\circ}\text{C}$  and  $10^{\circ}\text{C}$ . However, the impact of air void content on material stiffness (i.e., dynamic modulus values) at  $35^{\circ}\text{C}$  was statistically insignificant.
- In general, specimen thickness, gauge length, strain level, and test temperature, did not have a considerable impact on the dynamic modulus values.
- The temperature tolerance range of  $\pm 1.0^{\circ}\text{C}$  seems adequate because the change in dynamic modulus value was within the acceptable range; however, to maintain consistency with other specifications, the tolerance range of  $\pm 0.5^{\circ}\text{C}$  ( $\pm 1^{\circ}\text{F}$ ) is recommended for the IDT specification.
- No significant change was observed between the stiffness values at  $40\ \mu\epsilon$  and  $60\ \mu\epsilon$ . With the consideration of signal quality and damage to the sample, the horizontal strain level should be limited to  $50 \pm 5\ \mu\epsilon$ .
- An air void content tolerance of  $\pm 0.5\%$  should be reasonable because the dynamic modulus variation was less than 10% for almost all the cases investigated.

- Ruggedness analysis showed no major difference between the stiffness values for 38 mm and 50 mm thickness; therefore, the thickness of  $38 \pm 3$  mm is recommended for IDT samples, which is practical for obtaining field cores from pavement sections.
- The gauge length limit must be an appropriate representative volume element (RVE), especially for mixtures that contain large aggregate particles; so, the gauge length of  $101.6 \pm 3$  mm is recommended for IDT testing.
- Specimen geometry and gauge length (100-mm diameter, 150-mm height, and 70-mm gauge length) specified in AASHTO TP 79 and PP 61 yield dynamic modulus values that are in reasonable agreement with the results from other specimen geometries and meet conventional RVE requirements.
- Regarding direct tension cyclic fatigue testing, the specimen geometry of 100 mm in diameter and 130 mm in height leads to statistically the same damage characteristic curves as the other geometries investigated and increases the propensity for middle failure.
- SBS, as presented in the FHWA-ALF project, demonstrates the best performance for both fatigue cracking and rutting since it decreases the mixture modulus at low and intermediate temperatures, and increases the stiffness at high temperatures. Other modified binders, crumb rubber, and terpolymer, also improve the pavement life in terms of fatigue cracking.
- Warm mix additives seem to deteriorate the mixtures' fatigue resistance, although they decrease the stiffness and aging during compaction. Evotherm improves the fatigue behavior in MIT; this is while it increases the amount of cracking in NCAT test track project.

- It is accepted that the addition of RAP up to 20% does not have any major effect on virgin mixture performance, according to many asphalt agencies. The results of MIT-RAP project briefly admit this conclusion where utilization of RAP up to 15% did not change the mixture performance. The mixtures containing 50% RAP show lower fatigue life compared with the others.
- The pavement simulations indicate no significant change in the fatigue resistance or permanent deformation when using an anti-frost layer or increasing the sub-base layer thickness.
- One interesting observation is that the base layer material played the most important role in affecting both rutting and fatigue cracking in the KEC test road sections. The aggregate base layer exhibited greater rut depths and more cracking than the asphalt base layers, whereas the sections with an asphalt base layer (either the BB1 mix or BB3 mix) showed less distress than the aggregate base sections.
- The data obtained from the pavement analyses of the different base layer thicknesses briefly indicate that an increase in the base layer thickness reduces the pavement distresses, but the amount of improvement is dependent on the material type.
- For the multilayer pavement sections, the properties of the surface and intermediate layer materials, not just the bottom layer materials, are taken into account in the LVECD program.
- Regarding the prediction results, in terms of ranking, the LVECD program provided better agreement with the field measurements than the Pavement ME program.
- The S-VECD model coupled with the  $G^R$  failure criterion can be used for the accurate fatigue life predictions of asphalt mixtures, even when very different asphalt binders (unmodified, polymer-modified, crumb rubber-modified, WMA, RAP etc.) are analyzed since there is a strong agreement between the LVECD simulations and field observations.

- From both LVECD and Pavement ME observations, a sigmoidal function was chosen for representing the relation between field cracked area and simulated damaged area.
- The proposed damage-to-field cracked area transfer functions were validated for both the asphalt pavement new asphalt pavement projects. However, it should be pointed out that the proposed framework has not been validated for the overlays and the pavements with reflective cracking.

## **11.2 Future Work**

The following topics are suggested for future work:

- Verification of the dynamic modulus and damage properties of small specimens since these samples are more compatible with the field cores and they can be easily fabricated in the asphalt labs.
- Development of fatigue failure criterion for the binder and finding the relationship between binder and mixture fatigue life to reduce the amount of testing time in the lab.
- Modification of VECD cyclic tension fatigue testing to monotonic tension mode for more feasibility in mixture testing. A bridge which relates the failure criterion in cyclic and monotonic mode is necessary to predict the fatigue life of the mixture.
- Verification and re-calibration of the LVECD program once mixture aging and thermal cracking models are implemented in the new LVECD package.
- Calibration of LVECD software for the thin pavement (less than 4 in) and for the perpetual pavements.

## REFERENCES

- Abbasian-Hosseini, S. A., Leming, M. L., & Liu, M. (2015). Effects of Idle Time Restrictions on Excess Pollution from Construction Equipment. *Journal of Management in Engineering*, 04015046.
- Abbasian-Hosseini, S. A., Liu, M., & Leming, M. (2015). Comparison of Least-Cost and Least-Pollution Equipment Fleet Configurations Using Computer Simulation. *Journal of Management in Engineering*, 04015003.
- Abbasian-Hosseini, S. A., Nikakhtar, A., & Ghoddousi, P. (2014). Verification of lean construction benefits through simulation modeling: A case study of bricklaying process. *KSCE Journal of Civil Engineering*, 18(5), 1248-1260.
- Al-Qadi, I. and P. J. Yoo. "Surface Tangential Contact Stresses Effect on Flexible Pavement Response," *Journal of Association of Asphalt Paving Technologists*, Vol. 76, pp. 663-692, 2007.
- American Association of State Highway Transportation Officials (AASHTO) (2013). AASHTO PP60-13, Preparation of Cylindrical Performance Test Specimens Using the Superpave Gyratory Compactor (SGC).
- American Association of State Highway Transportation Officials (AASHTO) (2013). AASHTO PP61-10, 2013, Developing Dynamic Modulus Master Curves for Hot Mix Asphalt (HMA) Using the Asphalt Mixture Performance Tester (AMPT).
- American Association of State Highway Transportation Officials (AASHTO) (2014). AASHTO TP 107, Determining the Damage Characteristic Curve of Asphalt Concrete from Direct Tension Cyclic Fatigue Tests, *AASHTO*. Washington, D.C.
- American Association of State Highway Transportation Officials (AASHTO) (2007). AASHTO TP62-07, Determining Dynamic Modulus of Hot Mix Asphalt (HMA).
- American Society for Testing and Materials (ASTM) (1985) ASTM D 3497-79, Standard Test Method for Dynamic Modulus of Asphalt Mixtures. Annual Book of ASTM Standards, Vol. 04.03, ASTM International, West Conshohocken, PA.
- American Association of State Highway Transportation Officials (AASHTO) (2011). AASHTO TP 79, Standard Method of Test for Determining the Dynamic Modulus and Flow Number for Hot Mix Asphalt (HMA) Using the Asphalt Mixture Performance Tester (AMPT). *AASHTO*. Washington, D.C.

American Society for Testing and Materials (ASTM) (1985). ASTM C1067-12, 2012. Standard Practice for Conducting a Ruggedness or Screening Program for Test Methods for Construction Materials. West Conshohocken, PA.

American Society for Testing and Materials (ASTM) (2012). ASTM D6931-12, 2012, Standard Test Method for Indirect Tensile (IDT) Strength of Bituminous Mixtures.

Amini, A., Mashayekhi, M., Ziari, H, Nobakht, S., 2011. Life cycle cost comparison of highways with perpetual and conventional pavements. *International Journal of Pavement Engineering*, Vol 13, Issue 6.

Behiry, Ahmed Ebrahim. Fatigue and Rutting Lives in Flexible Pavements. *Ain Shams Engineering Journal*, 2012, 3, pp. 367-374.

Bhattacharjee, S., Swamy, A.K., Daniel, J.S., 2009. Application of the elastic-viscoelastic correspondence principle to determine the fatigue endurance limit of hot mix asphalt. Paper submitted for 88th Annual Meeting. Transportation Research Board, Washington, D.C.

Bonaquist, R. National Cooperative Highway Research Program Report 629: Ruggedness Testing of the Dynamic Modulus and Flow Number Tests with the Simple Performance Tester. Transportation Research Board, Washington, DC, 2008.

Bonaquist, R and D. Christensen. Refining the Simple Performance Tester for Use in Routine Practice. *NCHRP Report 614*, Transportation Research Board, National Research Council, Washington, D.C., 2008.

Buttlar, W. G. and R. Roque. Development and Evaluation of the Strategic Highway Research Program Measurement and Analysis System for Indirect Tensile Testing at Low Temperature. *Transportation Research Record 1454*, TRB, National Research Council, Washington, DC, pp. 163–171, 1994.

Cao, W., 2015. Experimental and analytical investigations of permanent deformation behavior of asphalt mixtures under confining pressure. Ph.D. Dissertation, North Carolina State University, Raleigh, NC.

Cao, W., Eslaminia, M., and Kim, Y.R., 2012. Fatigue performance modeling of Binzhou perpetual pavements using viscoelastic continuum damage finite element program. In: *Proceedings of the International Society for Asphalt Pavements 2012*, Nanjing, China.

Cao, W., A. H. Norouzi, and Y. R. Kim., 2015. Application of viscoelastic continuum damage approach to predict the fatigue cracking performance of Binzhou perpetual pavements. *Journal of Traffic and Transportation Engineering*, in press.

Chehab, G., E. O'Quinn, and Y. R. Kim, Specimen Geometry Study for Direct Tension Test Based on Mechanical Tests and Air-Void Variation in Asphalt Concrete Specimens Compacted by Superpave Gyrotory Compactor. Transportation Research Record, No. 1723, Transportation Research Board, National Research Council, Washington, D.C., 2000, pp 125-132.

Chehab, G., Y. R. Kim, R. A. Schapery, M. Witczack, and R. Bonaquist, Time-Temperature Superposition Principle for Asphalt Concrete Mixtures with Growing Damage in Tension State. Journal of Association of Asphalt Paving Technologists, Vol. 71, 2002, pp. 559-593.

Choi, Y. and Y. R. Kim. Development of Calibration Testing Protocol for Permanent Deformation Model of Asphalt Concrete. Transportation Research Record: Journal of the Transportation Research Board, No. 13-2555, 2012, pp. 34-43.

Daniel J. S. and Y. R. Kim, Development of a Simplified Fatigue Test and Analysis Procedure Using a Viscoelastic Continuum Damage Model, *Journal of Association of Asphalt Paving Technologists*, Vol. 71, 2002, pp. 619-650.

Darabi, M.K., Abu Al-Rub, R.K., Masad, E.A., Huang, C., Little, D.N., 2012. A modified viscoplastic model to predict the permanent deformation of asphaltic materials under cyclic-compression loading at high temperatures. *International Journal of Plasticity*, 35: 100-134.

Elwardany, Michael D. Performance of plant produced HMA mixtures with high RAP content in terms of low temperature cracking, fatigue cracking, and moisture induced damage. UNIVERSITY OF NEW HAMPSHIRE, 2012.

Eslaminia, M. and M. N. Guddati. Fourier-Finite Element Analysis of Pavements under Moving Vehicular Loading. *International Journal of Pavement Engineering*, 2012.

Eslaminia, M., S. Thirunavukkarasu, M. N. Guddati, and Y. R. Kim. Accelerated Pavement Performance Modeling Using Layered Viscoelastic Analysis. Proceedings of the 7th International RILEM Conference on Cracking in Pavements, Delft, The Netherlands, pp. 20-22, 2012.

Federal Highway Administration. Report FHWA-RD-03-031. Pavement Distress Identification Manual for the NPS Road Inventory Program, June 2003.

Heyden, T., A. Nijhuis, J. Smeyers-Verbeke, B. Vandeginste, and D. Massart. Guidance for Robustness/Ruggedness Tests in Method Validation, *Journal of Pharmaceutical and Biomedical Analysis*, Vol. 24, No. 5-6, pp. 723-753, 2011.

Hondros, G. Evaluation of Poisson's Ratio and the Modulus of Materials of a Low Tensile Resistance by the Brazilian (Indirect Tensile) Test with Particular Reference to Concrete. *Australian Journal of Applied Science*, Vol. 10, No. 3, pp. 243–268, 1959.

Hosseini, A., Nikakhtar, A., & Ghoddousi, P. (2012). Flow production of construction processes through implementing lean construction principles and simulation. *IACSIT International Journal of Engineering and Technology*, 4(4), 475-479.

Hosseini, S. A., Nikakhtar, A., Wong, K. Y., & Zavichi, A. (2012). Implementing Lean Construction Theory into Construction Processes' Waste Management. In *Reston, VA: ASCE Proceedings of the 2011 International Conference on Sustainable Design and Construction | d 20120000*. American Society of Civil Engineers.

Hou, T., B. S. Underwood, and Y. R. Kim. Fatigue Performance Prediction of North Carolina Mixtures Using Simplified Viscoelastic Continuum Damage Model. *Journal of the Association of Asphalt Paving Technologists*, Vol. 79, pp. 35-80, 2010.

Huang, Y. H. *Pavement Analysis and Design*. 2nd edition, Englewood Cliffs: Prentice-Hall, 2003.

Jackson, N. and J. Puccinelli. Long-Term Pavement Performance (LTPP) Data Analysis Support: National Pooled Fund Study TPF-5(013)-Effect of Multiple Freeze Cycles and Deep Frost Penetration on Pavement performance and Cost, Publication FHWA-HRT-06-121. FHWA, U.S. Department of Transportation, 2006.

Kim, D. Modulus and Permanent Deformation Characterization of Asphalt Mixtures and Pavements. Ph.D. dissertation, North Carolina State University, Raleigh, NC, 2015.

Kim, D. and Y.R. Kim. Determination of Dynamic Modulus of Asphalt Mixtures Using Impact Resonance Testing of Thin Disk Specimens. Submitted to the *ASTM Journal of Testing and Evaluation*, 2015.

Kim, Y.R., Little, D.N., 1990. One-dimensional constitutive modeling of asphalt concrete. *Journal of Engineering Mechanics*, 116(4): 751-772.

Kim, Y. R., D. N. Little, and R. L. Lytton. Fatigue and Healing Characterization of Asphalt Mixtures. *Journal of Materials in Civil Engineering*, Vol. 15, No. 1, pp. 75-83, 2003.

Kim, Y. R., Y. Seo, M. King, and M. Momen. Dynamic Modulus Testing of Asphalt Concrete in Indirect Tension Mode. *Transportation Research Record: Journal of the Transportation Research Board*, No. 1891, TRB, National Research Council, Washington, DC, pp. 163–173, 2004.

Kim, Y. R., Y. Lee, and H. J. Lee, Correspondence Principle for Characterization of Asphalt Concrete, *ASCE Journal of Material in Civil Engineering*, Vol. 7, No.1, 1995, pp. 59-68.

Underwood, B. S., Y. R. Kim, and M. N. Guddati, Improved Calculation Method of Damage Parameter in Viscoelastic Continuum Damage Model, *International Journal of Pavement Engineering*, Vol. 11, No. 6, 2010, pp. 459-476.

Kutay, M. E., N. H. Gibson, J. Youtcheff, and R. Dongre. Use of Small Samples to Predict Fatigue Lives of Field Cores: Newly Developed Formulation Based on Viscoelastic Continuum Damage Theory. *Transportation Research Record: Journal of the Transportation Research Board*, No. 2127, National Research Council, Washington, DC, pp. 90-97, 2009.

Lacroix, A. and Y. R. Kim. Performance Predictions of Rutting for NCAT Test Track. *Transportation Research Record: Journal of Transportation Research Board*, in press, 2014.

Lee, J. S., A. Norouzi, and Y. R. Kim. Determining Specimen Geometry of Cylindrical Specimens for Direct Tension Fatigue Testing of Asphalt Concrete. *Journal of Testing and Evaluation*, 2015, in press.

Lee, J.S., J.J. Lee, S.A. Kwon, and Y.R. Kim, Use of Cyclic Direct Tension Tests and Digital Imaging Analysis to Evaluate Moisture Susceptibility of Warm-Mix Asphalt Concrete, *Transportation Research Record No. 2372*, Transportation Research Board, National Research Council, Washington, D.C., 2013, pp. 61-71.

Maher, A., and T. Bennert, Evaluation of Possion's ratio for Use in the Mechanistic Empirical Pavement Design Guide, Final Report of FHWA-NJ-2008-004, New Jersey, <http://www.state.nj.us/transportation/refdata/research/reports/FHWA-NJ-2008-004.pdf>.

Majidzadeh, K., S. Khedr, and M. El-Mojarrush. Evaluation of Permanent Deformation in Asphalt Concrete Pavement. *Transportation Research Record: Journal of the Transportation Research Board*, No. 715, TRB, National Research Council, Washington, DC, 1979.

Mensching, David J., Jo Sias Daniel, Thomas Bennert, Marcelo S. Medeiros Jr, Michael D. Elwardany, Walaa Mogawer, Elie Y. Hajj, and Mohammad Zia Alavi. Low-temperature properties of plant-produced RAP mixtures in the Northeast. *Road Materials and Pavement Design* 15, no. sup1 (2014): 1-27.

Moghaddas Tafreshi, S. N., and A. H. Norouzi. Application of Waste Rubber to Reduce the Settlement of Pavement Systems. *Journal of Geomechanics and Engineering*, Vol. 9, No. 1, 2015.

Moghaddas Tafreshi, S. N., and A. H. Norouzi. Bearing Capacity of a Square Model Footing on Sand Reinforced with Shredded Tire—An Experimental Investigation, *Journal of Construction and Building Materials*, Vol. 35, Pages 547-556, 2012.

Myers, L. A., R. Roque and B. E. Ruth. Mechanisms of Surface-Initiated Longitudinal Wheel Path Cracks in High Type Bituminous Pavements, *Journal of Association of Asphalt Paving Technologists*, Vol. 65, pp. 401-432, 1998.

Myers, L. A. and R. Roque. Evaluation of Top-Down Cracking in Thick Asphalt Pavements and the Implications for Pavement Design, *Transportation Research Circular: Perpetual Bituminous Materials*. Washington, D.C, 2001.

NCHRP Report 602, Project 9-23. Calibration and Validation of the Enhanced Integrated Climatic Model for Pavement Design. Transportation Research Board, 2008. ISBN 978-0-309-09929-5.

Nikakhtar, A., Hosseini, A. A., & Wong, K. Y. (2012). Sensitivity analysis of construction processes using computer simulation: a case study. *Advanced Science Letters*, 13(1), 680-684

Nikakhtar, A., Hosseini, A. A., Wong, K. Y., & Zavichi, A. (2015). Application of lean construction principles to reduce construction process waste using computer simulation: a case study. *International Journal of Services and Operations Management*, 20(4), 461-480.

Norouzi A., M. Sabouri, and Y. R. Kim. Evaluation of the Fatigue Performance of High RAP Asphalt Mixtures. *Proceedings of 12th International Society for Asphalt Pavements*, Raleigh, NC, 2014.

Norouzi, A., and Y. R. Richard Kim. Mechanistic evaluation of fatigue cracking in asphalt pavements. *International Journal of Pavement Engineering*, 1-17, 2015.

Norouzi, A. H., and Y. R. Kim. Ruggedness Study on the Dynamic Modulus Testing of Asphalt Concrete in Indirect Tension Mode. *Journal of Testing and Evaluation*, 2015, in press.

Norouzi, A., D. Kim, and Y. R. Kim. Numerical Evaluation of Pavement Design Parameters on the Fatigue Cracking and Rutting Performance of the Asphalt Pavements, *Journal of Materials and Structures*, 2015, in press.

Park, H. J., M. Eslaminia, and Y. R. Kim. Mechanistic Evaluation of Cracking in in-Service Asphalt Pavements. *Journal of Materials and Structures*, pp. 1–20, 2014.

Park, S.W., Kim, Y.R., Schapery, R.A., 1996. A viscoelastic continuum damage model and its application to uniaxial behavior of asphalt concrete. *Mechanics of Materials*, 24: 241-255.

Park, S.W., Schapery, R.A., 1999. Methods of interconversion between linear viscoelastic material functions. Part I – a numerical method based on Prony series. *International Journal of Solids and Structures*, 36(11): 1653-1675.

Pellinen, T. Evaluation of Surface (top-down) Longitudinal Wheel Path Cracking in Indiana, Joint Transportation Research Program. Purdue University, West Lafayette, IN, 2002.

Pierce, L. M., McGovern, G. (2014). Implementation of the AASHTO Mechanistic-Empirical Pavement Design Guide and Software. Report NCHRP Synthesis 457.

Rad, Farhad Yousefi. Estimating blending level of fresh and RAP binders in recycled hot mix asphalt. Diss. University of Wisconsin Madison, 2013.

Rad, Farhad, Nima Sefidmazgi, and Hussain Bahia. Application of Diffusion Mechanism: Degree of Blending Between Fresh and Recycled Asphalt Pavement Binder in Dynamic Shear Rheometer. *Transportation Research Record: Journal of the Transportation Research Board* 2444 (2014): 71-77.

R. Reese, Properties of Aged Asphalt Binder Related to Asphalt Concrete Fatigue Life, *Journal of the Association of Asphalt Paving Technologists*, Vol. 66, pp. 604-632, 1997.

Roque, R. and W.G. Buttlar, The Development of a Measurement and Analysis System to Accurately Determine Asphalt Concrete Properties Using the Indirect Tensile Mode, *Proceedings, The Association of Asphalt Paving Technologist*, pp. 304-333, 1992.

Sabouri, M. and Y.R. Kim, Development of a Failure Criterion for Asphalt Mixtures under Different Modes of Fatigue Loading, *Transportation Research Record, Transportation Research Board, National Research Council, Washington, D.C.*, In press, 2014.

Sabouri, M., T. Bennert, J. S. Daniel, and Y. R. Kim. A Comprehensive Evaluation of the Fatigue Behavior of Plant Produced RAP Mixtures Laboratory-Produced RAP Mixtures. *Journal of Road Materials and Pavement Design*, 2014.

Sabouri M, T. Bennert, J. Daniel, and Y. R. Kim (2014). Evaluating Laboratory-Produced RAP Mixtures in Terms of Rutting, Fatigue, Predictive Capabilities, and High RAP Content Potential. *Transportation Research Record: Journal of the Transportation Research Board*.

Schapery, R.A. Correspondence principles and a generalized J integral for large deformation and fracture analysis of viscoelastic media. *International Journal of Fracture*, 25: 195-223, 1984.

Seo, Youngguk. Distress Evolution in Highway Flexible Pavements: A 5-Year Study at the Korea Highway Corporation Test Road. ID JTE 102107. *Journal of Testing and Evaluation*, Vol. 38, No. 1, 2010.

Shook, J. F., B. F. Kallas, and B. F. McLeod. Factors Influencing Dynamic Modulus of Asphalt Concrete. *Journal of Association of Asphalt Paving Technologists*, Vol. 38, 1969.

Tanesi, J., J. M. Gudimettla, G. L. Crawford, and A. A. Ardani. Ruggedness Study on The Coefficients of Thermal Expansion of Concrete Test Method (AASHTO T336), *Transportation Research Record: Journal of the Transportation Research Board*, No. 2342, Transportation Research Board of National Academies, Washington, DC, pp. 54-60, 2013.

Underwood, B. S., C. M. Baek, and Y. R. Kim. Use of Simplified Viscoelastic Continuum Damage Model as an Asphalt Concrete Fatigue Analysis Platform, *Transportation Research Record Issue 2296*, Transportation Research Board, National Research Council, Washington, D.C., 2012, pp. 36-45.

Underwood, B. S., Y. R. Kim, and M. N. Guddati. Characterization and Performance Prediction of ALF Mixtures Using a Viscoelastoplastic Continuum Damage Model. *Journal of the Association of Asphalt Paving Technologists*, Vol. 75, pp. 577-636, 2006.

Underwood, B. S., Y. R. Kim, and M. N. Guddati. Improved Calculation Method of Damage Parameter in Viscoelastic Continuum Damage Model. *International Journal of Pavement Engineering*, Vol. 11, 2010, pp. 459-476.

Wang, Yizhuang. Performance Evaluation of Warm Mix Asphalt Mixtures and Their Incorporation into the AASHTOWare Pavement ME Program. Master thesis, North Carolina State University, Raleigh, NC, 2014.

Wang, Y. D., A. Norouzi, and Y. R. Kim. Comparison of Fatigue Cracking Performance Predictions in Asphalt Pavements Using Pavement ME and LVECD Programs", *Journal of Transportation Research Records*, in press, 2015.

Witzak, M. W., K. Kaloush, T. Pellinen, M. El-Basyouny, and H. Von Quintus., Simple Performance Test for Superpave Mix Design, NCHRP Report 465, Transportation Research Board, National Research Council, Washington, D.C., 2002.

Witczak, M. W. and O. A. Fonseca. Revised Predictive Model for Dynamic Modulus of Asphalt Mixtures. Transportation Research Record: Journal of the Transportation Research Board, No. 1540, TRB, National Research Council, Washington, DC, 1996.

Witczak, M. W., R. Bonaquist, H. Von Quintus, and K. E. Kaloush. Specimen Geometry and Aggregate Size Effects in Uniaxial Compression and Constant Height Shear Tests. Journal of the Association of Asphalt Paving Technologists, Vol. 69, pp. 733–793, 2000.

Wu, C. and M. Zeng. Effects of Additives for Warm Mix Asphalt on Performance Grades of Asphalt Binders. Journal of Testing and Evaluation, Vol. 40, No. 2, 2012.

Xu, Q. and M. S. Rahman. Finite Element Analyses of Layered Viscoelastic System Under Vertical Circular Loading. International Journal for Numerical and Analytical Methods in Geomechanics, Vol. 32, pp. 897-913, 2008.

Yin, Q., 2011. Analysis on primary road performance of LSPM, Value Engineering, 30(11): 62-63.

Zhang J., M. Sabouri, Y. R. Kim, and M. N. Guddati. Development of a Failure Criterion for Asphalt Mixtures under Fatigue Loading. Journal of the Association of Asphalt Paving Technologists, Vol. 82, 2013. In press.

Zhao, Y., Huang, X. Design method and performance for large stone porous asphalt mixtures. Journal of Wuhan University of Technology – Mater. Sco. Ed., 25(5): 871-876, 2010.

